OPTICAL RECTIFICATION IN TELLURIUM FOR CO_2 LASER DETECTION

by

© Jean-François Ostiguy, B.Ing.
(Ecole Polytechnique de Montreal)

Department of Electrical Engineering
McGill University

August 1982
M.Eng.

OPTICAL RECTIFICATION IN TELLURIUM FOR CO_2 LASER DETECTION

by

Jean-Francois Ostiguy B.Ing.
(Ecole Polytechnique de Montreal)

A thesis submitted to the Faculty of Graduate Studies and Research in partial fulfillment of the requirements for the degree of Master of Engineering

Department of Electrical Engineering,
McGill University,
Montreal, Canada.

August 1982

ABSTRACT

This thesis presents a detailed theoretical investigation of the generalized conductivity in solids at optical frequencies, on the basis of the work of Butcher and McLean. Explicit expressions for the second order conductivity and the optical rectification tensor have been obtained and shown to be identical to the so-called bulk photovoltaic effect (BPVE) defined by von Baltz. Detailed experimental investigation in the case of Tellurium has been conducted and good qualitative agreement with the microscopic theory has been obtained.

RESUME

Cette thèse présente une étude théorique détaillée de la conductivité généralisée dans les solides aux fréquences optiques, sur la base des travaux de Butcher et McLean. Des expressions explicites pour la conductivité de second ordre ainsi que pour le tenseur de redressement optique ont été obtenues et démontrées identiques à l'effet photovoltaique de volume défini par von Baltz. Une étude expérimentale détaillée dans le cas du Tellure a été conduite et les resultats concordent bien au niveau qualitatif avec la théorie microscopique.

ACKNOWLEDGEMENTS

The author wishes to express his appreciation to Dr. A.A. Gundjian for his guidance and assistance throughout the period of research.

Thanks are also due to Dr. Ishiang Shih for supplying the Tellurium crystals and the resistivity data which appears in figures (6-17) to (6-20) of the present thesis. His comments have been deeply appreciated.

Acknowlegments are due Mrs Robert Kotiuga, Michel Belanger and James Reid for many helpful comments and moral support.

Finally, the author would like to thank J. Foldvari for his technical assistance.

TABLE OF CONTENTS

LIST OF ILLUSTRATIONS

CHAPTER I

Introduction

The advent of the transversly excited (TEA) CO_2 pulsed laser in the early seventies {1} has increased very significantly the upper limit of the available peak power levels at optical frequencies. This situation has led to the necessity of obtaining detectors suitable for the 10.6 μ radiation, operating at room temperature with satisfactory speed and responsivity.

The subsequent research efforts have led to the development of a variety of new detection schemes {2} and detectors. The most important of the latter that have found wide acceptance are the pyroelectric {3} and the photon-drag {4} detectors. The former generates an electrical signal when its spontaneous electric polarization is altered by a change in the crystal temperature upon absorption of the laser power. The photon-drag detector involves a transfer of photon momentum from the radiation field to the charge carriers in a semiconductor. Both share the advantage of room temperature operation and relatively high power density damage thresholds.

Pyroelectric detectors being thermal devices, show a very broad spectral response free of any stray signals, but their responsivity drops drastically with increased speed of response. Photon-drag detectors are fundamentally faster; however, they have a limited responsivity. Both pyroelectric and photon-drag detectors require almost complete absorption of the incident radiation.

A fundamental consideration for an efficient photon-drag device is the availability of a large photon absorption cross-section at the wavelength of interest. Among all semi-conductors Te is expected to be a favourable material since, due to its specific band structure it exhibits at 10.6 μ the highest known value of the absorption cross-section {5}. This material was therefore investigated as a potential CO_2 laser photon-drag detector and the results have been the subject of the doctoral dissertation of G. Ribakovs {6}, and of several publications {7,8,9,10}.

In the course of his experimentation, Ribakovs identified besides the photon-drag signal, another fast emf which could not be attributed to photon-drag because of a different tensorial behaviour. The existence of the latter had been also reported independently by Hermann and Vogel {11} and by Hammond, Jenkins and Stanley {12}. Since this fast emf reproduces faithfully the laser pulse shape and the signal levels are generally comparable in magnitude with those generated by the photon-drag effect, it was naturally considered to possess a good potential as a detection mechanism {10}.

The present thesis deals with a detailed discussion of this new emf. Since the latter constitutes a quadratic response to the optical field amplitude, the terminology "optical rectification" has been adopted to describe this phenomenon.

CHAPTER II

TEA-CO_2 Laser-Induced Rectified Optical Emfs in Tellurium

2.0 Introduction

In this chapter, we shall present a brief review of experimental observations that have motivated the present research. We shall also describe briefly the models which have been proposed to account for the observations. This will finally lead to the motivation for the theoretical discussion that is presented in the following chapters.

2.1 Experimental Observations

When single-crystal Tellurium is irradiated by high power TEA-CO_2 laser pulses, fast emfs faithfully reproducing the power envelope are generated {7}. These emfs have been found to be described phenomenologically in terms of a current density J_i related to the laser beam characteristics and crystal orientation as follows

$$J_i = \chi_{imn} W e_m e_n + T_{ijmn} W \hat{q}_j e_m e_n \qquad (2\text{-}1)$$

where W is the laser power density within the material, e_m and e_n are components of the unit vector of radiation electric field, $\hat{q}_j$ is a component of the unit photon wavevector and χ and T are third and fourth rank tensor

TABLE 2-1

SUMMARY OF RIBAKOV'S RESULTS AT ROOM TEMPERATURE

Tensor Component	Magnitude (cm/A)	
	Doped Sample ($p \simeq 10^{16}$ cm^{-3})	Undoped Sample
T^*_{1133}	1.1×10^{-7}	0.85×10^{-7}
T^*_{2233}	1.1×10^{-7}	0.85×10^{-7}
χ^*_{122}	0.7×10^{-7}	0.25×10^{-7}
χ^*_{212}	0.7×10^{-7}	0.25×10^{-7}
χ^*_{111}	0.7×10^{-7}	0.25×10^{-7}

NOTE $T^*_{ijkl} \equiv \rho_{ii} T_{ijkl}$

$\chi^*_{ijk} \equiv \rho_{ii} \chi_{ijk}$

coefficients, respectively. The subscripts take on the values 1,2,3 which correspond respectively to crystalline directions [1210] , [1010] , and [0001] . Thus, there exists two groups of signals, respectively consistent with a third and a fourth rank tensor behaviour.

It is recognized that there exists only a limited number of finite components for any tensorial parameter, determined by the prevailing tensor symmetry. Tellurium belonging to point group 32, there exists at the most five finite third rank χ_{imn} components of which only two are independent and twenty-five fourth rank components of which only ten are independent. Moreover, since the two subscripts m and n correspond to the directions of the radiation field, they are naturally interchangeable such that $\chi_{imn} = \chi_{inm}$ and $T_{ijmn} = T_{ijnm}$.

Ribakovs {9} has experimentally determined the magnitudes of both χ^* and T^* components for one doped and undoped crystals. It is to be noted that his results correspond to the product of the χ and T tensors with the resistivity of the measured material. Table 2-1 summarizes his results.

The fourth rank tensor T corresponds to the well accounted for photon-drag effect {8} which results in a signal that inverts its polarity when the laser beam propagation direction is reversed and is thus readily identifiable from the third rank tensor χ signal which retains its polarity under the same conditions.

Although some theories have been proposed to account for χ, its exact nature has not yet been satisfactorily determined. It is understood that since it relates quadratically the generated current density to the optical field amplitude it has been refered to as an optical rectification signal. For consistency we shall adopt this terminology in the present thesis which is exclusively devoted to the discussion of this phenomenon.

2.2 Physical Significance of Non-Centrosymmetric Lattice Structure

It is well-known that a necessary condition for the existence of a physical property describable in terms of a third rank tensor is the absence of inversion symmetry. The Tellurium lattice belonging to the point group symmetry 32 meets this requirement.

It is worthwhile at this point to illustrate the physical significance of inversion symmetry at the atomic level. This can be done by examining figure (2-1) which is a cross-sectional view of the Tellurium crystal structure in a plane perpendicular to the trigonal c-axis. The parallelogram defined by points A,B,C,D determines the primitive cell. From the juxtaposition of a few primitive cells a hexagonal feature evolves as shown in figure (2-1) which illustrates better the overall symmetry features of Tellurium.

Typically, an observation in direction 1 will clearly exhibit a non-centrosymmetric character. One will therefore expect the response of this crystal to an electric field acting in the positive direction to be different from that due to the same field in the negative direction; consequently, the response expressed as a power series in terms of the excitation field is expected to contain even order terms, hence the rectification effect.

It is interesting to note that from figure (2-1) the c-axis is not a pure rotation axis, but a screw axis, i.e. a symmetry element corresponding to a combination of both a rotation and a translation.

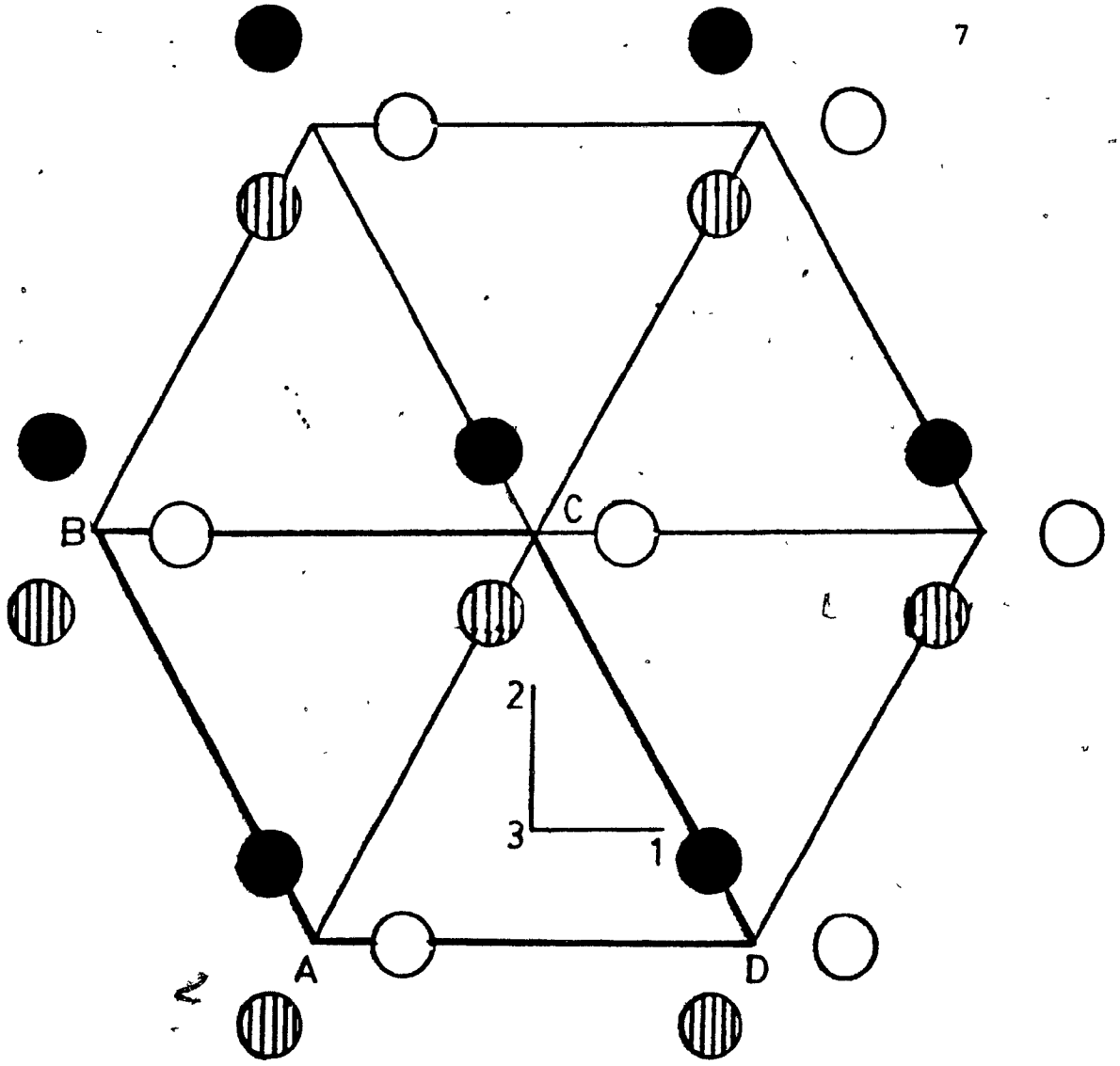

Figure (2-1) Cross-sectional View of the Te Crystal Structure in a Plane Perpendicular to the Trigonal Axis. ABCD determines the primitive cell.

2.3 Observation of Similar Optical Rectified Emfs Generated in Other Non-Centrosymmetric Materials

Rectified optical emfs of behaviour similar to the one under investigation in Tellurium have also been observed in other non-centrosymmetric materials. The case which bears the closest similarity to Tellurium is that of GaP.

Gibson and al. {13} have reported the occurence of a rectified signal in n-type GaP under experimental conditions similar to those of Ribakovs, but also at a wide range of frequencies other than the CO_2 laser 10.6 μ wavelength. This effect was also found to occur in p-type GaAs {14}, and in some dielectric materials like $BaTiO_3$ {15} and ZnS {16}. In our later discussions, critical reference will be made to the above cases to put the final interpretation in proper perspective.

2.4 Preliminary Critical Discussion of Different Possible Sources for the Rectified Emfs

2.4.1 Pseudo-Dember Effect

Auth and al. {17} have proposed the pseudo-Dember effect as a possible source of rectified emfs in CO_2 laser irradiated Tellurium. The pseudo-Dember effect is the analog of the well known Dember effect which would result from transitions within the sub-bands of the given material. The physical nature of this mechanism requires the reversal of the generated emfs as a result of the inversion of the direction of propagation of the incident laser beam. This behaviour eliminates completely the possibility for such a mechanism to contribute to any third rank tensor property.

2.4.2 Anisotropic Scattering Processes

Other authors have claimed that rectified optical signals could originate from various intra and inter-band anisotropic scattering processes.

Heyszenau {18} has suggested that a net photocurrent would be generated as a consequence of asymmetric charge distribution in energy bands due to photoexcitation from localized states, as illustrated in figure (2-2). Direct asymmetric generation being possible only for local states in polar systems, lattice defects would play an important role in this process. Such a mechanism should depend critically from crystalline quality and is hardly expected to be reproducible from one specimen to another, contrary to our observations.

Belinicher {19} has proposed that a photocurrent may appear because of an asymmetry in the intraband scattering of free carriers by impurities and by phonons in non-centrosymmetric materials under exposure to a propagating radiation field. This mechanism is expected to be strongly dependent on the variation of the free carrier density and temperature, a trend which is not supported by our observations.

Ivshenko and Pikus {20} have proposed that a " photogalvanic" current could appear if we allow interband phototransitions involving the participation of polar optical phonons. Although their rough numerical estimation of the photocurrent magnitude for one particular case seems to be in good agreement with the experimental data for GaP, again our experimental data concerning the temperature dependence of the generated signal in Tellurium does not support the above hypothesis.

2.4.3 Non-Linear Conductivity

Basically, the effect of optical radiation on a semiconductor can be described by considering that the sinusoidally varying radiation electric field acts on the charge carriers and consequently generates an alternating current. When this current is not linearly related to the applied field its average value could be non-vanishing, allowing the observation of a rectified optical signal.

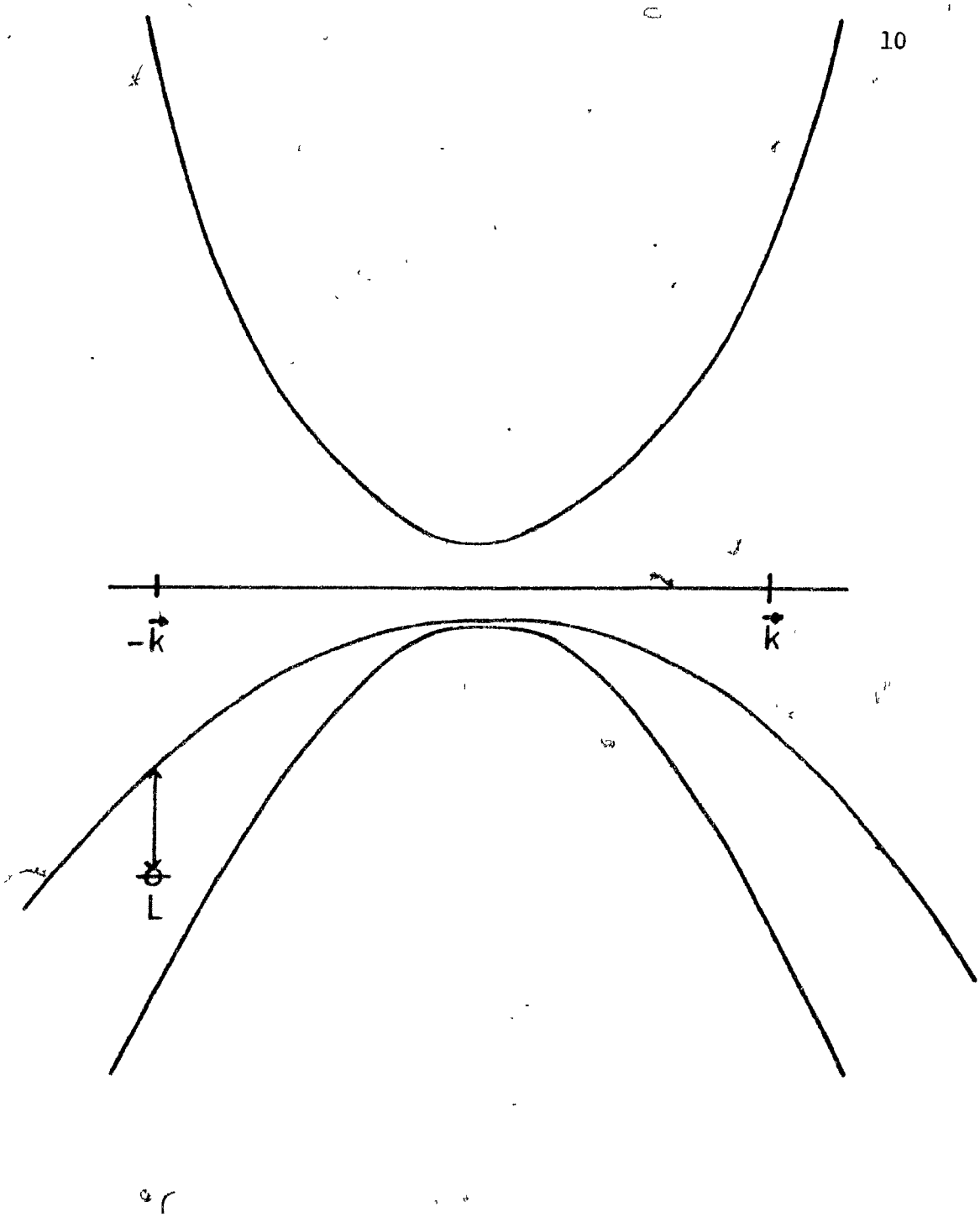

Figure (2-2) Photoexcitation from a Localized State

Herrmann and Vogel [11] who were the first to report the existence of a rectified signal in Tellurium, initially proposed that the latter could be ascribed to a non-linearity arising from the trogonal warping of the hole energy surfaces. These authors supported their interpretation with relation (2-2) due to Butcher and Mc Lean [21].

$$\sigma^{(2)}_{ijl}(\omega_1,\omega_2) = \frac{e^3}{2V\hbar^3\omega_1\omega_2} \sum_{n,k} f_{n\vec{k}} \frac{\partial^3 E_n(\vec{k})}{\partial k_i \partial k_j \partial k_l} \qquad (2\text{-}2)$$

which expresses the quadratic component of the conductivity tensor $\sigma^{(2)}_{ijl}(\omega_1,\omega_2)$ in terms of the energy band structure function $E_n(\vec{k})$ and the Fermi-Dirac distribution function $f_{n\vec{k}}$.

It has however properly been pointed out by Ribakovs [9] that the above claim overlooks the fundamental condition of time-reversal symmetry which will cause equation (2-2) to vanish identically. A careful examination of Butcher's complete work shows on the other hand, that relation (2-2) corresponds to a limiting case valid only for low frequencies where inter-band resonant transition effects are completely neglected. Therefore, a priori it appears that Butcher's general result does not necessarily vanish due to time-reversal symmetry.

A search of the pertinent literature reveals that other theories were proposed based on the existence of a quadratic component of the high frequency conductivity. In particular, Genkin and Mednis [22] and more recently von Baltz and Kraut [23] have proposed that a pure crystal can exhibit a bulk photovoltaic effect independently from possible contributions due to impurities, optical phonons or lattice defects. Their treatment being based fundamentally on premises similar to those of Butcher, it appeared to us that their work should bear a close relationship to that of the latter.

2.5 Conclusion

The different considerations presented in this chapter led us naturally to observe that high frequency non-linear conductivity in Tellurium remains the most likely source for the optical rectified signals under investigation. This provided the motivation to undertake a detailed theoretical and experimental discussion of the latter in conjunction with the concept of generalized non-linear conductivity.

CHAPTER III

Generalized Concept of Conductivity

3.0 Introduction

At the start of the development of a theoretical analysis for the phenomenon of non-linear conduction at optical frequencies, it has been found necessary to define as generally as possible the problem of electronic charge carrier response to an electric field excitation. This response is what we shall define as generalized conduction in the solid; in this approach it is clear that the distinction between free and bound charge carriers will initially be eliminated and therefore, the results are expected to account for the contribution to the final response from both types of carriers. This analysis and interpretation of generalized conduction was found to be essential in order not only to provide the proper mathematical basis for the discussion of our own observations, but also in order to bring out the common nature of analyses presented by several authors whose works will later be shown to merge to the same results merely put in slightly different formats.

3.1 Fundamental Notions

Conductivity is a measure of the ability of an electric field to set charge carriers into motion and hence produce an electric current. In the simple concept of conductivity, at relatively low frequencies, the electric field accelerates the free carriers, but the maximum velocity they can attain is limited by different scattering processes.

The time required to reach the maximum velocity is in general very small with respect to the period of the applied electric field and one is then justified to write

$$\vec{J} = \frac{n e \vec{E} \tau_n}{m_n^*} + \frac{p e \vec{E} \tau_p}{m_p^*} \qquad (3\text{-}1)$$

$$\vec{J} = (\sigma_p + \sigma_n)\vec{E} = \sigma \vec{E} \qquad (3\text{-}2)$$

where n represents the density of free electrons, p the density of free holes (if applicable) and e is the magnitude of the electronic charge. m_n^* and m_p^* are repectively the effective masses of electrons and holes. Equations (3-1) and (3-2) are merely a restatement of Ohm's law. The contribution of bound carriers due to the distortion of orbitals is not considered, since the latter is expected to be negligible for frequencies much smaller than resonance frequencies.

The validity of Ohm's law is thus restricted to slow time varying and relatively low amplitude electric fields. In the case of a high frequency optical electric field, the period of oscillation can become much shorter than the scattering times involved. This, combined with the fact that the field amplitude of the TEA CO_2 laser is extremely large, implies that in such a case it is no longer possible to assume band parabolicity and that the effective mass approximation breaks down.

In order to get an expression for the conductivity holding under more general conditions, an approach based on the solution of the generalized transport equation is required. In the next paragraphs, for the sake of clarity, we shall give a brief review of concepts in transport theory and discuss both the classical and quantum-mechanical approaches.

3.2 Statistical Description of Transport

In the standard , semi-classical description of free charge carriers in a semiconductor, all the quantum effects due to the rapidly changing potential of the lattice ions are merged into a single parameter, the effective mass. In general, this is a tensorial quantity, inversely proportional to the second order partial derivatives with respect to the wavenumber of the Bloch wave dispersion relation.

As long as the perturbing potentials, i.e. the externally applied fields are slowly varying with respect to the interatomic distances, they can be treated classically. As a consequence, by using the effective mass approximation, the transport problem can be considered to be entirely classical in nature, and full use can be made of classical statistical mechanics. The fundamental equation of the latter theory is the so-called Boltzmann equation, which expresses the conservation and the incompressibility of the phase space " fluid ". This fluid is composed of a large number of points, each representing one of the possible states of the system of charge carriers. The solution to Boltzmann's equation expresses the probability of having a given system in a given differential region of phase space. If one can solve this equation in the presence of an external perturbation, i.e. in presence of an electric field, the evaluation of conductivity becomes straightforward, since the current can be determined by an averaging process using Boltzmann function as a weighting factor.

We have seen previously that for large field intensities and high frequencies, the effective mass approximation is expected to break down. The transport problem must then be treated quantum-mechanically. The quantum analog to Boltzmann equation is called Liouville's equation and the analog to Boltzmann function has been given the name of density matrix. The procedure used to evaluate the current due to a perturbing electric field is similar to the classical one, except that the quantities which are manipulated are operators.

The density operator contains all of the statistical information required to evaluate the current density. Independently, however from the method of evaluation used, conductivity posseses some well known fundamental attributes that will now be discussed.

3.3 Time Invariance and Causality

3.3.1 Time Invariance

Time invariance expresses the fact that irrespective of the precise instant at which an arbitrary electrical excitation is applied, the response must be the same . In other words, a time-shifting of the excitation implies a corresponding time shifting of the response. Mathematically, this is expressed by writing

$$\text{If} \quad \vec{J}(t) = \Lambda \{ \vec{E}(t) \} \tag{3-3}$$

$$\text{Then} \quad \vec{J}(t-t_o) = \Lambda \{ \vec{E}(t-t_o) \} \tag{3-4}$$

where the symbol Λ stands for a functional operator characterizing the system; in our case the excitation is the applied electric field $\vec{E}$, and the current density $\vec{J}$ is the resulting response.

3.3.2 Causality

Causality expresses the fact that for any physical phenomenon the effect follows the cause. This might seem obvious, but it has profound mathematical consequences.

A function σ is said to be causal if

$$\sigma(t) = 0 \quad \text{for } t < 0 \tag{3-5}$$

For convenience, the application time of the excitation is assumed to be $t = 0$.

3.3.3 Mathematical Implications

It is well known from linear circuit theory that the most general time invariant and causal linear relationship between two scalar functions - say $J(t)$ and $E(t)$ - is provided by the convolution product

$$J(t) = \sigma(t) * E(t) \qquad (3\text{-}6)$$

or, more explicitely

$$J(t) = \int_{-\infty}^{t} \sigma(t-\tau)\, E(\tau)\, d\tau \qquad (3\text{-}7)$$

There is clearly, a priori no reason to expect a linear dependence of the current density with respect to the electric field. Moreover, for a non isotropic solid, relation (3-7) takes a tensorial form and, when generalized to include higher order terms with respect to the electric field, it takes the following form

$$\begin{aligned} J_i &= \int_{-\infty}^{t} \sigma_{ij}^{(1)}(t-\tau_1) E_j(\tau_1) d\tau_1 \\ &\quad + \int_{-\infty}^{t}\int_{-\infty}^{t} \sigma_{ijk}^{(2)}(t-\tau_1; t-\tau_2) E_j(\tau_1) E_k(\tau_2) d\tau_1 d\tau_2 + \ldots \\ &= J_i^{(1)}(t) + J_i^{(2)}(t) + J_i^{(3)}(t) + \ldots \end{aligned} \qquad (3\text{-}8)$$

$\sigma_{ij}^{(1)}$ and $\sigma_{ij}^{(2)}$ are the first and second order conductivity tensors components etc., and the Einstein's summation convention is used.

The various terms of the infinite series (3-8) are sometimes given the name of time-ordered products.

Equation (3-8) can be put into a very handy form by using Fourier transforms. For the purpose of this discussion, let us for example consider the second term in equation (3-8) and let us drop temporarily the tensorial description of this component.

Let the transform of the function E(t) be defined as

$$E(\omega) = \frac{1}{2\pi}\int_{-\infty}^{\infty} E(t)e^{j\omega t}\,dt \qquad (3\text{-}9)$$

and its inverse by

$$E(t) = \int_{-\infty}^{\infty} E(\omega)e^{-j\omega t}\,d\omega \qquad (3\text{-}10)$$

where ω is real.

Replacing the electric field by its transform we get

$$J^{(2)}(t) = \int_{-\infty}^{t}\int_{-\infty}^{t}\left[\int_{-\infty}^{\infty}\int_{-\infty}^{\infty} E(\omega_1)E(\omega_2)e^{-j\omega_1 t_1}e^{-j\omega_2 t_2}\,d\omega_1 d\omega_2\right] \times \sigma^{(2)}(t-t_1;t-t_2)\,dt_1 dt_2 \qquad (3\text{-}11)$$

Now let $t-t_1 = \tau_1$ and $t_1-t_2 = \tau_2$; then

$$J^{(2)}(t) = \int_{0}^{\infty}\int_{0}^{\infty}\left[\int_{-\infty}^{\infty}\int_{-\infty}^{\infty} E(\omega_1)E(\omega_2)e^{-j\omega_1 t}e^{j\omega_1\tau_1}e^{-j\omega_2 t}e^{j\omega_2\tau_2}\,d\omega_1 d\omega_2\right] \times \sigma^{(2)}(\tau_1,\tau_2)d\tau_1 d\tau_2 \qquad (3\text{-}12)$$

Interchanging the order of integration

$$J^{(2)}(t) = \int_{-\infty}^{\infty}\int_{-\infty}^{\infty}\left[\int_{-\infty}^{\infty}\int_{-\infty}^{\infty} \sigma^{(2)}(\tau_1,\tau_2)e^{j\omega_1\tau_1}\, e^{j\omega_2\tau_2}\, d\tau_1\, d\tau_2\right] E(\omega_1)E(\omega_2)$$
$$\times \quad e^{-j\omega_1 t}\, e^{-j\omega_2 t}\, d\omega_1 d\omega_2 \qquad (3\text{-}13)$$

Integrating over τ_1 and τ_2 and making use of the causality of $\sigma^{(2)}(\tau_1,\tau_2)$

$$J^{(2)}(t) = \int_{-\infty}^{\infty}\int_{-\infty}^{\infty} \sigma^{(2)}(\omega_1,\omega_2)\, E(\omega_1)E(\omega_2)\, e^{-j\omega_1 t}e^{-j\omega_2 t}\, d\omega_1 d\omega_2 \qquad (3\text{-}14)$$

where $\sigma^{(2)}(\omega_1,\omega_2)$ represents the two-dimensional Fourier transform of $\sigma(\tau_1,\tau_2)$.

We can now rewrite equation (3-8) in terms of Fourier transforms as well as reintroduce the tensorial notation to obtain the expression for the current density.

$$J_i(t) = \int_{-\infty}^{\infty} \sigma^{(1)}_{ij}(\omega_1)E_j(\omega_1)e^{-j\omega_1 t}\, d\omega_1 + \int_{-\infty}^{\infty}\int_{-\infty}^{\infty} \sigma^{(2)}_{ijk}(\omega_1,\omega_2)E_j(\omega_1)E_k(\omega_2)e^{-j\omega_1 t}e^{-j\omega_2 t}d\omega_1 d\omega_2 + \ldots \qquad (3\text{-}15)$$

which can also be put under the form

$$J_i(t) = \int_{-\infty}^{\infty} J_i^{(1)}(\omega_1)\, e^{-j\omega_1 t}\, d\omega_1 + \int_{-\infty}^{\infty}\int_{-\infty}^{\infty} J_i^{(2)}(\omega_1,\omega_2)\, e^{-j\omega_1 t}e^{-j\omega_2 t}\, d\omega_1 d\omega_2 \qquad (3\text{-}16)$$

where

$$J_i^{(n)}(\omega_1, \ldots, \omega_n) = \sigma_{i..n}^{(n)}(\omega_1, \ldots, \omega_n) E_1(\omega_1) \cdots E_n(\omega_n) \tag{3-17}$$

is the n^{th} order current density component Fourier transform.

It must therefore be observed that the usual concept of current being the product of a conductivity term with electric field components is valid only in the frequency domain.

3.4 Conclusion

From the treatment in this chapter it is important to realize that equations (3-16) and (3-17) express generally the current density as a response to the electric field excitation subject only to the conditions of time invariance and causality in the system and therefore they can account for contributions to the current density from all charge carriers, specifically from both bound and free carriers; thus $\sigma_n(\omega_1, \ldots, \omega_n)$ will be called the n^{th} order generalized conductivity.

CHAPTER IV

Quantum Mechanical Evaluation of the Second Order Generalized Conductivity

4.0 Introduction

We shall now evaluate the first and second order conductivity tensors as defined in the previous chapter by solving first quantum mechanically for the electronic charge carrier distribution perturbation in presence of an external electric field. In view of the fact that an exact solution of Liouville equation is not possible, an adaptation of Kubo's perturbational approach {24} is utilized. We shall then evaluate the current density resulting from this perturbation. The analysis is based on the work of Butcher and Mc Lean {21}, and a phenomenological relaxation constant has been introduced.

Before undertaking the derivation as such, and for the sake of convenience, we shall recall some results from potential theory and give a brief outline of some relevant concepts of statistical quantum theory.

4.1 Coulomb's Gauge

The analysis of electromagnetic fields is facilitated by auxiliary functions known as potentials. The starting point for the definition of the latter is provided by Maxwell's equations

$$\vec{\nabla} \times \vec{E} = -\partial \vec{B}/\partial t \qquad (4\text{-}1)$$

$$\vec{\nabla} \times \vec{H} = \vec{J} + \partial \vec{D}/\partial t \qquad (4\text{-}2)$$

$$\vec{\nabla} \cdot \vec{B} = 0 \qquad (4\text{-}3)$$

$$\vec{\nabla} \cdot \vec{D} = \rho \qquad (4\text{-}4)$$

According to (4-3), $\vec{B}$ is solenoidal and as a consequence can be expressed by the curl of another vector that we will call $\vec{A}_o$.

$$\vec{B} = \vec{\nabla} \times \vec{A}_o \qquad (4\text{-}5)$$

From vector analysis, it is well known that equation (4-5) does not define $\vec{A}_o$ uniquely. We could add to a given $\vec{A}_o$ the gradient of an arbitrary scalar function. Using Ψ to represent such an arbitrary function

$$\vec{A} = \vec{A}_o - \vec{\nabla} \Psi \qquad (4\text{-}6)$$

By replacing B in equation (4-7) by the curl of A as defined by equation (4-6) we obtain

$$\vec{\nabla} \times (\vec{E} + \partial\vec{A}/\partial t) = 0 \qquad (4\text{-}7)$$

This shows that $(\vec{E} + \partial\vec{A}/\partial t)$ is irrotational and can be expressed as the gradient of a scalar function $-\phi$.

$$\vec{E} = - \vec{\nabla} \phi - \partial\vec{A}/\partial t \qquad (4\text{-}8)$$

Since $\vec{A}$ is arbitrary up to a term $-\vec{\nabla}\Psi$, it is easy to see that ϕ is arbitrary up to a term $\partial\Psi/\partial t$. The arbitrariness that exists in the choice of $\vec{A}$ and is referred to as the invariance of the potential with respect to gauge transformations. It is sometimes convenient to choose the potentials in such a way that the scalar potential ϕ vanishes. We then say that the potentials are represented in Coulomb's gauge. Equation (4-8) becomes

$$\vec{E} = - \partial\vec{A}/\partial t \qquad (4\text{-}9)$$

that is

$$\vec{A}(t) = - \int_{-\infty}^{t} \vec{E}(t_1)\, dt_1 \qquad (4\text{-}10)$$

4.2 The Liouville Equation

Let us discuss in a more detailed fashion the mathematical formulation of the transport problem we have discussed earlier in very general terms (see section 3.2). We shall not discuss here the origin of Liouville's equation; the interested reader is referred to one of the texts treating of this problem, the classical reference beeing [25].

Explicitely, Liouville's equation reads

$$d/dt\ \{\rho(t)\} = (i\hbar)^{-1} \left[H, \rho(t)\right] \qquad (4\text{-}11)$$

H represents the total Hamiltonian operator of the system considered. $\rho(t)$ is the density operator and the bracket is the commutator of H and ρ. It is important to realize that this equation is an operator equation: its solution requires techniques somewhat different from those used in the solution of standard differential equations because of the non-commutability characterizing operators.

Classically, the analog of ρ, called the Boltzmann function f contains all of the statistical information and is used as the weighting factor in the averaging process relating microscopic to macroscopic parameters. The generalization of this averaging process to quantum mechanics is obtained by evaluating the trace of the density operator with the relevant quantum operator O.

$$< O > = Tr \{\rho O\} \qquad (4\text{-}12)$$

Since our objective is the determination of the current generated by the application of an electric field, it is clear that we will require to evaluate $\langle \vec{J} \rangle$, the average of the current density operator. This is the subject of the following paragraph.

4.3 The Current Density Operator

Fundamentally, the generalized current is the sum of the contributions from all moving charge carriers. In a crystal, the only moving carriers are electrons. Ions beeing heavy, their movement is neglected. Also, inter-electronic interaction is neglected, and hence our derivation deals only with one-particle operators.

To construct the current density operator $\vec{J}$, we start naturally from the elementary formula

$$\vec{J} = - e n \vec{v} \qquad (4\text{-}13)$$

where n is the <u>total</u> electronic density including both free and bound carriers, e is the elementary charge magnitude and $\vec{v}$ is a " velocity operator " . Velocity is usually defined in terms of the momentum operator

$$\vec{p} = \vec{p}_{mech} + e\vec{A} \qquad (4\text{-}14)$$

where

$$\vec{p}_{mech} = m\vec{v} \qquad (4\text{-}15)$$

is the mechanical contribution to the overall momentum and $e\vec{A}$ is due to the electromagnetic field and can be expressed in terms of the position operator and of the time.

Clearly, $\vec{p}_{mech}$, the mechanical component of the generalized momentum operator can be indirectly defined by writing

$$\vec{p}_{mech} = \vec{p} - e\vec{A} \qquad (4\text{-}17)$$

The current density is then, in operator form

$$\vec{J} = -\frac{n\,e(\vec{p} - e\vec{A})}{m} \qquad (4\text{-}18)$$

Refering to equation (4-12), we see that the macroscopic current density is given by

$$\langle \vec{J} \rangle = Tr\,\{\rho\vec{J}\} \qquad (4\text{-}19)$$

4.4 Second Order Conductivity

4.4.1 Outline of the Procedure

Because the mathematics are somewhat bulky, it seems necessary at this point to outline briefly the procedure that shall be followed to obtain an expression for the second order generalized conductivity.

(1) First, it is necessary to find an expression for the density operator in presence of an externally applied electric field. This will be done by using time-dependent perturbation theory.

(2) Second, from the knowledge of the density matrix, $\langle \vec{J} \rangle$, the observable current density will be obtained from an evaluation of $Tr\{\rho \vec{J}\}$.

(3) Third, since the previous steps are making use of the auxiliairy potential $\vec{A}$, $\vec{J}$ will depend implicitely on $\vec{E}$ through $\vec{A}$. It will be necessary to render this dependence explicit.

(4) Finally, the result will be put under the general form expressed by equations (3-16) and (3-17).

4.4.2 The Density Matrix Under Perturbation

A solution of Liouville's equation is in general, very difficult to obtain. For practical reasons, certain simplifying assumptions are required.

(1) As previously mentioned, it will be assumed that the one-electron approximation holds, that is, each electron sees an average potential due to all others.

(2) The period of oscillation of the very high optical frequency radiation is expected to be much shorter than all relaxation processes involved; consequently, the latter are not expected to play a significant role. However, relaxation will be explicitely accounted for by the introduction of a phenomenological time constant τ, which beside its physical significance, will be found to be extremely convenient in the mathematical manipulations.

(3) The wavelength of the optical excitations considered beeing much larger than the typical lattice periodicity, the vector potential $\vec{A}$ can be assumed to be constant at the lattice level i.e. this is a local theory.

Thus

$$\vec{B} = \vec{\nabla} \times \vec{A}(t) = 0 \qquad (4\text{-}20)$$

In other words, the effects due to the radiation magnetic field are neglected.

The single-electron Hamiltonian can now be written as

$$H = \frac{(\vec{p} + e\vec{A})^2}{2m} + V(\vec{r}) \qquad (4\text{-}21)$$

This can be expanded, taking into account the assumed independence of $\vec{A}$ on position coordinates.

$$H = \vec{p}^2 + V(\vec{r}) + e\vec{A}\cdot\vec{p} + e^2\vec{A}^2 \qquad (4\text{-}22)$$

$$= H_o + H_1 + H_2 \qquad (4\text{-}23)$$

where, for convenience, we have defined

$$H_o = \frac{\vec{p}^2}{2m} + V(\vec{r}) \qquad (4\text{-}24)$$

$$H_1 = \frac{e}{m}\vec{A}\cdot\vec{p} \qquad (4\text{-}25)$$

$$H_2 = \frac{e^2}{2m}\vec{A}^2(t) \qquad (4\text{-}26)$$

The time evolution of the density operator is governed by Liouville's equation. In order to account in the simplest manner for relaxation mechanisms which are not contained in our Hamiltonian, we shall use a well accepted phenomenologically modified form of Liouville's equation.

$$d/dt\{\rho(t)\} = (i\hbar)^{-1}\left[H,\rho\right] - \frac{(\rho - \rho_o)}{\tau} \qquad (4\text{-}27)$$

where ρ_o represents the density operator under thermodynamic equilibrium.

We note at once that the term H_2 commutes with the density matrix, beeing time-dependent only, and can be ignored as far as equation (4-27) is concerned.

Using the unitary operator

$$U(t) = e^{i/\hbar\, H_o t} \qquad (4\text{-}28)$$

we transform the density operator in the interaction picture and differentiate the result with respect to t.

$$d/dt\ \{U\ \rho U^{\dagger}\} = dU/dt\ \rho\ U^{\dagger} + U\ d\rho/dt\ U^{\dagger} + U\ \rho\ dU^{\dagger}/dt \qquad (4\text{-}29)$$

Using equation (4-27) to substitute for $d\rho/dt$ and equation (4-28) for U, it comes

$$d/dt\ \{U\ \rho\ U^{\dagger}\} = iH(U\rho U^{\dagger}) + (i\hbar)^{-1} U\left[H,\rho\right] U^{\dagger} + (i\hbar)^{-1}\ U\ (\rho - \rho_0)\ U^{\dagger} + U\rho U^{\dagger}\ (-iH_o/\hbar) \qquad (4\text{-}30)$$

We now expand the commutator $U\left[H,\rho\right]U^{\dagger}$

$$\begin{aligned} U\ [H,\rho]\ U^{\dagger} &= U\,H\,\rho\,U^{\dagger} - U\,\rho\,H\,U^{\dagger} \\ &= U\,H\,U^{\dagger}U\,\rho\,U^{\dagger} - U\,\rho\,U^{\dagger}U\,H\,U^{\dagger} \\ &= (H_o + H_1')\,\rho' - \rho'(H_o + H_1') \\ &= \left[H_o,\rho'\right] + \left[H_1',\rho'\right] \end{aligned} \qquad (4\text{-}31)$$

where the prime indicates that the operator is to be seen in the interaction picture. Inserting equation (4-31) into (4-30) we get

$$d/dt\ \rho' = (i\hbar)^{-1}\left[H_1',\rho'\right] - \frac{\{\rho' - \rho_o\}}{\tau} \qquad (4\text{-}32)$$

We now transform this result into an integral equation. This can be done using the Green function $G(t,t_1)$

$$\rho'(t) = \int_{-\infty}^{\infty} (i\hbar)^{-1}\left[H_1',\rho'(t_1)\right] + \frac{\rho_o}{\tau}\,G(t,t_1)\,dt_1 \qquad (4\text{-}33)$$

where $G(t,t_1)$ is given by

$$G(t,t_1) = \begin{cases} 0 & t < t_1 \\ e^{-(t-t_1)/\tau} & t > t_1 \end{cases} \qquad (4\text{-}34)$$

Since

$$\int \rho_o/\tau\ e^{-(t-t_1)/\tau}\,dt_1 = \rho_o$$

equation (4-33) becomes

$$\rho'(t) = \rho'_o + (i\hbar)^{-1} \int_{-\infty}^{t} \left[H'_1(t_1), \rho'(t_1) \right] \; e^{-(t-t_1)/\tau} \, dt_1 \tag{4-35}$$

This is a standard integral equation and it can be solved by iterations. For convenience, let us substitute δ for $1/\tau$. As a first guess for $\rho'(t)$, we use $\rho_o = \rho'_o$.

$$\rho'(t) \simeq \rho_o + (i\hbar)^{-1} \int_{-\infty}^{t} \left[H'_1(t_1), \rho_o \right] \; e^{-\delta(t-t_1)} \, dt_1 \tag{4-36}$$

Using this result as a second approximation, and substituting again into equation (4-35)

$$\rho'(t) \simeq \rho_o + (i\hbar)^{-1} \int_{-\infty}^{t} \left[H'_1(t_1), \rho_o \right] \; e^{-\delta(t-t_1)} \, dt_1 + (i\hbar)^{-2} \int_{-\infty}^{t} \int_{-\infty}^{t_1} \left[H'_1(t_1), \left[H'_1(t_2), \rho_o \right] \right] \; e^{-\delta(t-t_1)} e^{-\delta(t_1-t_2)} \tag{4-37}$$

This procedure could be extended up to an arbitrary n^{th} order. For the purpose of this work, we shall not go beyond second order.

Going back to Schroedinger's picture:

$$\rho(t) = \rho_o + (i\hbar)^{-1} \int_{-\infty}^{t} U^{\dagger} \left[H'_1(t_1), \rho_o \right] U \; e^{-\delta(t-t_1)} \, dt_1 + (i\hbar)^{-2} \int_{-\infty}^{t} \int_{-\infty}^{t_1} U^{\dagger} \left[H'_1(t_1), \left[H'_1(t_2), \rho_o \right] \right] U \; e^{-\delta(t-t_1)} e^{-\delta(t_1-t_2)} dt_1 dt_2 \tag{4-38}$$

The integrands may be expressed more explicitly . Thus, for the first of them

$$U^{\dagger}\left[H_1'(t_1),\rho_o\right]U = \left[U^{\dagger}H_1'(t_1)\,U,\rho_o\right] \qquad (4\text{-}39)$$

Using equation (4-28)

$$U^{\dagger}(t)\,H_1'(t_1)\,U(t) = e^{-i/\hbar\, H_o(t-t_1)}H_1\, e^{i/\hbar\, H_o(t-t_1)} \qquad (4\text{-}40)$$

Substituting for H_1 from equation (4-25) leads to

$$U^{\dagger}\left[H_1'(t_1),\rho_o\right]U = e/m\, A_{\alpha}(t_1)\left[p_{\alpha}(t_1-t),\rho_o\right] \qquad (4\text{-}41)$$

where $p\,(t_1-t_2)$ is defined by

$$p_{\alpha}(t) = e^{i/\hbar\, H_o t}\, p_{\alpha}\, e^{-i/\hbar\, H_o t} \qquad (4\text{-}42)$$

and summation over the repeated index α is implied.

With the help of the substitutions

$$(t_1-t)\rightarrow t_1 \qquad (4\text{-}43)$$

$$(t_2-t)\rightarrow t_2 \qquad (4\text{-}44)$$

the same procedure applied to the second integral leads to

$$\rho(t) = \rho_o + (i\hbar)^{-1}(e/m)\int_{-\infty}^{0}\left[p_\alpha(t_1),\rho_o\right]A_\alpha(t+t_1)\,e^{\delta t_1}\,dt_1$$
$$+ (i\hbar)^{-2}(e/m)^2\int_{-\infty}^{0}\int_{-\infty}^{t_1}\left[p_\alpha(t_1),\left[p_\beta(t_2),\rho_o\right]\right]A_\alpha(t+t_1)A_\beta(t+t_2)e^{\delta t_1}e^{\delta(t_2-t_1)}dt_2dt_1 \qquad (4\text{-}45)$$

This represents the final form of our expression for the density operator.

4.4.3 Evaluation of the Observable Current Density

The macroscopic current density $\langle\vec{J}\rangle$ can now be found by evaluating

$$\langle\vec{J}\rangle = \mathrm{Tr}\{\rho\vec{J}\} \qquad (4\text{-}46)$$

where the operator $\vec{J}$ is defined by equation (4-18). Substituting (4-18) into (4-46), using the fact that $\vec{A}$ commutes with ρ and that $\mathrm{Tr}\{\rho\} = 1$, we obtain

$$\langle\vec{J}\rangle = -(e/m)\,n\,\mathrm{Tr}\{\rho\vec{p}\} - e^2n/m\,\vec{A} \qquad (4\text{-}47)$$

It must be noted once more that in this expression, while $\vec{p}$ is the momentum operator, n represents the <u>total</u> density of electrons per unit volume and should not be confused with n representing the free carrier density utilized in a simple description of current density.

4.4.4 Explicit Expression of the Dependence on the Electric Field

Expression (4-47) depends implicitely on the electric field through the vector potential $\vec{A}$. An explicit expression of $\vec{E}(t)$ could be obtained using equation (4-11). However, we shall transform (4-47) directly into the form of equations (3-16) and (3-17). This will be done by noting that

$$A(t+t_1) = \int_{-\infty}^{(t+t_1)}\int_{-\infty}^{\infty}E_\alpha(\omega_1)\,e^{-i\omega_1}\,d\omega_1 d\tau \qquad (4\text{-}48)$$

4.4.4 Explicit Expression of the Dependence on the Electric Field

Equation (4-47) depends implicitly on the electric field through the vector potential $\vec{A}$. An explicit expression in terms of $\vec{E}(t)$ could be obtained using equation (4-11). However, we shall transform (4-47) directly into the form of equations (3-16) and (3-17). This will be done by noting that

$$A_\alpha (t+t_1) = \int_{-\infty}^{(t+t_1)} \int_{-\infty}^{\infty} E_\alpha(\omega_1)\, e^{-j\omega_1 \tau}\, d\omega_1 d\tau \qquad (4\text{-}48)$$

By straighforward manipulations of (4-47) after substituting equation (4-45) for ρ and expressing the vector potential explicitly in terms of the Fourier transform of the field, one gets

$$\sigma^{(1)}_{\mu\alpha}(\omega_1) = \frac{je^2 n}{m\omega}\,\delta_{\mu\alpha} + \frac{e^2 n}{\hbar\omega_1} \int_{-\infty}^{0} \mathrm{Tr}\{ [p_\alpha(t_1), \rho_o] p_\mu \}\, e^{-j\omega_1 t_1}\, e^{\delta t_1}\, dt_1 \qquad (4\text{-}49)$$

$$\sigma^{(2)}_{\mu\alpha\beta}(\omega_1,\omega_2) = \frac{-e^3 n}{\hbar^2 \omega_1 \omega_2 m^3} \times \int_{-\infty}^{0} \int_{-\infty}^{t_1} \mathrm{Tr}\{ [p_\alpha(t_1), [p_\beta(t_2), \rho_o]\, p_\mu \}\, e^{-j\omega_1 t_1}\, e^{-j(\omega_2 + j\delta)t_2}\, dt_2 dt_1 \qquad (4\text{-}50)$$

Equations (4-49) and (4-50) can be put under a more suggestive form by evaluating the trace in the unperturbed energy representation. Before proceeding to the evaluation as such, ρ_o can be taken out of the commutators by expanding the quantum-mechanical brackets and using the cyclic property of the trace. This leads to the following results

$$\mathrm{Tr}\{\left[p_\alpha(t_1),\rho_o\right]\ p_\mu\} = \mathrm{Tr}\{\rho_o\left[p_\mu,p_\alpha(t_1)\right]\} \qquad (4\text{-}51)$$

$$\mathrm{Tr}\{\left[p_\alpha(t_1),\left[p_\beta(t_2),\rho_o\right]\right]p_\mu \quad \mathrm{Tr}\ \rho_o\left[\left[p_\mu,p_\alpha(t_1)\right],p_\beta(t_2)\right] \qquad (4\text{-}52)$$

The left hand side of equation (4-51) can be written using Dirac's notation $|k\rangle$ for the electronic states in the unperturbed energy representation and using the convention of summation over repeated indices.

$$\mathrm{Tr}\{\rho_o\left[p_\mu,p_\alpha(t_1)\right] = \langle k|\rho_o|l\rangle\langle l|p_\mu|m\rangle\langle m|p_\alpha(t_1)|k\rangle$$
$$= -\langle k|\rho_o|l\rangle\langle l|p_\alpha(t_1)|m\rangle\langle m|p_\mu|k\rangle \qquad (4\text{-}53)$$

Recall that ρ_o represents the equilibrium value of the density operator. From Liouville's equation, it is seen that in order for $d\rho/dt$ to be constant, ρ has to be a function of the Hamiltonian operator. In the unperturbed energy representation, this means that the matrix elements $\langle k|\rho_o|l\rangle$ are diagonal.

In fact, it can be shown [25] that

$$\langle k|\rho_o|l\rangle = f(E_k)\delta_{kl} = f_k' \qquad (4\text{-}54)$$

where

$$f_k = \frac{1}{1 + \exp\frac{(E_k - E_F)}{kT}} \qquad (4\text{-}55)$$

is the Fermi-Dirac distribution function.

Using (4-54), equation (4-53) then becomes

$$\mathrm{Tr}\ \{\rho_o \left[p_\mu, p_\alpha(t_1)\right]\} = f_k \langle k|\left[p_\mu, p_\alpha(t_1)\right]|k\rangle \qquad (4\text{-}56)$$

using the same procedure, we obtain from (4-52)

$$\mathrm{Tr}\ \{\rho_o \left[\left[p_\mu, p_\alpha(t_1)\right], p_\beta(t_2)\right]\} = f_k \langle k|\left[\left[p_\mu, p_\alpha(t_1)\right], p_\beta(t_2)\right]|k\rangle \qquad (4\text{-}57)$$

In order to perform explicitely the integration with respect to t_1 and t_2 in relations (4-49) and (4-50), the dependent terms in (4-56) and (4-57) will be factored out. For a typical matrix element (4-58) shows the followed procedure

$$\langle k|p_\alpha(t_1)|l\rangle = \langle k|e^{it_1 H_o/\hbar} p_\alpha e^{-it_1 H_o/\hbar}|l\rangle$$

$$= \exp(it_1/\hbar\ (E_k - E_l))\ \langle k|p_\alpha|l\rangle \qquad (4\text{-}58)$$

Explicit integration with respect to t_1 and t_2 of (4-49) and (4-50) leads to

$$\sigma^{(1)}_{\mu\alpha}(\omega_1) = \frac{ien}{\omega_1 m} + \frac{ie^2 n_2}{\hbar\omega_1 m^2} f_1\left\{\frac{\langle 1|\mu|m\rangle\langle m|\alpha|1\rangle}{\omega_{1m}+\omega_1+i\delta} + \frac{\langle 1|\alpha|m\rangle\langle m|\mu|1\rangle}{\omega_{1m}-\omega_1-i\delta}\right\} \tag{4-59}$$

$$\sigma^{(2)}_{\mu\alpha\beta}(\omega_1,\omega_2) = -\frac{e^3 n}{\hbar^2\omega_1\omega_2 m^3} \times$$

$$\left[f_r \frac{\langle r|\beta|s\rangle\langle s|\alpha|t\rangle\langle t|\beta|r\rangle}{(\omega_{rs}+\omega_1+\omega_2+i\delta)(\omega_{rt}+\omega_2+i\delta)} + \right.$$

$$f_r \frac{\langle r|\beta|s\rangle\langle s|\mu|t\rangle\langle t|\alpha|r\rangle}{(\omega_{rs}-\omega_2-i\delta)(\omega_{st}+\omega_1+\omega_2+i\delta)} + f_r \frac{\langle r|\alpha|s\rangle\langle s|\mu|t\rangle\langle t|\beta|r\rangle}{(\omega_{rt}+\omega_2+i\delta)(\omega_{ts}-\omega_1-\omega_2-i\delta)} +$$

$$\left. f_r \frac{\langle r|\beta|s\rangle\langle s|\alpha|t\rangle\langle t|\mu|r\rangle}{(\omega_{rs}-\omega_2-i\delta)(\omega_{rt}-\omega_1-\omega_2-i\delta)} \right] \tag{4-60}$$

where $\langle 1|\mu|m\rangle$ is used as a short hand for $\langle 1|p_\mu|m\rangle$ and ω_{1m} represents $(\omega_1 - \omega_m) = (E_1 - E_m)/\hbar$.

4.4.5 Symmetrization with Respect to Permutations in the Field Components

As it has been mentioned earlier (see chapter III) $\sigma_{\mu\alpha\beta}(\omega_1,\omega_2)$ can be put under a symmetric form with respect to permutations of $\{\alpha,\omega_1\}$, $\{\alpha,\omega_2\}$, to reflect the fact that the permutations of the electric field components are immaterial. This can be achieved by summing (4-60) over permutations of $\{\alpha,\omega_1\}$, $\{\alpha,\omega_2\}$ and dividing by their total number. We shall use the following shorthand notation

$$\sigma_{\mu\alpha\beta} \rightarrow 1/2 \sum_P P(\alpha\omega_1,\beta\omega_2)\,\sigma^{(2)}_{\mu\alpha\beta}(\omega_1,\omega_2) \tag{4-61}$$

4.4.6 Low Frequency Limit

In order to be able to interpret physically the implications of the expressions (4-59) and (4-60) it will be useful at this stage to consider the low frequency limit of the latter as discussed by Butcher {21}.

The results (4-59) and (4-60) can be expressed in terms of partial derivatives with respect to the wavevector of the Bloch wave dispersion relation. It has been shown by Kane {26} that the coefficients of the Taylor series expansion of the band energy $E_n(\vec{k})$ about an arbitrary value of the wavevector $\vec{k}$ can be related to the complicated sums of momentum matrix elements products of equations (4-59) and (4-60) in the limit where $\omega \to 0$. The coefficients of the Taylor series are defined by

$$E_n(\vec{k}+\vec{q}) = E_n(\vec{k}) \sum_{r=0}^{\infty} E^{(r+1)}_{\mu\alpha_1\cdots\alpha_r}(n,\vec{k}) q_\mu q_\alpha \cdots q_{\alpha_r} \qquad (4\text{-}62)$$

where, for example

$$E^{(2)}_{\mu\alpha\beta} = 1/3! \frac{\partial E_n(\vec{k})}{\partial k_\mu \partial k_\alpha \partial k_\beta} \qquad (4\text{-}63)$$

Kane has shown that

$$E^{(2)}_{\mu\alpha}(n,\vec{k}) = \hbar/2m^2 \frac{\langle n|\mu|m\rangle\langle m|\alpha|n\rangle}{\omega_{nm}} + \frac{\langle r|\alpha|m\rangle\langle m|\mu|n\rangle}{\omega_{nm}} + \hbar^2/2m\ \delta_{\mu\alpha} \qquad (4\text{-}64)$$

Comparing with equation (4-59), one can conclude by inspection that

$$\sigma_{\substack{\mu\alpha(\omega_1) \\ \omega\to 0}} = \frac{2ie^2 n}{\omega_1 \hbar^2} \sum_{n,\vec{k}} f_{n\vec{k}} E^{(2)}_{\mu\alpha}(n,\vec{k}) \qquad (4\text{-}65)$$

A result similar to (4-64) holds for $E^{(3)}$ and leads to

$$\sigma^{(2)}_{\substack{\mu\alpha\beta(\omega_1,\omega_2) \\ \omega_1\to 0 \\ \omega_2\to 0}} = \frac{3e^3 n}{\omega_1\omega_2 \hbar^3} \sum_{n,\vec{k}} f_{n\vec{k}} E^{(2)}_{\mu\alpha\beta}(n,\vec{k}) \qquad (4\text{-}66)$$

Equations (4-65) and (4-66) are very important as they permit to interpret the general results (4-59) and (4-60) in terms of a semi-classical picture, as we shall see in the next chapter.

Note that (4-65) and (4-66) are divergent. This is perfectly conform with the hypothesis of adiabaticity . A field with a vanishing frequency is a DC field, and in the absence of any relaxation mechanism, it is normal for the current to grow without limit.

4.5 Conclusion

By using time-dependent perturbation theory, we have obtained very general expressions for the first and second order conductivities. In the limit of low frequencies the latter are expressible in terms of the familiar Bloch wave dispersion relation with respect to the wavevector components. The next step shall be to evaluate explicitely the optical rectification effect resulting from the presence of the second order conductivity component $\sigma^{(2)}_{ijk}(\omega_1,\omega_2)$ at optical frequencies.

CHAPTER V

Optical Rectification

5.0 Introduction

We have already discussed in chapter II how the presence of a quadratic component in the conductivity of a material could be responsible for a rectification effect. We shall now evaluate formally the expected magnitude of the latter in terms of $\sigma^{(2)}_{\mu\alpha\beta}(\omega_1,\omega_2)$. It will be shown that the result obtained is strictly identical to the result obtained by von Baltz [27] who did not recognize the connection of his work with the existing discussions of generalized conductivity. We shall then discuss the physical significance of the results.

5.1 Origin of Optical Rectification

Let us assume the incident electric field to be of the form

$$\vec{E}(t) = \vec{E}_o(t)\cos(\omega t) \qquad (5\text{-}1)$$

where $E_o(t)$ represents a slowly varying function of time while ω corresponds to a high frequency. A laser pulse electric field would be represented by such an expression . The current density component along a given direction can be expressed as follows

$$J(t) = \int_{-\infty}^{\infty} \sigma^{(1)}(\omega_1)E(\omega_1)d\omega_1 + \int_{-\infty}^{\infty}\int_{-\infty}^{\infty} \sigma^{(2)}(\omega_1,\omega_2)E(\omega_1)E(\omega_2)e^{-j\omega_1 t}e^{-j\omega_2 t}d\omega_1 d\omega_2 \qquad (5\text{-}2)$$

Since the tensorial character of the conductivity component is not relevant to the discussion, abstraction has been made of the tensor notation.

$E(\omega_1)$ is the Fourier transform of equation (5-1)

$$E(\omega_1) = 1/2\pi \int_{-\infty}^{\infty} E_o(t) \cos \omega t \, e^{-j\omega_1 t} \, dt \qquad (5-3)$$

Expressing $\cos \omega t$ in terms of complex exponentials, this equation can be integrated into

$$E(\omega_1) = 1/2 \{E_o(\omega_1+\omega) + E_o(\omega_1-\omega)\} \qquad (5-4)$$

Using this result, the second term of equation (5-2) becomes

$$J^{(2)}(t) = 1/4 \int_{-\infty}^{\infty}\int_{-\infty}^{\infty} \sigma^{(2)}(\omega_1,\omega_2) \{E_o(\omega_1+\omega)E_o(\omega_2+\omega) + E_o(\omega_1-\omega)E_o(\omega_2+\omega) + E_o(\omega_1 \omega)E_o(\omega_2-\omega) + E_o(\omega_1-\omega)E_o(\omega_2-\omega)\} e^{-j\omega_1 t} e^{-j\omega_2 t} d\omega_1 d\omega_2$$

If we assume that $E_o(\omega-\omega_o)$ occupies a very narrow spectral band centered at ω_o, in the limit it can be considered to become a δ function and $\sigma^{(2)}(\omega_1,\omega_2)$ can be pulled out of the integral.

$$J^{(2)}(t) = 1/4\, \sigma^{(2)}(-\omega,-\omega) \int_{-\infty}^{\infty}\int_{-\infty}^{\infty} E_o(\omega_1+\omega)E_o(\omega_2+\omega)\, e^{-j\omega_1 t} e^{-j\omega_2 t} \, d\omega_1 d\omega_2$$
$$+ 1/4\, \sigma^{(2)}(\omega,-\omega) \iint E_o(\omega_1-\omega)E_o(\omega_1+\omega)\, e^{-j\omega_1 t} e^{-j\omega_2 t} \, d\omega_1 d\omega_2$$
$$+ 1/4\, \sigma^{(2)}(-\omega,\omega) \iint E_o(\omega_1 \omega)E_o(\omega_1-\omega)\, e^{-j\omega_1 t} e^{-j\omega_2 t} \, d\omega_1 d\omega_2$$
$$+ 1/4\, \sigma^{(2)}(\omega,\omega) \iint E_o(\omega_1-\omega)E_o(\omega_2-\omega)\, e^{-j\omega_1 t} e^{-j\omega_2 t} \, d\omega_1 d\omega_2$$

$$= I_1' + I_2 + I_3 + I_4 \qquad (5\text{-}6)$$

The above integrals may be performed explicitely. For example, the first can be evaluated using the substitutions

$$(\omega_1 + \omega) \rightarrow \omega \qquad (5\text{-}7)$$

$$(\omega_2 + \omega) \rightarrow \omega' \qquad (5\text{-}8)$$

$$1/4\ \sigma^{(2)}(-\omega,-\omega)\int_{-\infty}^{\infty}\int_{-\infty}^{\infty} E_o(\omega)e^{j\omega t}\, E_o(\omega')e^{j\omega t}\, e^{-j\omega t}e^{-j\omega' t}\, d\omega d\omega'$$

$$= 1/4\ {}^{(2)}(-\omega,-\omega)\ e^{2j\omega t} E_o^2(t) \qquad (5\text{-}9)$$

Equation (5-6) becomes

$$J^{(2)}(t) = 1/4\{\sigma^{(2)}(-\omega,-\omega)\ e^{2j\omega t} + \sigma^{(2)}(\omega,\omega)e^{-2j\omega t}\}\ E_o^2(t)$$

$$+ 1/4\{\sigma^{(2)}(-\omega,\omega) + \sigma^{(2)}(\omega,-\omega)\}\ E_o^2(t) \qquad (5\text{-}10)$$

Now using the identity

$$\sigma^*(\omega_1,\omega_2) = \sigma(-\omega_1,-\omega_2) \qquad (5\text{-}11)$$

we obtain, finally

$$J^{(2)}(t) = 1/2\ \sigma^{(2)}(\omega,\omega)\ \cos(2\omega_o t)\ E_o^2(t)$$

$$+ 1/2\ \mathrm{Re}\{\sigma^{(2)}(\omega,-\omega)\}\ E_o^2(t) \qquad (5\text{-}12)$$

The second term of this equation shows that when $E_o(t)$ is a slowly varying function of t, there will be an observable current proportional to the power of the incident signal.

5.2 Formal Evaluation of the Rectification Coefficient

From equations (4-60) and (4-61) and the result we obtained in the last section, it is possible to obtain a quantum-mechanical formal expression for the rectification coefficient.

Initially, in order to simplify the mathematical form of the expressions, we shall consider the particular case when the incoming radiation is polarized along one of the coordinate axes. This is equivalent to set $\alpha = \beta$. It has the advantage of rendering equation (4-60) symmetric, eliminating the need for further symmetrization, as described in section 4.4.5. We thus get from equation (4-60)

$$\sigma^{(2)}_{\mu\alpha\alpha}(\omega,-\omega) = -\frac{e^3 n}{\hbar^2 \omega^2 m^3} \quad X$$

$$\Bigg[f_r \frac{\langle r|\mu|s\rangle\langle s|\alpha|t\rangle\langle t|\alpha|r\rangle}{(\omega_{rs}+i\delta)(\omega_{rt}-\omega+i\delta)} + f_r \frac{\langle r|\alpha|s\rangle\langle s|\mu|t\rangle\langle t|\alpha|r\rangle}{(\omega_{rs}+\omega+i\delta)(\omega_{st}+i\delta)} + f_r \frac{\langle r|\alpha|s\rangle\langle s|\mu|t\rangle\langle t|\alpha|r\rangle}{(\omega_{rt}-\omega+i\delta)(\omega_{ts}-i\delta)} + f_r \frac{\langle r|\alpha|s\rangle\langle s|\alpha|t\rangle\langle t|\mu|r\rangle}{(\omega_{rs}+\omega-i\delta)(\omega_{rt}-i\delta)} \Bigg] \qquad (5\text{-}13)$$

It is clear that this term represents the optical rectification effect which will be evaluated and discussed in details in the subsequent sections of this thesis.

The complex conjugate for the latter is

$$\sigma^{(2)*}_{\mu\alpha\alpha}(\omega,-\omega) = \sigma^{(2)}_{\mu\alpha\alpha}(-\omega,\omega)$$

hence

$$1/2 \ \mathrm{Re}\{\sigma^{(2)}_{\mu\alpha\alpha}(-\omega,\omega)\} =$$

$$-\frac{e^3 n}{4\hbar^2\omega^2} \sum_{\Omega=\pm\omega}$$

$$\left[f_r \frac{\langle r|\mu|s\rangle\langle s|\alpha|t\rangle\langle t|\alpha|r\rangle}{(\omega_{rs}+i\delta)(\omega_{rt}-\Omega+i\delta)} \right.$$

$$f_r \frac{\langle r|\alpha|s\rangle\langle s|\mu|t\rangle\langle t|\alpha|r\rangle}{(\omega_{rs}+\Omega-i\delta)(\omega_{st}+i\delta)} + f_r \frac{\langle r|\alpha|s\rangle\langle s|\mu|t\rangle\langle t|\alpha|r\rangle}{(\omega_{rt}-\Omega+i\delta)(\omega_{ts}-i\delta)} +$$

$$\left. f_r \frac{\langle r|\alpha|s\rangle\langle s|\alpha|t\rangle\langle t|\mu|r\rangle}{(\omega_{rs}+\Omega-i\delta)(\omega_{rt}-i\delta)} \right] \qquad (5\text{-}14)$$

This result can be put under the more compact form

$$-\frac{e^3 n}{4\hbar^2 m^3} \sum_{\Omega=\pm\omega} \frac{(f_r-f_s)\langle r|\alpha|s\rangle}{(\omega_{rs}-\Omega-i\delta)} \left\{ \frac{\langle s|\alpha|t\rangle\langle t|\mu|r\rangle}{(\omega_{rt}-i\delta)} - \frac{\langle s|\mu|t\rangle\langle t|\alpha|r\rangle}{(\omega_{ts}-i\delta)} \right\}$$

(5-15)

Note that this is strictly identical with equation (25) of reference {27}. It has however been obtained directly from the premises of Butcher's generalized conductivity concept. von Baltz, on the other hand, in reference {27} and his later publications {23,28} believes having identified a novel photovoltaic effect.

This point must therefore be rectified and von Baltz's bulk photovoltaic effect must be recognized to be merely the result of the presence of second order generalized conductivity in a material.

By a procedure similar to that leading to equation (5-15) where the steps are distinctly more tedious since the equivalent of equation (5-13) would contain eight terms, it can be shown that in the general case where $\alpha \neq \beta$ {23}

$$\chi_{\mu\alpha\beta} = -\frac{e^3 n}{16\pi^3 \hbar^2 \omega^3 m^3} \operatorname{Re}\left\{ \sum_{\Omega=\pm\omega} \int_{\substack{\text{Brillouin}\\ \text{Zone}}} (f_l - f_n) \frac{\langle n,\vec{k}|\vec{e}\cdot\vec{p}|l,\vec{k}\rangle\langle l,\vec{k}|\vec{e}\cdot\vec{p}|m,\vec{k}\rangle\langle m,\vec{k}|\vec{p}|n,\vec{k}\rangle d^3k}{(\omega_{nm} - i\delta)(\omega_{nl} + \hbar\Omega - i\delta)} \right\} \quad (5\text{-}16)$$

where the sum over wavevector and spin has been replaced by an integration over the first Brillouin zone according to

$$\sum_{k,s} \cdots = 2 \cdot 1/(2\pi)^3 \int d^3k \quad (5\text{-}17)$$

$\vec{p}$ represents the momentum operator and $\vec{e}$ is the unit electric polarization vector.

From the properties of Bloch functions, it is possible to verify that (5-16) would indeed be zero for a crystal with a center of symmetry as required from macroscopic considerations for a property represented by an odd-rank tensor.

5.3 Discussion

Clearly, relation (5-16) is extremely complicated if not impossible to be evaluated explicitly in the case of Tellurium since, as it stands, it would require an explicit knowledge of the momentum matrix elements.

However, since expression (5-16) exhibits explicit singularities at preferred frequencies, it is expected that valuable information can be extracted from the latter by discussing its behaviour as a function of the frequency ω of the incident radiation.

5.3.1 Photon Frequencies Inferior to all Possible Interband Transition Frequencies

If we assume that the incident electric field has a frequency such that the energy of the associated photons is inferior to all of the interband and sub-band transition frequencies, in other words if

$$\omega \ll \omega_{nm} = \frac{E_n - E_m}{\hbar} \qquad (5\text{-}21)$$

one can neglect ω in the denominator. Assuming a large relaxation time, i.e. a small value of δ, the situation becomes mathematically equivalent with the case of vanishing frequency. We have seen in paragraph 4.4.5 that in that case

$$\sigma^{(2)}_{\mu\alpha\beta}(\omega_1,\omega_2) = \frac{3e^3 n}{\omega_1\omega_2\hbar^3} \sum_{n,k} f_{n\vec{k}}\, E^{(2)}_{\mu\alpha\beta}(n,\vec{k}) \qquad (5\text{-}22)$$

where

$$E^{(2)}_{\mu\alpha\beta} = 1/3! \quad \frac{\partial E_n(\vec{k})}{\partial k_\mu \partial k_\alpha \partial k_\beta} \qquad (5\text{-}23)$$

But, a consequence of the time reversal invariance of the unperturbed Hamiltonian is Kramer's theorem {29}

$$E_n(\vec{k}) = E_n(-\vec{k}) \qquad (5\text{-}24)$$

This implies that all odd order partials are odd functions of the wave vector $\vec{k}$. Since $f_{n\vec{k}}$, the Fermi function, is an even function of the latter (beeing a function of the energy only), one can conclude that

$$\sigma^{(2)}_{\mu\alpha\beta}(\omega_1,\omega_2) = 0 \qquad (5\text{-}25)$$

But, we have shown that the optical rectification tensor is expected to be given by

$$\chi^{(2)}_{\mu\alpha\beta} = 1/2\ \mathrm{Re}\{\sigma^{(2)}_{\mu\alpha\beta}(\omega_1=-\omega,\omega_2=\omega\ \} \qquad (5\text{-}26)$$

Hence

$$\chi_{\mu\alpha\beta} = 0 \qquad (5\text{-}27)$$

5.3.1.1 Semi-Classical Interpretation of the Preceeding Result

The result we have just obtained can be interpreted in terms of the semi-classical model which considers the electrons in a solid as quasi-particles with an effective mass tensor $m^*_{\mu\beta}$ specified by

$$\left(\frac{1}{m^*}\right)_{\mu\beta} = (1/\hbar^2)\ \frac{\partial^2 E(\vec{k})}{\partial k_\mu \partial k_\beta} \qquad (5\text{-}28)$$

(a) first order conductivity

Let us first discuss the meaning of equation (4-65) which describes the first order conductivity. Recall that within the adiabatic approximation, no energy is transfered to the lattice, or equivalently, scattering is non-existent. Therefore, in a infinitesimal time interval dt, an electric field increases the velocity of an electron within a given band by an amount

$$d\vec{v} = -\frac{e\vec{E}}{m^*}\,dt \qquad (5\text{-}29)$$

where m* represents the effective mass tensor in the direction of the field. If we assume that while the electron is moving its mass does not vary appreciably (a first order approximation), the total velocity change will be

$$\Delta\vec{v} = -\int_0 \frac{e\vec{E}}{m^*}\,dt \qquad (5\text{-}30)$$

In the frequency domain, this becomes

$$\Delta\vec{v}(\omega_1) = \frac{j\,e}{\omega_1 \hbar\, m^*}\,\vec{E}(\omega_1) \qquad (5\text{-}31)$$

If there are n electrons per unit volume the first order conductivity can be obtained by analogy with the elementary vector equation

$$\sigma^{(1)}(\omega_1)\,\vec{E}(\omega_1) = n\,e\,\vec{v}(\omega_1) \qquad (5\text{-}32)$$

Hence

$$\sigma^{(1)}(\omega_1) = \frac{j\,e^2\,n}{\omega_1 \hbar\, m^*} \qquad (5\text{-}33)$$

And, for a field oriented in an arbitrary direction

$$\sigma^{(1)}_{\mu\alpha}(\omega_1) = \frac{j\,e^2\,n}{\omega_1 \hbar}\,\{1/m^*\}_{\mu\alpha} \qquad (5\text{-}34)$$

Substituting (5-28) into this result, we get

$$\sigma^{(1)}_{\mu\alpha}(\omega_1) = \frac{j\,e^2\,n}{\omega_1 \hbar}\,\frac{\partial^2 E_n(\vec{k})}{\partial k_\mu\, \partial k_\alpha} \qquad (5\text{-}30)$$

This is almost similar to equation (4-65) except for the absence of the Fermi function as a weighting factor; we can introduce this aspect by noting that in our derivation we have implicitely assumed that all of the electrons were occupying the same position within the band structure, which is obviously not true.

In fact, the probability for an electron to occupy the position defined by $E_n(k)$ is given by the Fermi function, and equation (5-30) must be modified accordingly. Hence

$$\sigma^{(1)}_{\mu\alpha}(\omega_1) = \frac{j e^2 \hbar}{\omega_1} \sum_{n,\vec{k}} f_{n\vec{k}} \frac{\partial^2 E_n(\vec{k})}{\partial k_\mu \partial k_\alpha} \quad (5\text{-}31)$$

and we find a result strictly identical with (4-65).

It is well known that in expression (5-31) only partially filled bands will contribute to the total value of the sum; hence, the summation over the band index n is to be performed only over partially filled bands. To the first order, the theory is thus seen to be in perfect agreement with the semi-classical theory of electrons and holes.

(b) Second order conductivity

We are now in a position to examine the significance of equation (4-66). We have assumed in the foregoing paragraph that, to the first order the mass of an electron occupying a position $\vec{k}$ in the band structure was not modified while it was slightly shifted by an amount $\vec{\Delta k}$ under the action of an external perturbing field $\vec{E}$. To the second order, this mass does change and to the first order, this change is proportional to the first order derivative of the effective mass with respect to the wavevector. Hence, it is natural that $\sigma^{(2)}(\omega_1, \omega_2)$ depends on the third order derivatives of $\vec{E}_n(\vec{k})$.

Therefore, as long as hypothesis (5-21) holds, one can see that $\sigma^{(2)}(\omega_1, \omega_2)$ results from a first order dependence of the band curvature with respect to the wavevector. This result, obtained from semi-classical considerations is identical to the one obtained from the general quantum-mechanical approach of chapter IV.

Consequently, based on Kramers' theorem {29}, $\sigma^{(2)}(\omega_1,\omega_2)$ will be identically zero. This fact has escaped the attention of many workers such as {11} who attributed erroneously a second order component to the conductivity of electrons in non-parabolic bands.

5.3.2 Photon Frequencies Comparable with Interband and Sub-Band Transition Frequencies

When the photon energy is comparable to interband energies, the singularities in relation (4-60) and (5-16) play a major role and therefore expression (4-66) cannot be used anymore. Moreover, in the vicinity of a singularity, it is clear that the precise numerical value of δ, which was phenomenologically introduced to take into account the presence of a relaxation mechanism becomes determinant.

Although at this stage it is found to be practically impossible to evaluate explicitely expression (4-66) in the neighbourhood of a singularity due to its extreme complexity, we will however discuss its physical significance.

Let us recall from chapter IV that the observable current density has been found by evaluating

$$\langle \vec{J} \rangle = \mathrm{Tr}\{\rho \vec{J}\} \qquad (5\text{-}35)$$

where ρ and $\vec{J}$ are operators given by matrices in the unperturbed energy representation; these matrices are of infinite dimensionality since there is an infinite number of basis vectors in that representation. However, for the sake of clarity, let us assume that we are dealing with a two-dimensional space. Then

$$\rho\vec{J} = \begin{pmatrix} \rho_{11} & \rho_{12} \\ \rho_{21} & \rho_{22} \end{pmatrix} \begin{pmatrix} \vec{J}_{11} & \vec{J}_{12} \\ \vec{J}_{21} & \vec{J}_{22} \end{pmatrix} =$$

$$\begin{pmatrix} (\rho_{11}\vec{J}_{11} + \rho_{12}\vec{J}_{21}) & (\rho_{11}\vec{J}_{12} + \rho_{12}\vec{J}_{22}) \\ (\rho_{21}\vec{J}_{11} + \rho_{22}\vec{J}_{21}) & (\rho_{21}\vec{J}_{12} + \rho_{22}\vec{J}_{22}) \end{pmatrix} \qquad (5\text{-}36)$$

and

$$\langle \vec{J} \rangle = \mathrm{Tr}\{\rho\vec{J}\} = \rho_{11}\vec{J}_{11} + \rho_{12}\vec{J}_{21} + \rho_{21}\vec{J}_{12} + \rho_{22}\vec{J}_{22}$$

$$= \rho_{11}\vec{J}_{11} + \rho_{22}\vec{J}_{22} + (\rho_{12}\vec{J}_{21} + \rho_{21}\vec{J}_{12}) \qquad (5\text{-}37)$$

We note the presence of two different kinds of terms in the preceeding result, i.e. terms involving real diagonal elements of ρ and $\vec{J}$ and terms involving complex conjugate non-diagonal elements.

A diagonal element of $\vec{J}$ represents the observable current density associated with the corresponding Bloch function. For example, $\vec{J}_{11} = \langle 1|\vec{J}|1\rangle$ is the current density associated with the state $|1\rangle$. As for ρ_{11}, it merely expresses the relative importance of this particular eigenstate with respect to the overall average quantum state of the system.

The case of the non-diagonal elements is slightly more complicated. First, it must be noted that non-diagonal elements ρ_{12} and ρ_{21} correspond to the probability of transition between states $|1\rangle$ and $|2\rangle$.

On the other hand, non-diagonal current density matrix elements represent the current associated with such a transition. Finally, in relation (5-37), the terms in parentheses must be considered as a whole since the observed current is a real quantity.

When photon frequencies correspond to interband or sub-band transition frequencies, it is clear that diagonal elements of the density matrix become important. If the corresponding diagonal elements of the current density do not vanish identically by symmetry, it must be noted that there will be a contribution to the overall current density.

The fact that there is a current associated with the presence of an electron in a particular state in $\vec{k}$-space is a familiar notion. The significance of the existence of a current when an electron undergoes a transition from one state to another is more difficult to interpret.

When a transition occurs, there is an induced dipole moment, i.e. a change may take place in the position of the center of gravity of the electronic charge with respect to that of the rigid lattice of positive ions. This induced dipole moment is expected to follow in a specific manner to be determined the exciting field and, in view of the variation of the latter an alternating current is generated since

$$\vec{J} = \partial\vec{P}/\partial t \qquad (5\text{-}38)$$

Relation (5-38) makes it easy to understand why the first order conductivity as expressed by (4-59) becomes very large when the optical frequency corresponds to a transition frequency. This merely means that if the atoms are considered like small charged oscillators, the electric field oscillates at a characteristic resonance frequency, generating an oscillating current of a large amplitude. Experimentally, one observes for such a frequency a marked increase in the absorption, in agreement with this simplist picture.

Moreover, it is to be noted that when $\omega_1 = \omega_{\ell m}$ the first part of the second term in expression (4-59) may be neglected with respect to the second. This term is observed to be real and therefore represents a component of the current in phase with the electric field which is the condition for real electric power absorption.

As for the second order conductivity, the polarization model can be used to explain second harmonic generation {30}, which is closely related to the high frequency component of the current which has been discarded in equation (5-12).

The DC rectified current component would appear at first sight to be explainable trough this same polarization model; however, a close examination leads to serious difficulties as discussed below.

5.3.2.1 Characteristics of Rectified Current Resulting from the Polarization Model

the non-linear oscillator model

Although it constitutes a very simplified model, the one-dimensional non-linear oscillator provides a good qualitative insight to the non-linear interaction of the electrons with the electric field. Indeed, it has been used by Bloembergen {31} to discuss the non-linear optical susceptibility and by Garrett and Robinson {32} to derive an expression for the one-dimensional non-linear coefficient. The model assumes that the electronic response to a driving electric field can be simulated by that of an electron in an anharmonic potential well. The equation of motion is

$$\ddot{x} + \gamma\dot{x} + \omega_o^2 x + dx^2 = -\frac{e\,E(t)}{m} \qquad (5\text{-}39)$$

where x is the deviation from the potential minimum, mdx^2 is the anharmonic restoring force, $-eE(t)$ is the driving force due to the optical field and $m\gamma\dot{x}$ is a phenomenological damping term. The dipole moment is given by

$$p(t) = e\,x(t) \qquad (5\text{-}40)$$

(a) Frequency Inferior to Transition Frequency: the Case of Dielectrics

When the frequency of the exciting field is smaller than the transition or resonance frequency, both the inertial and the damping forces can be neglected. Then

$$\omega_o^2 x + bx^2 = -\frac{eE(t)}{m} \qquad (5\text{-}41)$$

Using the fact that

$$(1 + y)^{\frac{1}{2}} \approx 1 + y/2 + y^2/8 + \ldots \qquad (5\text{-}42)$$

we get

$$x(t) = -\frac{eE(t)}{m\omega_o^2} - \frac{be^2E^2(t)}{m^2\omega_o^6} \qquad (5\text{-}43)$$

Because of the presence of a term quadratic in the field, x is seen to have a non-zero average value and as a consequence there exists a non-zero average dipole moment.

Now, if

$$E(t) = E_o(t) \cos \omega_o t \qquad (5\text{-}44)$$

where $E_o(t)$ is a slowly varying function of the time t

$$x(t) \simeq - \frac{eE_o(t) \cos \omega_o t}{m \omega_o^2} - \frac{b e^2 E_o^2(t)}{2 m^2 \omega_o^6} (1 - \sin 2\omega_o t) \qquad (5\text{-}45)$$

The observable " slow " current will be proportional to the time derivative of the slow component of the polarization.

$$J = e \, dx/dt = - \frac{b e^2}{2 m^2 \omega_o^6} \, d/dt \{E_o^2(t)\} \qquad (5\text{-}46)$$

Equation (5-40) shows that far away from resonance, the current should be proportional to the time derivative of the amplitude of the field squared, i.e. proportional to the time derivative of the incident power. It must be noted that this represents the situation that prevails in dielectric materials.

(b) Frequency Corresponding to the Resonance Frequency: the Case of Semiconductors.

When the frequency of the laser electric field coincides with the resonance frequency, and if the amplitude of the excitation is a slowly varying function of the time, to a very good approximation the oscillation will grow as the integral of the excitation.

Naturally, this cannot go on forever, and in practice the growth is limited by a relaxation mechanism, the maximum amplitude beeing attained when both the energy input and the relaxation rate (i,e. the losses) are equal.

If a small anharmonicity is present ($d \neq 0$), the average value of the induced polarization which is zero in the linear case, will also grow with time, generating a current. The growth of the average polarization should therefore be roughly proportional to the integral of the field amplitude squared multiplied by the anharmonic coefficient d.

It is thus clear that the simple one-dimensional non-linear oscillator model may account for the presence of a polarization current on a transient basis. However, in the presence of energy relaxation mechanisms which result in the saturation of the response, it cannot account for a steady-state DC current such as the one originating from the second term of equation (5-12).

5.3.3 Discussion of the Time Response of the Generated Signals

Optical rectification has been experimentally observed to occur, both in dielectrics [33] and semiconductors [13], upon irradiation by powerful pulsed coherent light from Q-switched or TEA lasers; in all cases the effect has been observed under the form of an induced voltage in the bulk material. In order to account for the time-domain behaviour of the induced signal, we shall now give a very simple circuit model of a corresponding detector in order to discuss the fundamental differences between the cases of dielectric an semiconducting materials.

To find how the observed terminal signal voltage is related to the bulk current density generated by the incoming laser beam, it is necessary to solve Maxwell's equations for the average macroscopic fields $\vec{E}$ and $\vec{H}$ in the material.

It is important to realize that these fields are completely different from the local fields at the atomic level as well as the laser radiation field.

$$\vec{\nabla} \times \vec{H} = \vec{J} + \partial\vec{D}/\partial t \qquad (5\text{-}47)$$

In this equation $\vec{J}$ represents the free carrier current density. Hence we write

$$\vec{J} = \sigma\vec{E} \qquad (5\text{-}48)$$

where σ represents the usual low-frequency conductivity. $\partial D/\partial t$ can be written as

$$\partial\vec{D}/\partial t = \varepsilon\partial\vec{E}/\partial t \qquad (5\text{-}49)$$

where ε is the usual low frequency permittivity of the material.

Phenomenologically, two possible sources for the induced current must be considered. The direct effect of the laser beam may consist in either an induced polarization or an induced conduction current varying slowly in magnitude according to the modulation envelope of the laser pulse; the high frequency components of these signals average out to zero and therefore our discussion will concern only the rectified components of the signals.

We thus rewrite (5-47) as

$$\nabla \times \vec{H} = \sigma\vec{E} + \varepsilon\ \partial\vec{E}/\partial t + \vec{J}_s + \vec{J}_p \qquad (5\text{-}50)$$

where the " polarization " current density is defined by

$$\vec{J}_p = \partial \vec{P}_s / \partial t \qquad (5\text{-}51)$$

$\vec{J}_s$ and $\vec{P}_s$ are respectively the laser induced slowly varying current density and polarization vectors. To a very good approximation, magnetic flux induction effects can be assumed to be inexistent.

Hence, the curl of $\vec{H}$ is zero and

$$\sigma \vec{E} + \varepsilon \frac{\partial \vec{E}}{\partial t} + \vec{J}_s + \vec{J}_p = 0 \qquad (5\text{-}52)$$

$$\vec{E} = 1/\sigma \ (\vec{J}_s + \vec{J}_p) + \varepsilon/\sigma \ \partial \vec{E}/\partial t \qquad (5\text{-}53)$$

To make things simple, let us assume that the crystal is a uniform square plate of side a and thickness t as shown in figure (5-1), homogeneously illuminated and with transverse electrodes. The signal voltage V_s is the integral of the field $\vec{E}$ over a distance a

$$V_s = E \cdot a = a/\sigma \ (J_s + J_p) + \varepsilon/\sigma \ \partial V_s / \partial t \qquad (5\text{-}54)$$

which can be rewritten as

$$V_s = (I_s + I_p) R + RC \ \partial V_s / \partial t \qquad (5\text{-}55)$$

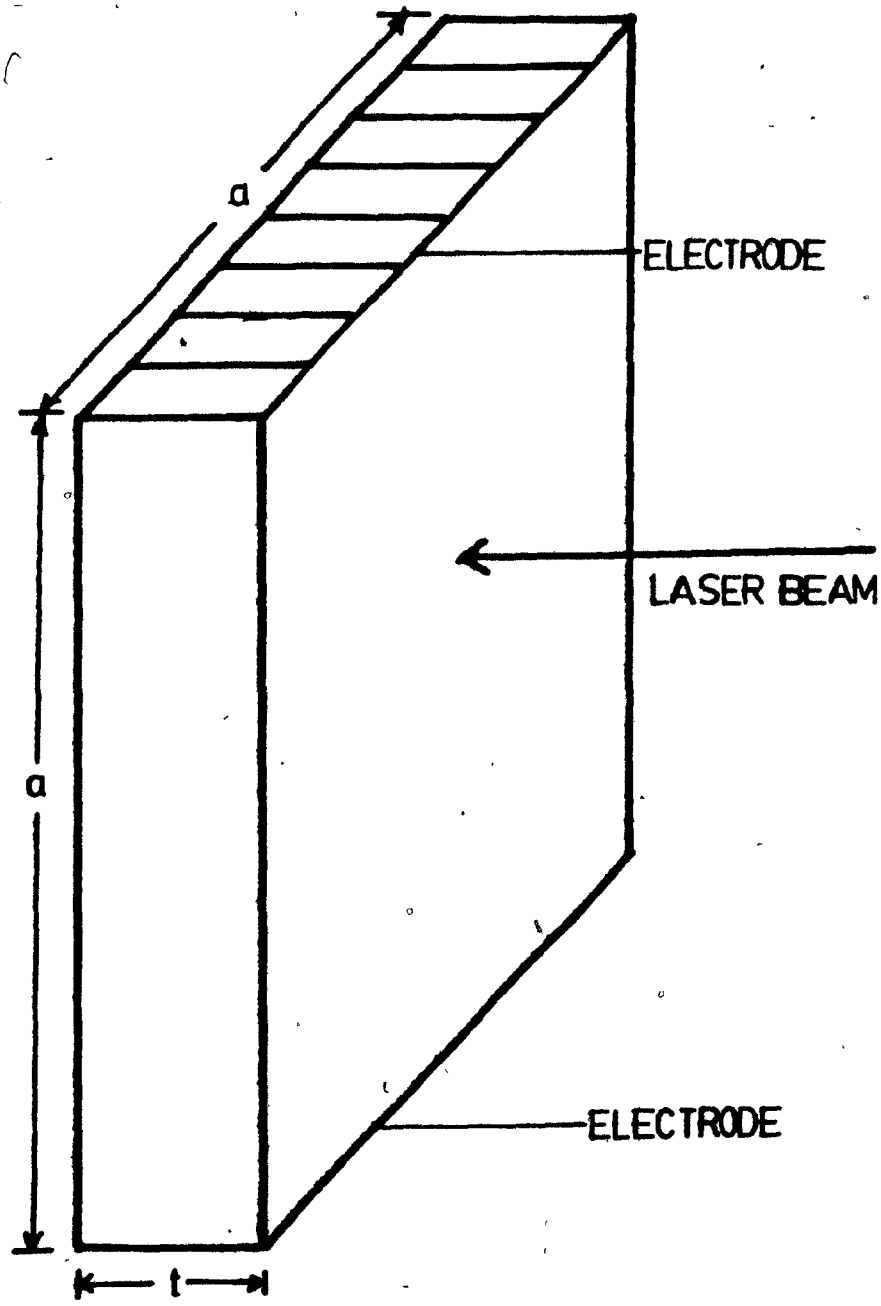

Figure (5-1) Idealized Sample Shape

or

$$(I_s + I_p) = V_s/R + C\partial V_s/\partial t \qquad (5\text{-}56)$$

where

$$R = 1/\sigma \quad a/ (a \cdot t) \qquad (5\text{-}57)$$

is the resistance of the crystal and

$$C = \varepsilon \frac{a \cdot t}{a} \qquad (5\text{-}58)$$

its capacitance.

Equation (5-56) is modeled by the simple circuit of figure (5-2).

The discussion presented in this chapter requires the consideration of three distinct situations.

(1) Dielectric Materials with Current Source I_p Only

In dielectric materials, no steady-state rectified current can be generated, since the radiation frequency is smaller than allowable transition frequencies. This situation corresponds to the discussion of paragraph 5.3.1

As we have seen in paragraph 5.3.2.1 however, the presence of a polarization current on a transient basis is not excluded. Since a laser pulse constitutes a transient excitation, one must conclude that if signals are observed at all in a dielectric material, they are due exclusively to the source I_p.

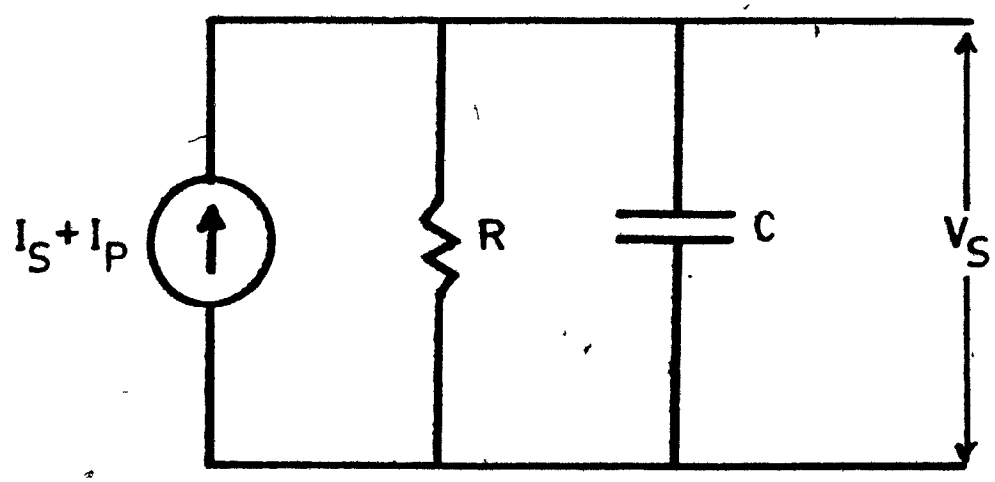

Figure (5-2) A simple Circuit Model to Account for the Time Domain Behaviour of the Induced Signal.

For such a material, the time constant RC is normally large compared to the observed laser pulse widths; the signal voltage is consequently proportional to the time integral of I_p. Since the polarization is itself proportional to the field modulation amplitude squared i.e. to the laser power and since I_p is the derivative of the polarization, V_s should be proportional to the laser power.

(2) Semiconducting Materials with the Current Source I_p Only

(a)

In semiconductors as well, a polarization current similar in nature to the one occuring in dielectrics may exist. However, since the resistance of a semiconductor may be quite small, the time constant RC will also be small. In such a case V_s is proportional to the time derivative of the laser power.

(b)

A different situation will arise when the laser frequency corresponds to a transition frequency. The polarization then gets integrated as discussed in paragraph 5.3.2.1 b).

If RC is smaller than the pulse width and if the latter is smaller than the characteristic relaxation time of the " oscillator " model discussed in 5.3.2.1 b), V_s will clearly be proportional to the laser power.

(3) Semiconducting Materials with the Current Source I_s Only

The analysis presented in chapter IV predicts the occurence of a net steady-state DC conduction current I_s in a semiconductor under constant irradiation when the laser frequency corresponds to a "resonant" transition frequency.

In this case I_s is directly proportional to the incident laser power and since the equivalent circuit time constant RC is expectedly small compared to the observed laser pulse width, the measured signal voltage V_s will be proportional to the laser power.

The above time domain behaviour analysis of the observed signal V_s will be used in our later discussion of the experimental results to help determine the nature of the process responsible for the observed laser generated voltages.

5.4 Conclusion

Starting with Butcher's analysis and the expression obtained in chapter IV for the second order generalized conductivity, we have derived a formal expression for a steady-state rectified DC current proportional to the laser power that would be generated in non-centrosymmetrical materials under constant irradiation. We have shown that the result recently obtained by von Baltz {27} is identical to the above; the latter has not recognized the connexion of his work with the fundamental work of Butcher and McLean {21}.

In a detailed discussion of our results, it has been shown that the rectified conductive current may exist only when the excitation laser frequency corresponds to an interband transition and reduces identically to zero due to time-reversal symmetry (i.e Kramers' theorem) when only intraband transitions prevail. The rectified DC current has also been shown not to be ascribable to any induced non-linear polarization effect.

Finally, the time-domain behaviour of the induced signals in both dielectrics and semiconductors has been discussed.

CHAPTER VI

Experimental Observation of Optical Rectification in Tellurium

6.0 Introduction

For reasons that have been discussed in chapter II, it has been found necessary to devote an important part of this thesis to a detailed theoretical discussion of non-linear conductivity in solids and the associated phenomena of optical rectification.

Having this thorough discussion as a background, we now undertake an experimental program in an attempt to resolve or verify questions raised in the former. The results that shall be presented here are similar to those obtained by Ribakovs (see section 2.1). However, special care has been given in the present work such that the resistivity of the samples be explicitely taken into account. In particular, the temperature control system has been improved, lower temperatures have been reached and a wider range of doping levels have been investigated. This approach has been motivated by the theoretical discussion which indicates a potential dependence of the phenomenon on energy band populations.

6.1 The Experimental Set-up

6.1.0 Introduction

The object of the experimental set-up is essentially to provide the possibility of measuring the electric signals induced in a Tellurium sample exposed to the radiation from a TEA CO_2 laser, from ambient down to approximately liquid nitrogen temperature.

6.1.1 The Laser

The high power radiation was provided by a Lumonics series 101 TEA CO_2 laser. The transverse excitation scheme allows operation at atmospheric pressure while keeping the discharge voltage at reasonable levels. The latter was beeing supplied by a Universal Voltronics model BAC-32-25 variable high voltage source (maximum 40 KV) connected through a 700 KΩ resistor bank to protect against overloading. Linear polarization of the beam is assured by a KCl Brewster window.

The variable N_2 - CO_2 - He gas mixture was maintained in proportions 1 : 2 : 10 and the operating voltage was set to 38 KV. The laser output power density is estimated to be approximately 200 KW/cm^2 with a beam cross-sectional area of about 2.5 cm^2.

A typical radiation pulse, figure (6-1), has a half power width of 180 ns with a rise time of 70 ns. The tail of the pulse of which the magnitude and width can be controlled by varying the proportion of the N_2 content in the laser gas mixture shows a slow component with microsecond decay times.

Although the laser is capable of repetition rates up to 5 pulses per second, the pulse rate was maintained at about 1 pulse per second to assure good pulse reproducibility.

6.1.2 The Tellurium Samples

The Tellurium samples were cut from good quality single crystals grown in the department of Electrical Engineering by the Czochralsky method. The ingots, pulled along the c-axis were hexagonal prisms with cross-section diameters varying from 1 to 2 cm, and a few centimeters in length. Tellurium beeing an extremely fragile material due to weak binding forces between atomic chains [34], single crystals are readily mechanically damaged. In order to preserve the good crystalline quality of the samples, a specially constructed saw has been used.

It essentially consisted of a polyester thread continuously extracting fresh acid from a reservoir and bringing it into contact with the crystal surface so that only a non-abrasive chemical action is involved. The acid solution consisted of a mixture of chromic trioxide, hydrochloric acid and water in 1 : 1: 2 proportions by weight.

The samples were then polished by rubbing them very gently on a flat piece of glass immersed into a solution of chromic trioxide, nitric acid and water in 1 : 2 : 4 proportions by weight.

Electrical contacts were made to the sample surfaces by alloying small strips of a solder made of a mixture of antimony, lead and indium in proportions 1.7 : 1.3 : 1. This solder has a low melting point of approximately 150^{o}C which helps to avoid exposing the sample to a thermal shock. Fine copper wire was then soldered to the alloyed strips to complete the contact fabrication.

6.1.3 The Cryostat

Samples were mounted on the cold finger of an Oxford Instrument CF-104B cryostat. Two dielectric coated germanium windows allowed transmission of the laser beam through the sample while avoiding back reflections from the cryostat wall.

The sample temperature was sensed with a cryogenic linear temperature sensor (CLTS) constituted of two photolitographically made thin-film resistors having opposite non-linearities an positionned very close to each other; a constant current flowing through the CLTS generates a voltage linearly related with the temperature.

6.1.4 The Temperature Controller

Temperature was both controlled an monitored by an Oxford intrument model EA-2349 temperature controller.

First, this unit controls the coolant gas flow through a valve and a flow meter, providing the coarse temperature control. The fine control is obtained by the generation of a feedback voltage which activates a small heater in the cryostat itself. As a consequence, the coarse temperature setting has to be slightly inferior to the desired temperature. The temperature is then raised to the required value by the heating element.

The controller possesses a very stable current source to supply the CLTS. The resulting voltage is fed into a comparator circuit and the error signal is used both to display the temperature and to control the heater feedback supply circuitry.

6.1.5 Signal Measuring Apparatus

The photo voltages induced in Tellurium samples beeing in the millivolt range are applied via a coaxial cable from the cryostat to the 50 Ω input of a Hewlett-Packard model 462 wide-band amplifier. The latter posesses a 40 dB gain and a 4 ns rise-time. The output sinal from the amplifier is then fed at the input of a Tektronix model 7623 storage oscilloscope shunted by a 50 Ω load resistance. Signals down to about 50 μV and 10 ns rise time are measurable with this set-up.

6.1.6 The Pyroelectric Detectors

The laser output pulse shape and power were monitored with two different pyroelectric detectors, namely a Molectron model P3-01 and a Molectron model P5-00 having known responsivities.

6.1.7 Special Difficulties

6.1.7.1 Noise

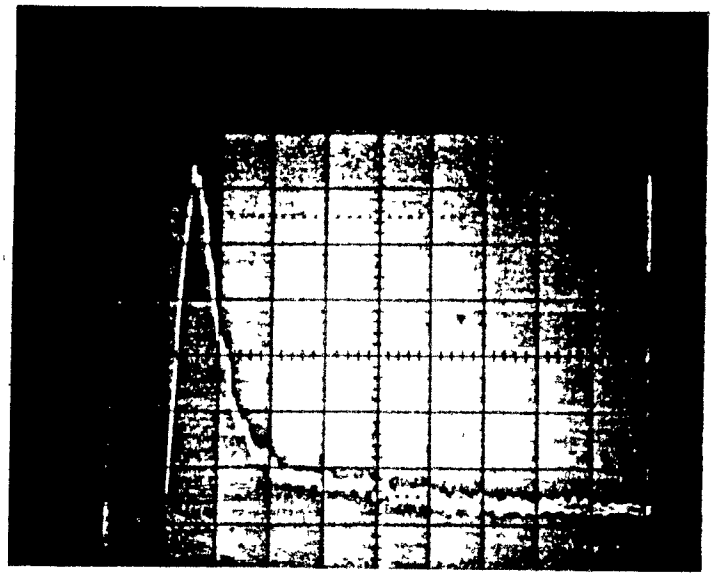

Figure (6-1) A Typical Radiation Pulse . Note the absence of parasitic piezoelectric oscillations and the presence of the distinctive plateau in the tail of the pulse. The time scale is 200 ns/cm and the vertical scale is 200 μV/cm.

Because of the very low level of the signal, and the proximity of the severe electric discharge condition in the laser, noise is a very serious problem. In order to eliminate the latter, it has been found necessary to shield both the laser and the sample containing set-up with two separate Faraday cages, communicating through small holes for the laser beam.

6.1.7.2 Sample Mounting

It has been mentioned that the samples were mounted on the cold finger of the cryostat. Since Tellurium is extremely fragile, it is essential to avoid any mechanical stress which could originate from sample mounting, especially when cooling down below 180^{O}K.

On the other hand, it is necessary to assure a good thermal contact between the sample and the cold finger. Because glue has a tendency to solidify at low temperature, and since in general its thermal expansion coefficient is different from that of Tellurium, it was found preferable to use vacuum grease as a binder, the latter having the advantage of beeing a good thermal conductor.

The samples were therefore mounted on a copper plate from which they were electrically insulated with a very thin mica sheet which continues to maintain a good thermal conduction path, as illustrated in figure (6-2).

6.1.7.3 Contact Masking

Figure (6-3) shows the mask used to prevent the laser beam from illuminating the electrical contact region, as this is known to generate spurious signals {9 }. The mask was made by opening a small square window into a piece of mylar. The outside surface of this piece was covered with a piece of aluminium foil to eliminate any radiation transmission.

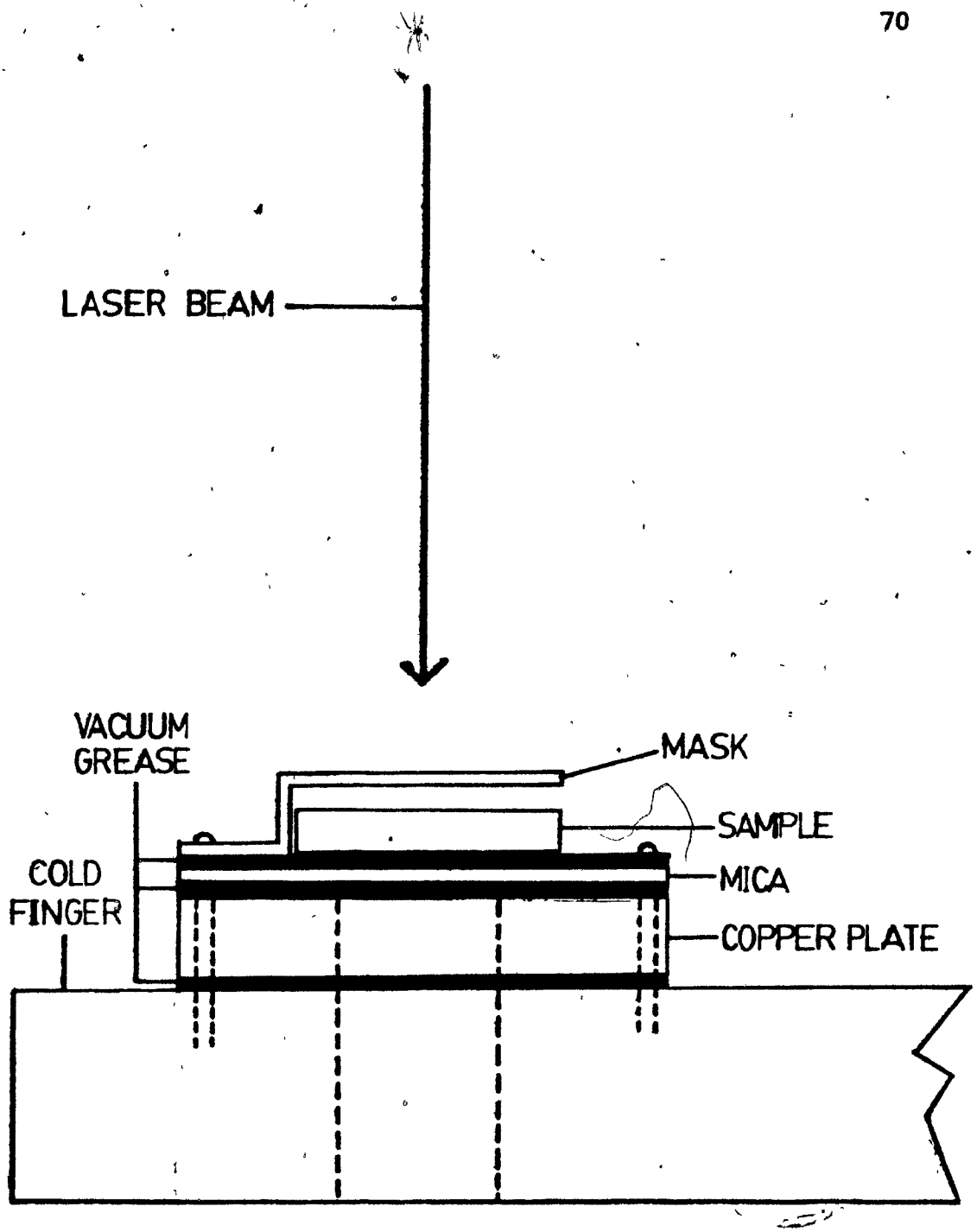

Figure (6-2) Sample Mounting on the Cold Finger of the Cryostat.

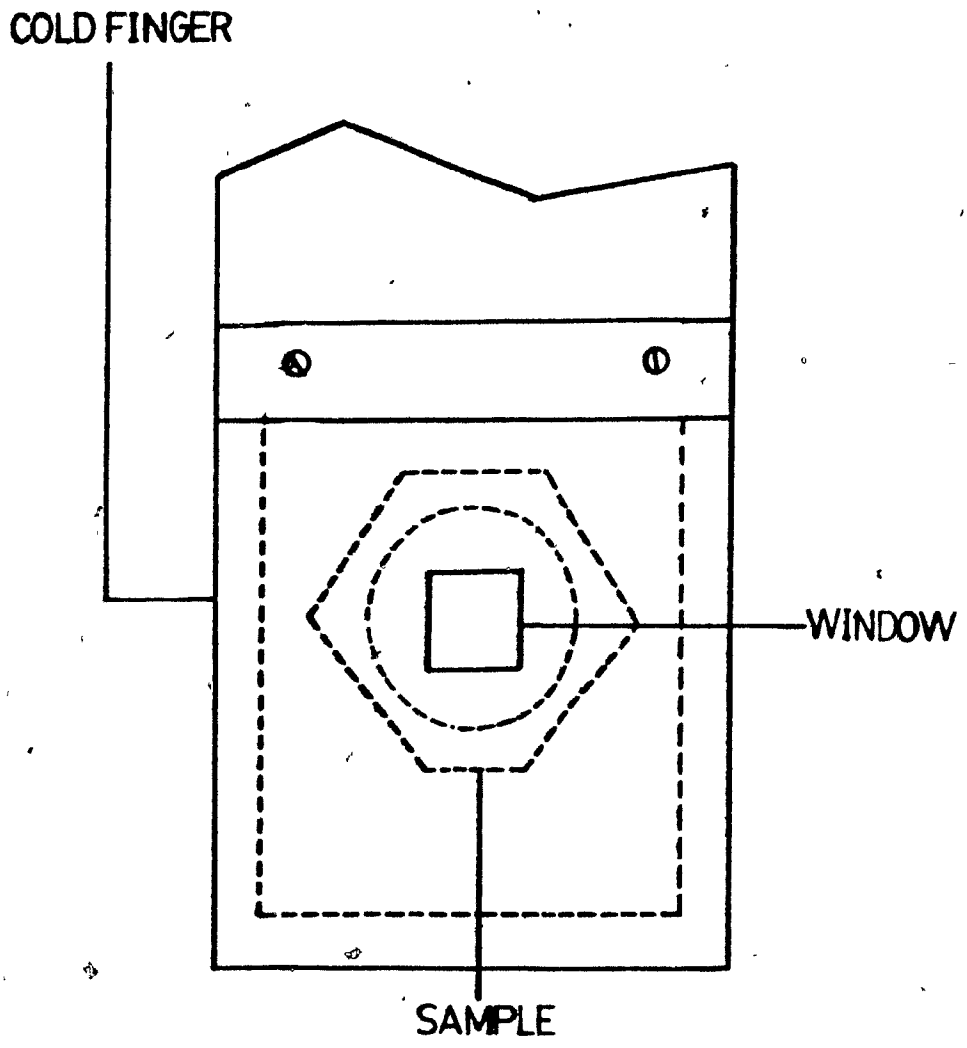

Figure (6-3) Mask used to prevent the laser beam to illuminate the electrodes.

6.1.7.4 Signal Voltage and Sample Resistance

As the resistance of intrinsic crystals at low temperatures may excede 100 Ω, it must be noted that the 50 Ω input impedance of the wide-band amplifier cannot be neglected and the measured signal has to be normalized to take into account voltage division.

6.2 Experimental Results

6.2.0 Introduction

The object of the experimental program was to measure the dependence on both temperature and doping level of the optical rectification tensor in Tellurium. The experiment consisted essentially in the measurement of the amplitude of the fast induced open circuit voltage at temperatures ranging from 90 to 300°K in four different samples described in table 6-1.

The extrinsic samples are p-type antimony doped and the different samples used in the experiment are identified by the ingot they originate from; normally, several samples are cut from the same ingot.

6.2.1 Characteristics of the Signal Observed

As it has been mentionned earlier, the voltage induced in the sample upon irradiation, is a true replica of the laser pulse shape. Figure (6-1) is a typical oscillogram of the observed signal, and is to be compared with figure (6-4) and (6-5) which are the output from the two different pyroelectric detectors described in section 6.1.6.

Note the presence in the laser pulse of the well known distinctive plateau (figure (6-1)). The pyroelectric detectors signals, figures (6-4) and (6-5) are clearly unable to display clearly this feature because of unavoidable stray piezoelectric resonance oscillations.

TABLE 6-1

SAMPLE IDENTIFICATION

Sample Identification	% Sb (per weight)	approximate doping level (cm^{-3})
CZ-77-15	undoped	undoped
CZ-76-13	0.01	3.0×10^{18}
CZ-77-11	0.1	3.0×10^{19}
CZ-77-12	1.0	3.0×10^{20}

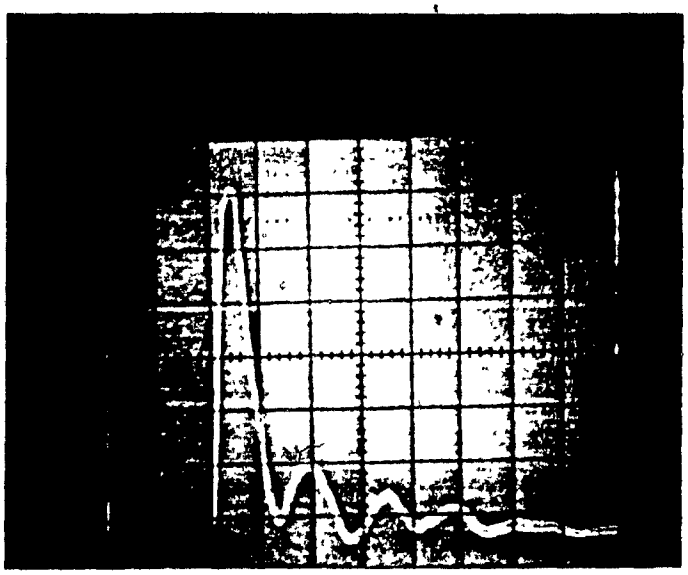

Figure (6-4) Output from the Molectron P3-01 Pyroelectric Detector. The time scale is 500 ns/cm and the vertical scale is 1 V/cm.

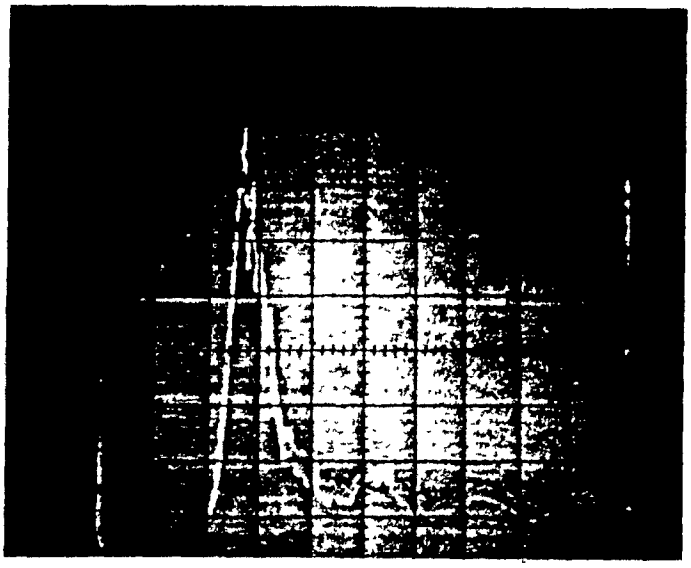

Figure (6-5) Output from the Molectron P5-00 Pyroelectric Detector. The time scale is 200 ns/cm and the vertical scale is 5 mV/cm.

A slow parasitic signal of unknown origin has been observed to occur sometimes in undoped samples at temperatures inferior to about 200 ^{o}K same as reported earlier by Ribakovs { 9 } ; its amplitude increases as the temperature decreases. Although this stray signal is clearly dependent on the presence of the laser beam, it exhibits a slowly decaying feature which is unrelated to the laser radiation modulation envelope. Figure (6-6) is a typical oscillogram of the signal. It should be noted that the latter is not reproducible from one sample to another and that it sometimes does not manifest at all. Such signals have not been observed in doped samples.

6.2.2 Measurements

6.2.1.1 Orientation

The samples were oriented in order to obtain a signal which could be attributed to the unique tensor component χ_{111} , as illustrated in figure (6-7)

6.2.1.2 Experimental Parameters

In all cases, the interelectrode spacing d was 5 mm, the sample thickness t 3 mm, and the illuminated area 5 mm x 5 mm. As it has been mentionned in paragraph 6.1.1, the laser power density, estimated from the known responsivities of the pyroelectric detectors is approximately 200 kW/cm^2. The anti-reflection coated Germanium windows of the cryostat are assumed to be perfectly transparent.

6.2.3 Results

(a) Verification of the Bulk Nature of the Observed Signals

The genuine bulk nature of the observed signals has been determined by the signals for the three different electrode configurations shown in figure (6-8) , namely front surface electrodes, back surface electrodes, and side surface electrodes.

Figure (6-6) A Typical Oscillogram of the Parasitic Signal Occuring in Undoped Samples. In this particular case, the temperature was 160°K. The time scale is 200 ns/cm and the vertical scale is 200 μV/cm.

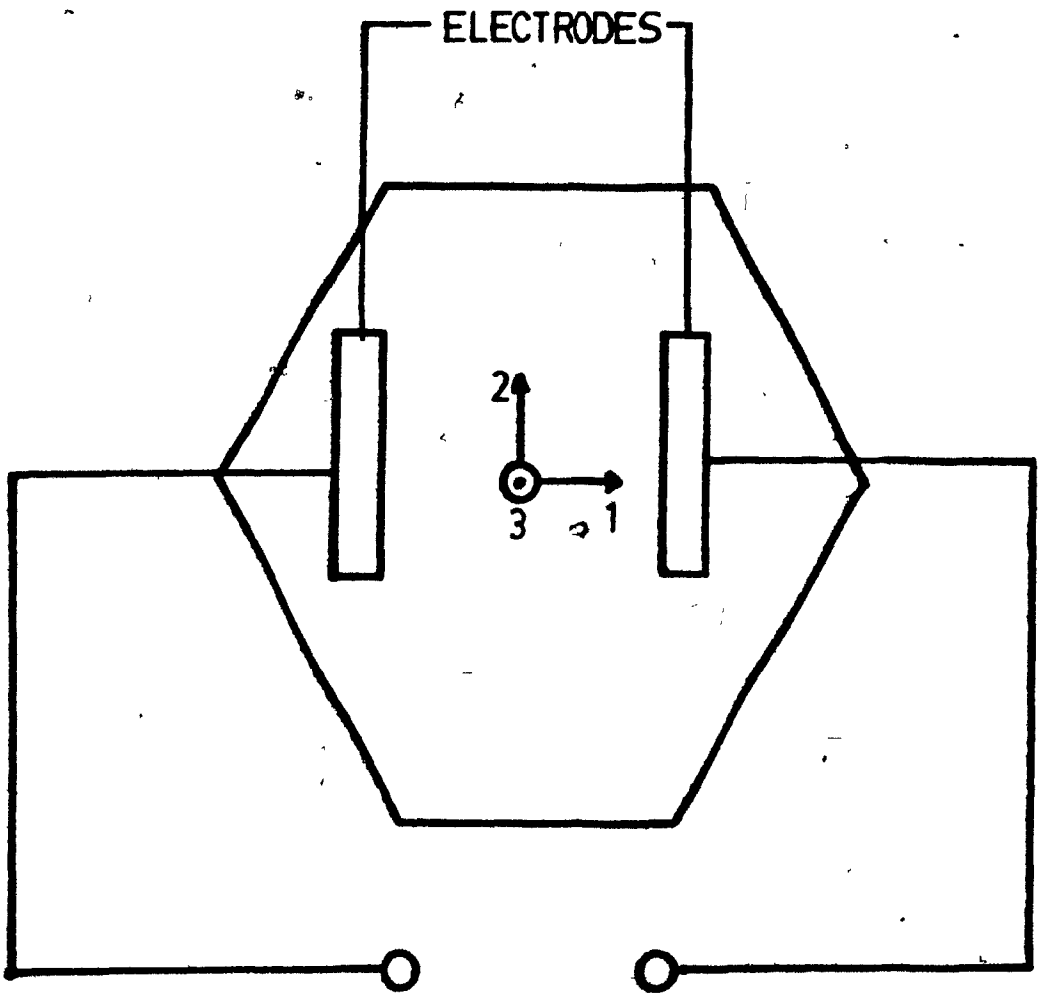

Figure (6-7) Orientation of the Sample in Order to Obtain a Signal Which Could Be Attributed to the Unique Tensor Component χ_{111}.

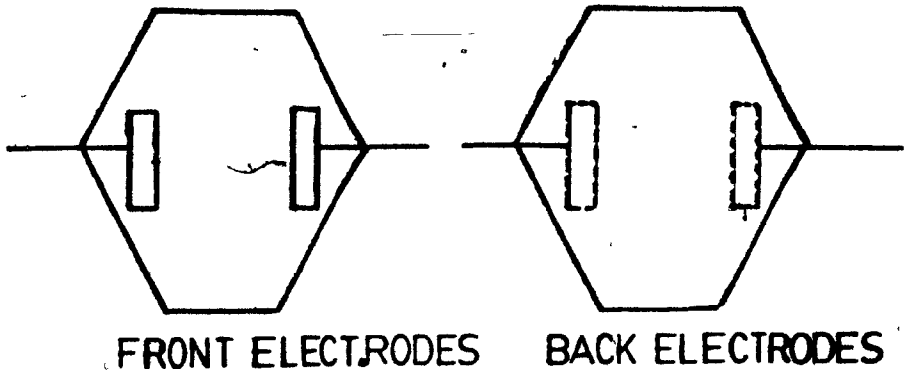

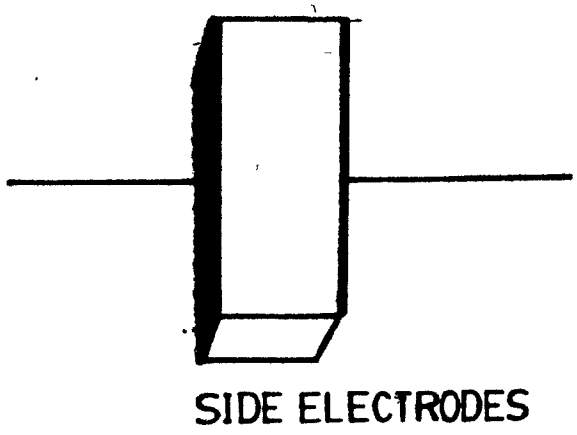

Figure (6-8) The Three Different Electrode Configurations Used to Verify the Genuine Bulk Nature of the Signals.

The response beeing identical in all cases, one must conclude that there is no appreciable surface effect involved.

(b) Linearity of the Signal Amplitude with Respect to the Power Density

The rectified pulse amplitude exhibits a linear dependence with respect to the laser power. This fact has been verified by gradually attenuating the incident power with an increasing number , up to three, of n-type silicon wafers having a resistivity of 7.1 Ω - cm and a thickness of 6.9 mils, which exhibit a transmission coefficient of about 50%. Thus, linearity has been demonstrated from $(0.5)^3 \times 200$ kW/cm^2 up to 200 kW/cm^2. Figure (6-9) is a graph illustrating the results obtained.

It is to be noted that the above results differ from a case reported by Hammond and al. {12} who describes the obtained signals to be essentially independent from the power density.

(c) Angular Dependence of the Induced Signal

Although we were not specifically interested from an experimental point of view on the detailed tensor behaviour of the induced signals which has been thoroughly investigated by Ribakovs { 6}, we felt necessary to verify the expected cos $(2\theta+\phi)$ dependence of the signal amplitude in order to make sure that the voltage pulses were the manifestation of a genuine third rank tensor. Figure (6-10) shows the angular dependence of the measured signals which has the expected behaviour.

(d) Variation of the Signal Amplitude with Temperature for Different Sample Doping Levels

The variation of the signal amplitude with respect to the temperature is presented for each doping level in figures (6-11), (6-12) and (6-13) for each sample identified in table 6-1 except for samples from ingot CZ-77-12. The latter are the most heavily doped samples; they have not produced any observable signals.

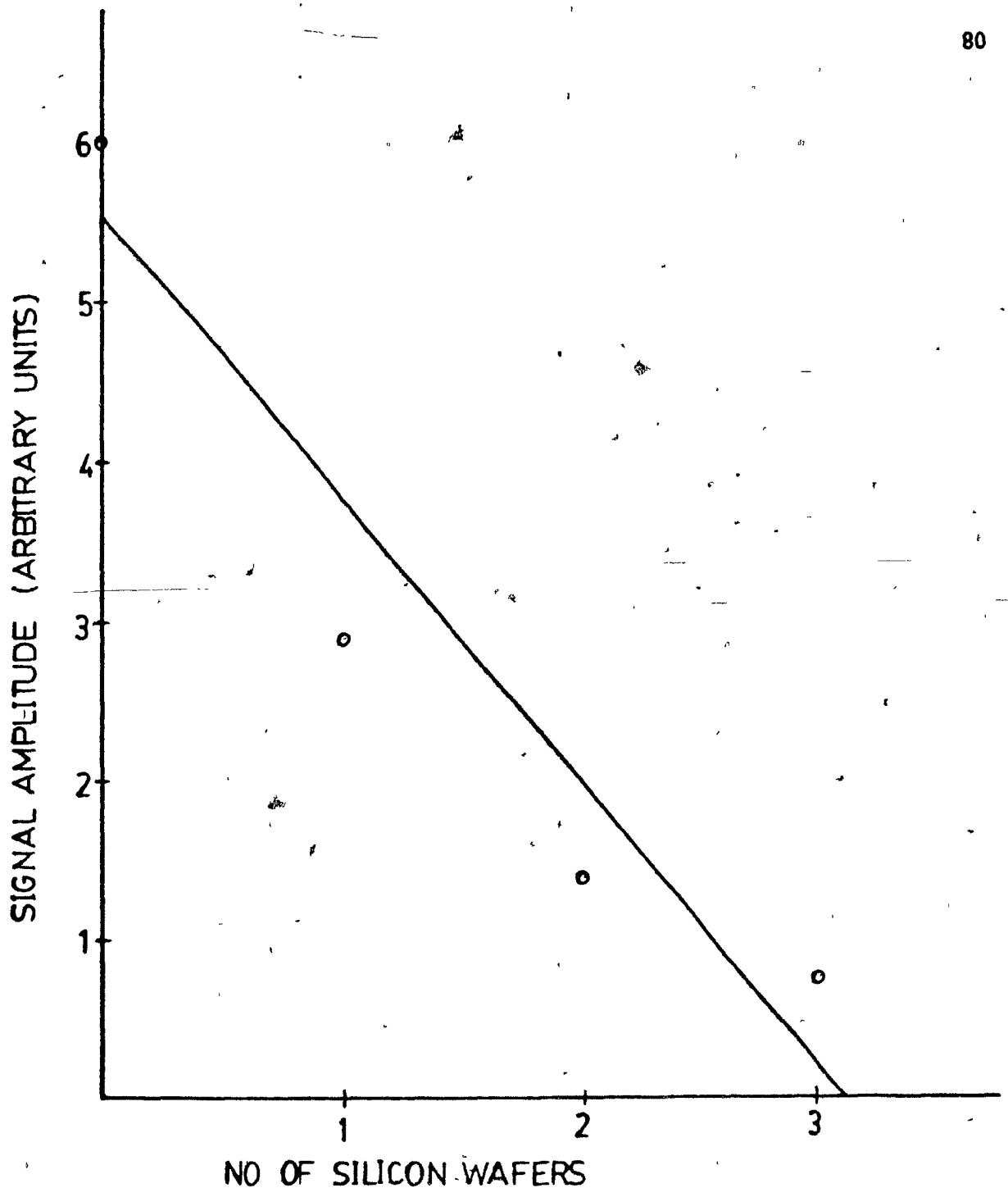

Figure (6-7) Linearity of the Signal Amplitude With Respect to the Power Density.

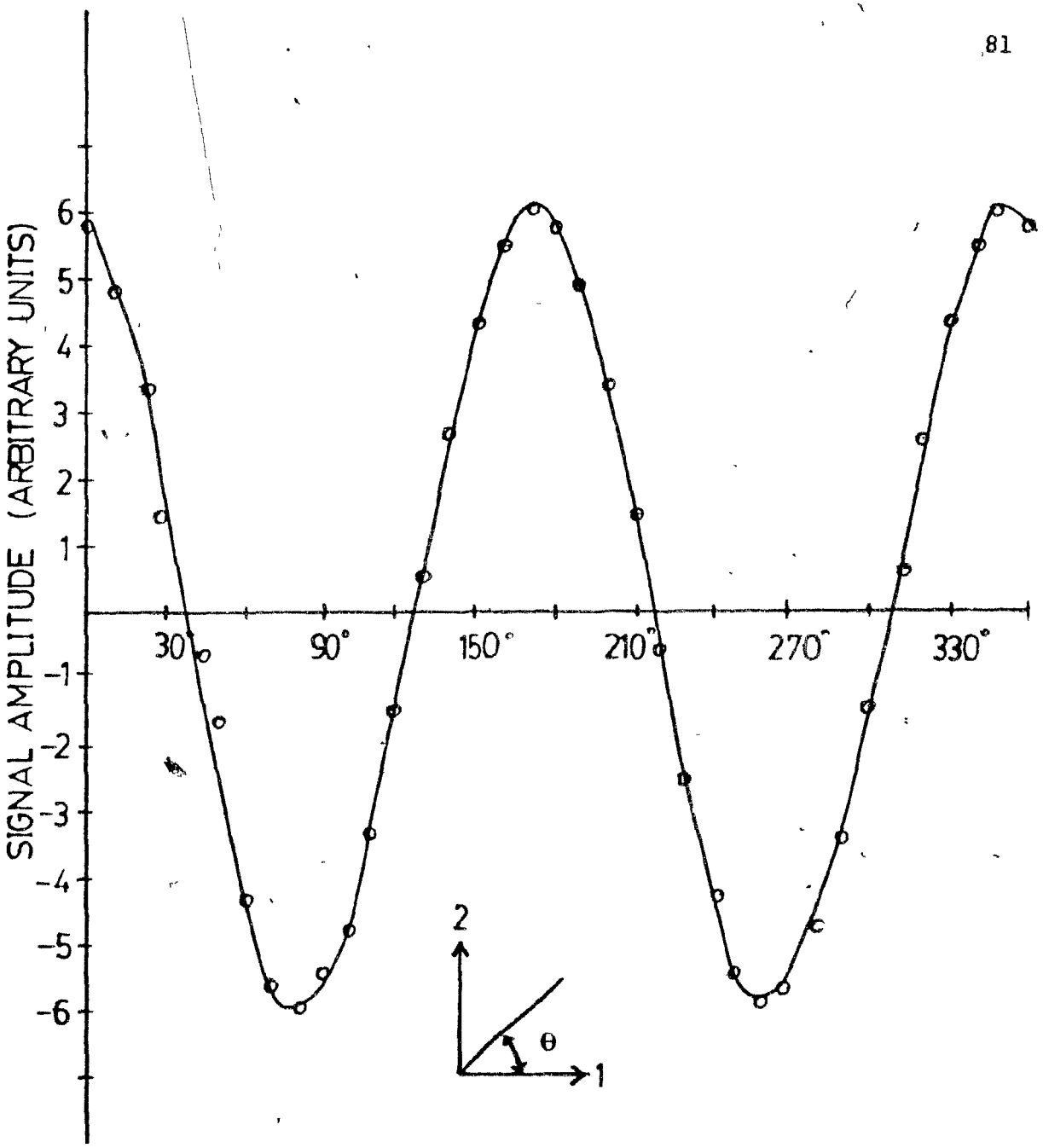

Figure (6-10) Angular Dependence of the Measured Signals. Note the angular shift due to optical activity.

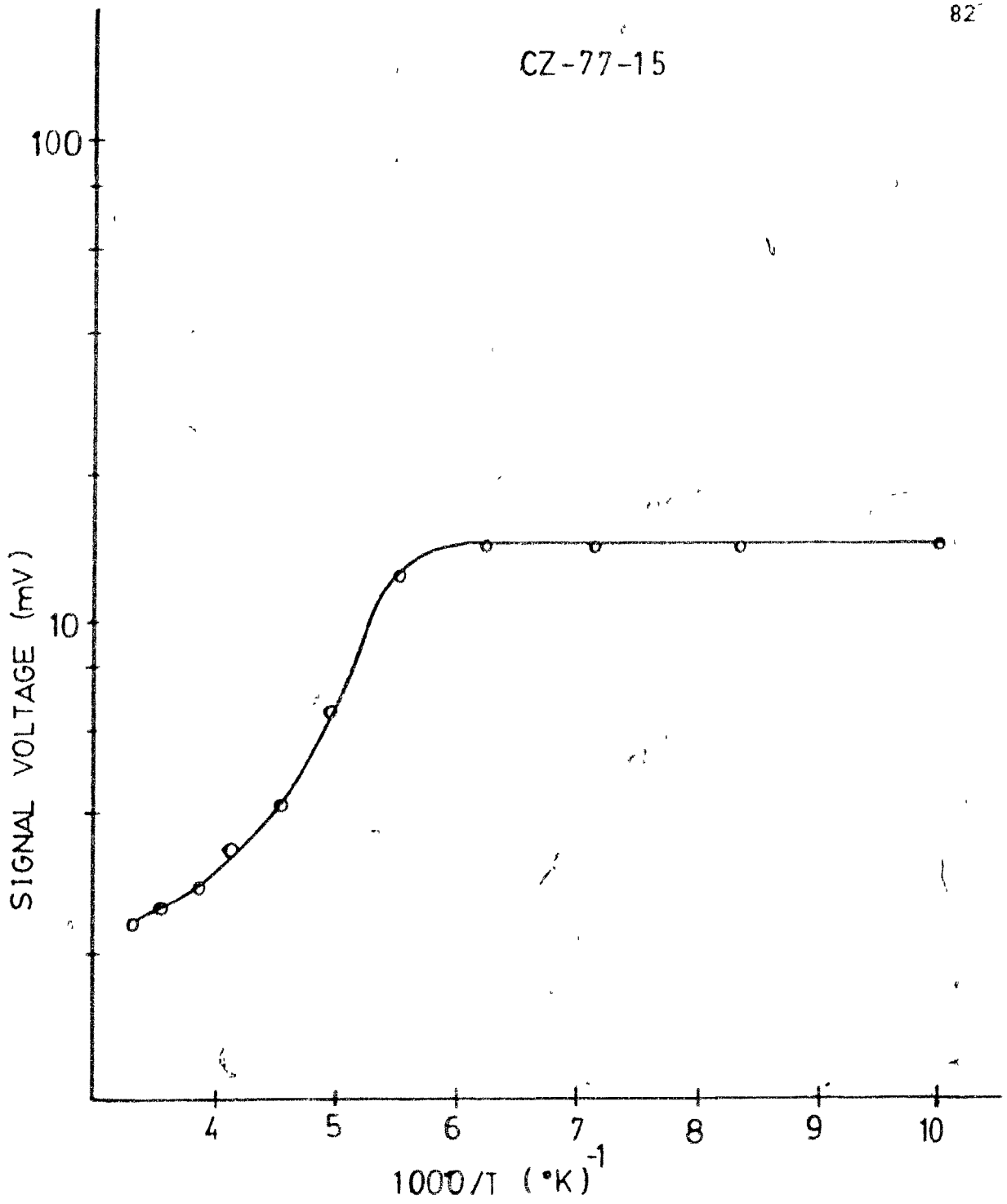

Figure (6-11) Variation of the Signal Amplitude in Function of the Temperature in Samples Originating from Ingot CZ-77-15

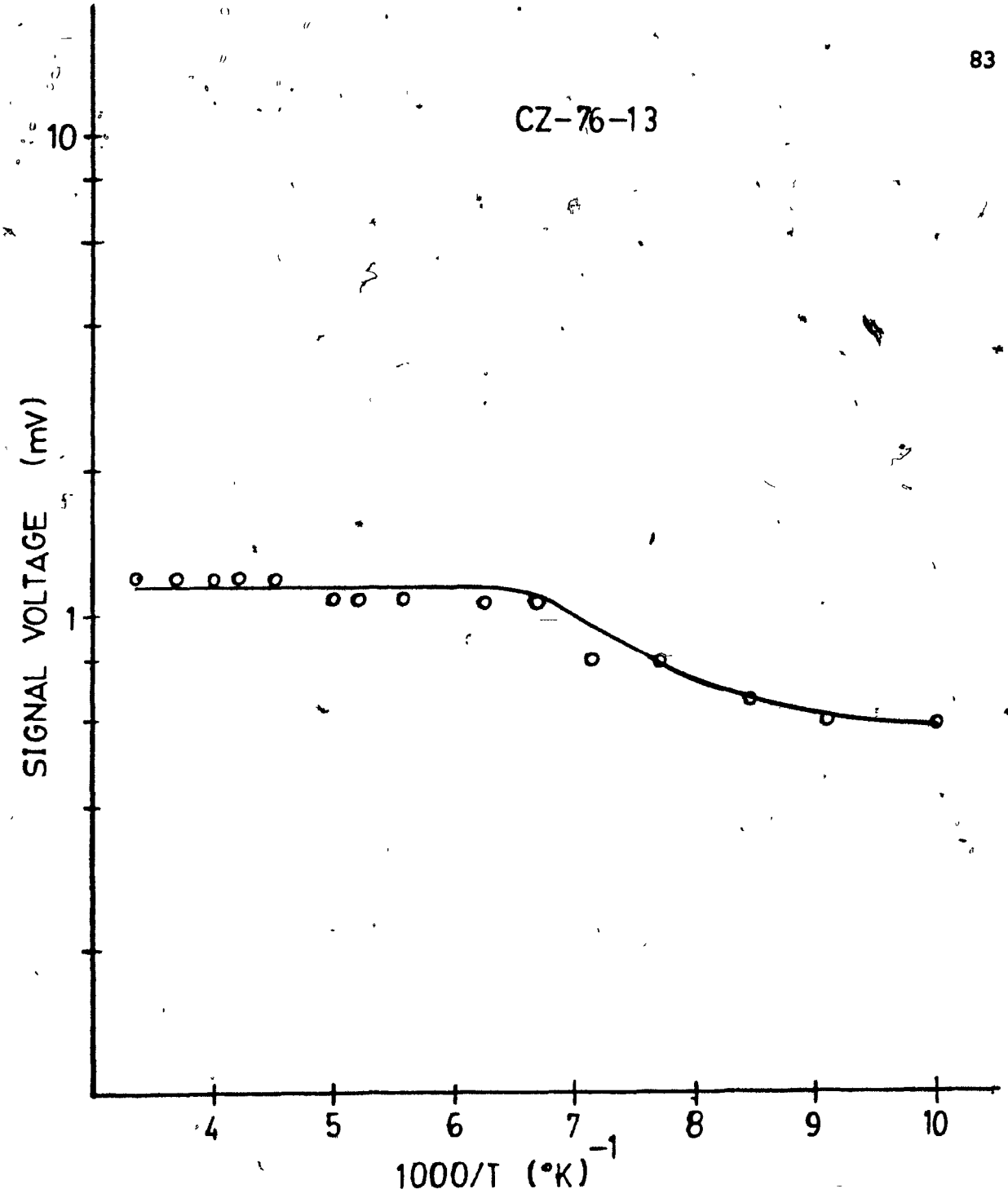

Figure (6-12) Variation of the Signal Amplitude in Function of the Temperature in Samples Originating fron Ingot CZ-76-13.

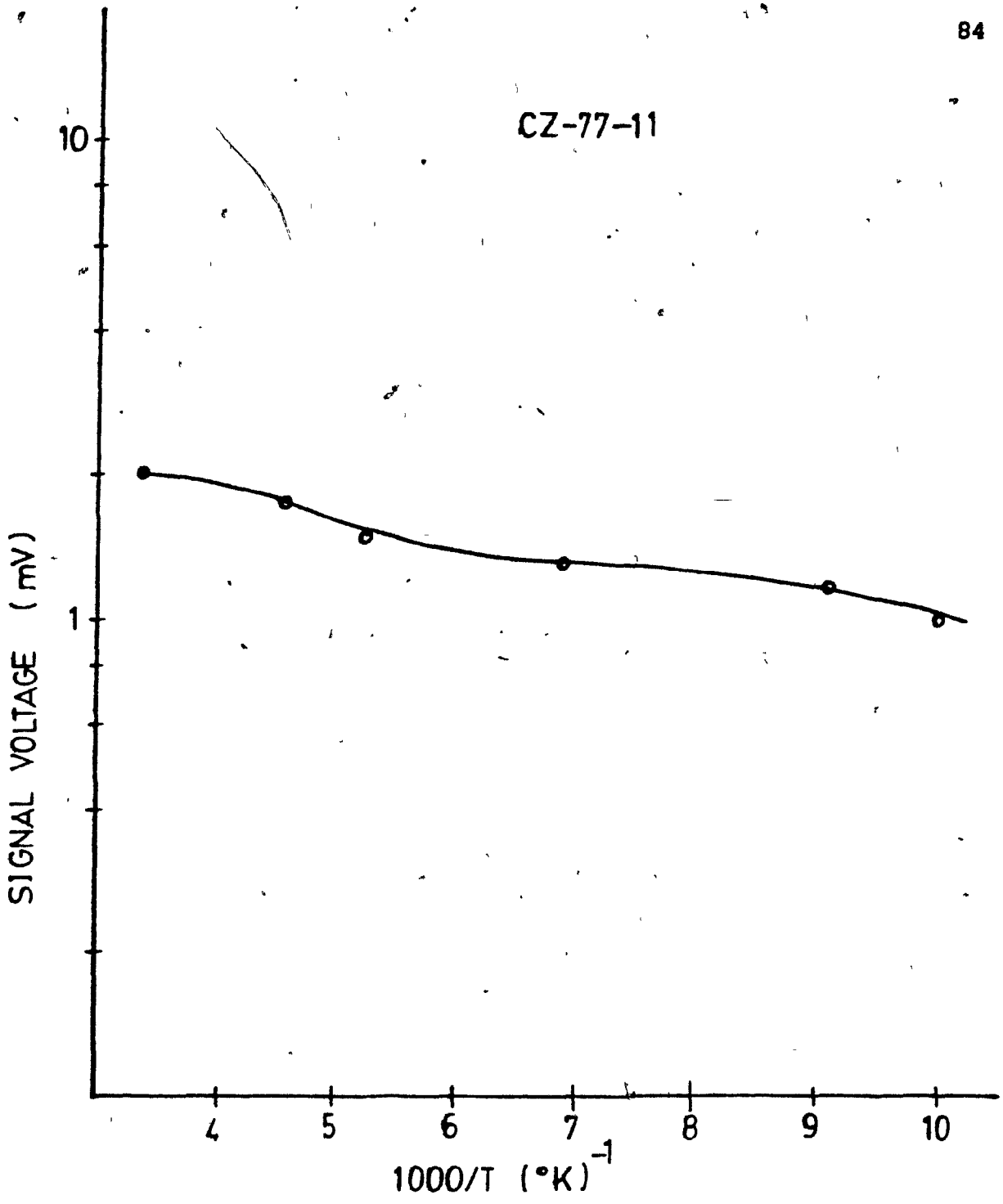

Figure (6-13) Variation of the Signal Amplitude in Function of the Temperature in Samples Originating from Ingot CZ-77-11

In the case of the undoped samples, the signal is seen to increase rapidly as the temperature decreases from about 300 ^{o}K to about 180 ^{o}K where it becomes essentially constant.

On the other hand, the curves corresponding to the doped samples have the same general behaviour. They present essentially no structure except for a slight monotonic decrease of the induced signal as the temperature decreases. These results are consistent with the observations of G. Ribakovs.

(e) Observations of Signals in Thin Samples at Room Temperature

Since the mechanism of signal generation is expected to correspond to a current source, it has been thought important to observe the effect on the induced signals due to variations in the resistive characteristics of the samples. In particular, an increase of the latter with an increase of the resistivity at a given doping level is expected. This is more thoroughly discussed later.

To verify this hypothesis, a simple experiment has been devised. Typically, it would have been interesting to obtain a real thin film which would be constituted of a few atomic layers, Such films are , however, technically difficult to fabricate, especially when a single crystal is required. It was, therefore, decided instead to polish samples by the standard procedure described in section 6.1.2 down to thicknesses of the order of 50 μ. This represents the minimum practically achievable thickness by such a procedure. The results are summarized in table 6-2. Interestingly, compared to the previous thick sample observations, enhanced signals have been observed in all cases; particularly, a distinctively observable signal has been obtained in the thin sample from ingot CZ-77-12, figure (6-14), where in a thick sample, no signal has been observed.

6.2.4 Relationship Between the Optical Rectification Tensor χ and the Experimentally Measured Signals

Clearly, the experimental results presented in the last section provide the induced voltages between the electrodes fixed on the samples.

TABLE 6-2

MEASUREMENTS ON THIN SAMPLES*

Sample Identification	Signal Amplitude (mV)	χ^{*}_{111} (cm/A)
CZ-77-15	5.0	0.5×10^{-7}
CZ-76-13	10.0	1.0×10^{-7}
CZ-77-12	2.5	0.25×10^{-7}

* Absorption is considered to be negligible in thin samples.

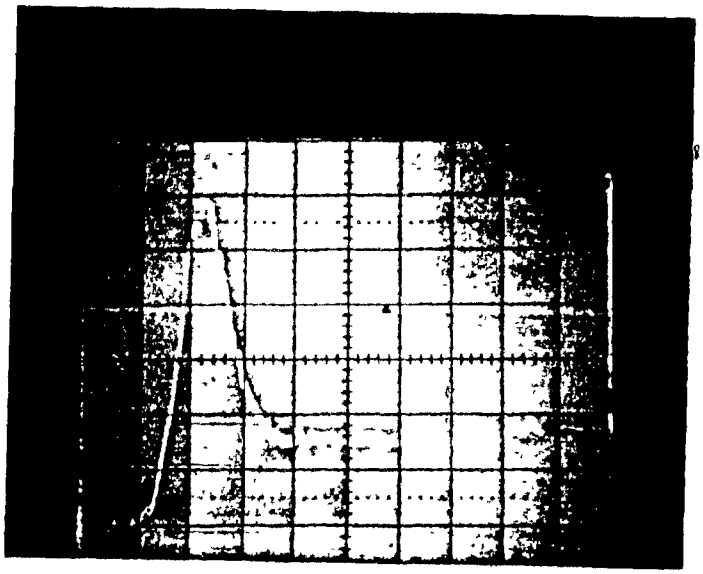

Figure (6-14) Signal Observed in Thin Sample from Ingot CZ-77-12.

We obtain the optical rectification tensor χ by relating these induced voltages to the optically rectified current density $\vec{J}$ with the help of the simple configuration shown in figure (6-7).

Although Tellurium is a semiconductor, its conductivity is relatively large. As a consequence, it is legitimate to neglect the intrinsic capacitance of the samples and to suppose that the signal voltage generated by the CO_2 laser radiation is entirely due to the flow of the rectified current through the resistance. In terms of the equivalent circuit model of paragraph 5.3.3, it implies that all the current from the current source passes through the resistance R. Equation 6-1 relates the incident power density to the induced current density.

$$\vec{J} = \chi W \qquad (6\text{-}1)$$

Under the hypothesis of a negligible sample capacitance one can also define a modified rectification tensor χ^* relating the generated voltage to the incident power density

$$V = \rho\chi dW = \chi^* dW \qquad (6\text{-}2)$$

where χ^* is merely defined as the product of χ and the appropriate value of the resistivity and d is the inter-electrode distance.

The results of Ribakovs, which have been summarized in chapter II have been expressed in terms of this modified rectification tensor. For the sake of comparison table 6-3 presents the experimentally obtained values in this thesis for the modified rectification tensor at room temperature; these results compare very well with those of Ribakovs.

6.2.5 Different Considerations Affecting the Experimental Results

(a) optical activity

A linearly polarized electric field rotates by about 11° per mm while propagating in the c-direction through Tellurium, due to optical activity.

TABLE 6-3

EXPERIMENTAL RESULTS IN TERMS
OF RIBAKOV'S χ^* AT ROOM TEMPERATURE

Sample Identification	resistivity (Ω-cm)	χ^* (cm/A)	χ $(V)^{-1}$
CZ-77-15	1.0	0.25×10^{-7}	0.25×10^{-5}
CZ-76-13	0.2	0.15×10^{-7}	0.75×10^{-5}
CZ-77-11	0.08	0.33×10^{-7}	4.1×10^{-5}
CZ-77-12	0.025	-	-

It is straightforward to demonstrate that this effect shifts the expected cos 2θ dependence of the measured signal by an angle $\phi = rt/2$ degrees, where r represents the "rotary power" in degrees per mm and t is the thickness of the sample. Experimentally, the effect of the presence of such an angular shift on the signal magnitude can be taken into account by slightly rotating the sample until a signal of maximum amplitude is obtained. Our measurements have been performed following this procedure.

(b) absorption

In order not to complicate matters unnecessarily, it is usually assumed that the laser power density is constant throughout the sample under investigation. In most cases, this constitutes a good approximation since absorption is relatively small and samples are only a few mm thick. However, the situation is different in heavily doped crystals, and the amplitude of the measured signal voltage is affected since the latter depends roughly on the average value of the power density over the sample thickness. Neglecting multiple reflections, the ratio between the average power and the incident power at the air-Tellurium interface can be shown to be

$$P_A/P_o = (1-R)/\alpha t \{1-e^{-\alpha t}\} \qquad (6-3)$$

where P_A is the effective power, P_o is the incident power, R is the reflection coefficient , α is the absorption coefficient and t is the sample thickness.

At 10.6 μ absorption in intrinsic Tellurium is dominated by free carriers. Figure (6-15) is a plot of the absorption coefficient α vs the wavelength λ of the radiation {35}. The absence of structure in the neighborhood of $\lambda = 10.6\ \mu$, and the straight feature of the curve are characteristic of the above mentionned type of absorption. For an intrinsic crystal, α is seen to be about 0.18 cm^{-1}. Although no results are available at other doping levels, it is normal to expect a significant increase in the absorption at higher impurity concentrations.

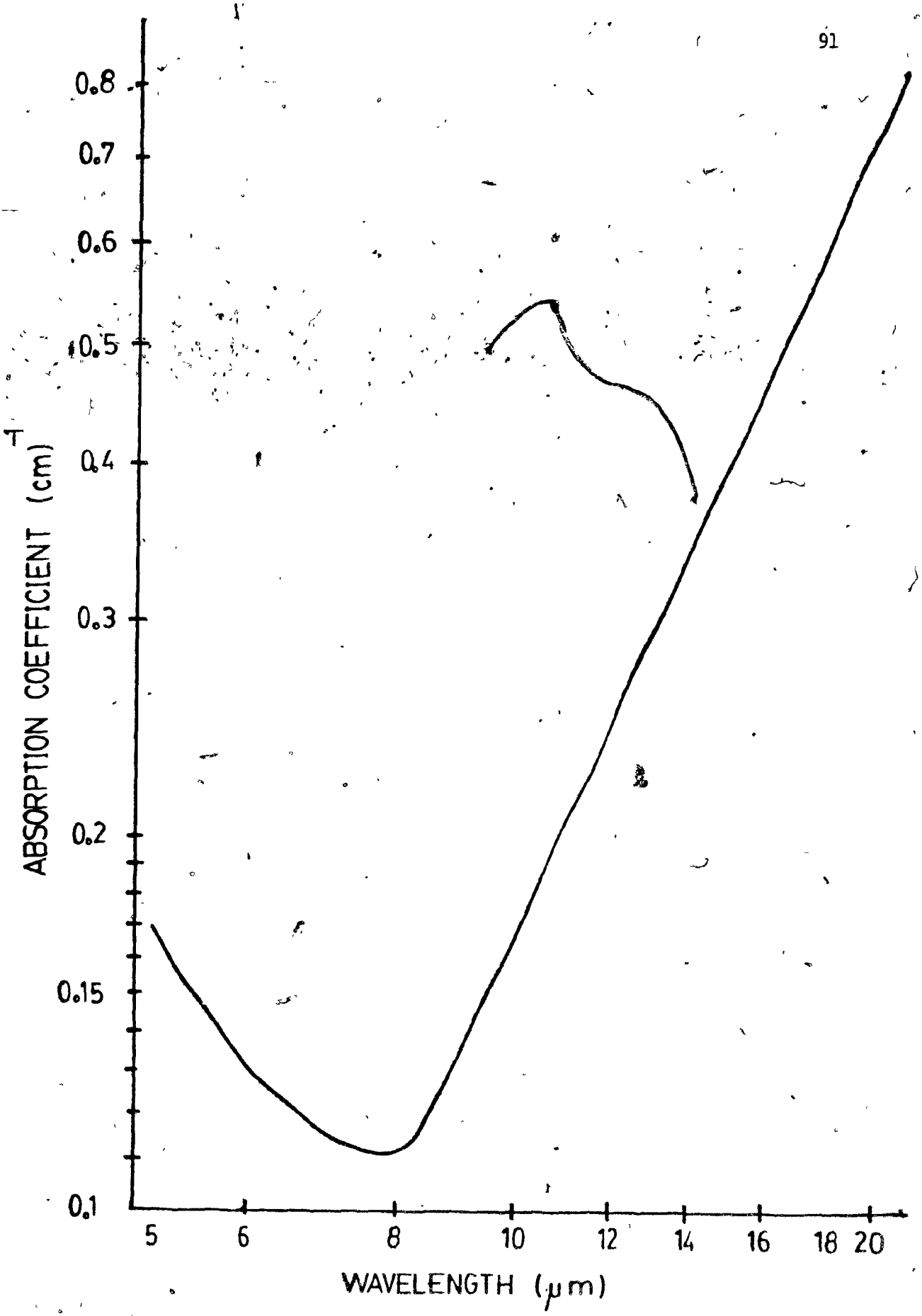

Figure (6-15) The Absorption in Undoped Tellurium at Room Temperature.
From S. Ades, M.Eng. Thesis, McGill University, 1975

TABLE 6-4

ESTIMATES OF THE FREE CARRIER ABSORPTION COEFFICIENT

Sample Identification	Absorption coefficient $(cm)^{-1}$
CZ-77-15	0.18 *
CZ-76-13	0.90
CZ-77-11	2.25
CZ-77-12	7.2

* actual measured value

A rough estimate of the behaviour of α with respect to the conductivity can be obtained by resorting to Drude's classical theory (see appendix B) which assumes that the absorption of light by free charge carriers can be treated as a transport problem. Table (6-4) summarizes the results obtained.

It is obvious from equation (6-3) and from table (6-4) that the useful power, that is, the value of the power density which sould be used in evaluating the rectification tensor component χ_{111}, is significantly smaller for doped samples than for undoped samples. However, we shall not perform any explicit computation of P_A at this stage since it will be seen in (d) that the effect of multiple reflections must also be taken into account.

(c) Reflection Coefficient

Closely related to the increased absorption in heavily doped samples is the phenomenon of the increase in the reflection coefficient R. The value of the latter is of prime importance in the evaluation of χ as it directly affects the actual power density transfered to the sample. Here again, a rough estimate of the reflexion coefficient behaviour can be obtained from the results of classical electromagnetic theory.

At normal incidence, the reflexion coefficient R affecting the radiation intensity is given by the well-known formula {36}

$$R = \frac{(n-1)^2 + k^2}{(n+1)^2 + k^2} \qquad (6-4)$$

where n and k are determined from formulea (A-4) and (A-5) (see appendix A).

Since the values of k are about four orders of magnitude smaller than those of n, it appears that despite inportant variations in the doping level, the reflection coefficient does not vary significantly.
With n = 4.8, we get for R

$$R \simeq \frac{(4.8 - 1)^2}{(4.8 + 1)^2} = 0.43 \qquad (6\text{-}5)$$

which is in very good agreement with the published experimental data [37].

(d) Multiple Reflections

Since both the air-Tellurium and Tellurium-air interfaces are characterized by a reflexion coefficient, figure (6-16), a certain proportion of the radiation is constrained to bounce back and forth inside the sample. As the signal voltage polarity is independent from the beam propagation direction, multiple reflections will enhance the measured signal voltage magnitude. It is easy to demonstrate that the useful power for a single pass through the sample as expressed by equation (6-3) gets multiplied by a factor

$$\Gamma = \frac{1}{1 - R/\alpha t\,(1 - e^{-\alpha t})} \qquad (6\text{-}5)$$

when multiple reflections are taken into account.

Thus finally, table 6-5 presents estimates of the useful power P_A in the samples after taking into account the effect of both absorption and multiple reflections. It is to be noticed that for the most heavily doped samples the useful power represents only about 30% of the incident power whereas in the case of the undoped samples it represents almost 100% of the latter. One thus expects a reduction of the observed voltages in doped samples, due to these considerations.

(e) Interference Effects

In (d), we have discussed the influence of multiple reflections by making abstraction of interference effects. This approximation holds as long as we are dealing with samples such as the ones used in our experiments, which are relatively thick with respect to the radiation wavelength and where the front and back surfaces are not perfectly parallel and/or highly polished.

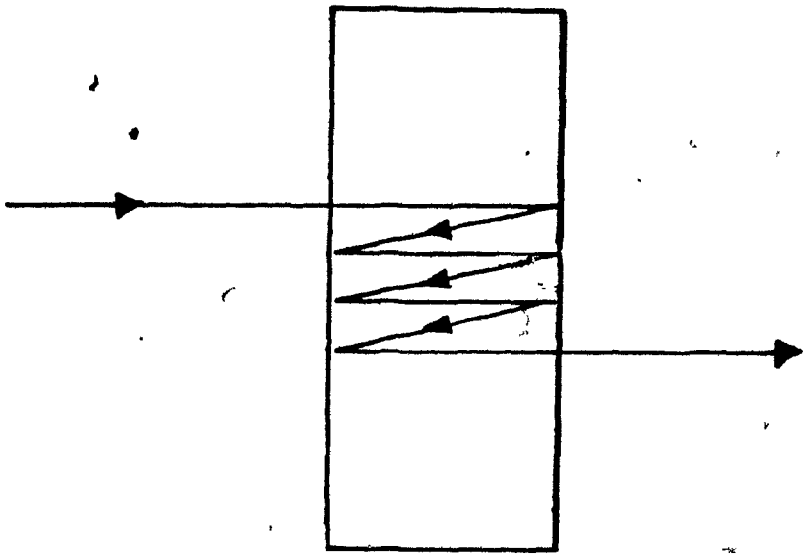

Figure (6-16) Multiple Reflections.

TABLE 6-5

ESTIMATES OF THE USEFUL POWER P_A

Sample Identification	P_A/P_o
CZ-77-15	0.95
CZ-76-13	0.81
CZ-77-11	0.61
CZ-77-12	0.28

6.3 Interpretation of the Experimental Results Related to the Theory

6.3.1 Time Dependence

In paragraph 5.3.3, we have examined theoretically the expected time response of the optically generated signals for various postulated source mechanisms. It was shown that in semi-conducting materials such as Tellurium, the current source may either be of the type I_p, in which case the signal is proportional to the time derivative of the laser power, or, of the type I_s, which leads to a rectified voltage directly proportional to the laser power.

Clearly, from the experimentally observed pulse shape, it appears that we are in presence of a current source of the type I_s; we must then conclude that the rectified signal is due to a second order non-linear conductive effect as derived in details in section 5.2 and not to some induced non-linear polarization current.

6.3.2 Derivation of the Optical Rectification Tensor χ from Measured Induced Potentials

Since the theory presented in this work deals with the optical rectification tensor χ itself, it will be desirable to obtain numerical values for the latter from the measured radiation-induced potential results presented in figures (6-11), (6-12), (6-13) and from the known temperature dependent sample resistivities given in figures (6-17) to (6-20). This is simply achieved by using relation (5-2). The results are presented in figures (6-21), (6-22) and (6-23).

6.3.3 General Observations on the Behaviour of χ in Doped and Undoped Samples

It is seen that the behaviour of the undoped samples is vastly different from that of the doped ones. In particular, χ in undoped samples is seen to decrease rapidly from room temperature down to about $180^{\circ}K$ where it reaches a minimum; it then increases slightly and saturates throughout the rest of the temperature range.

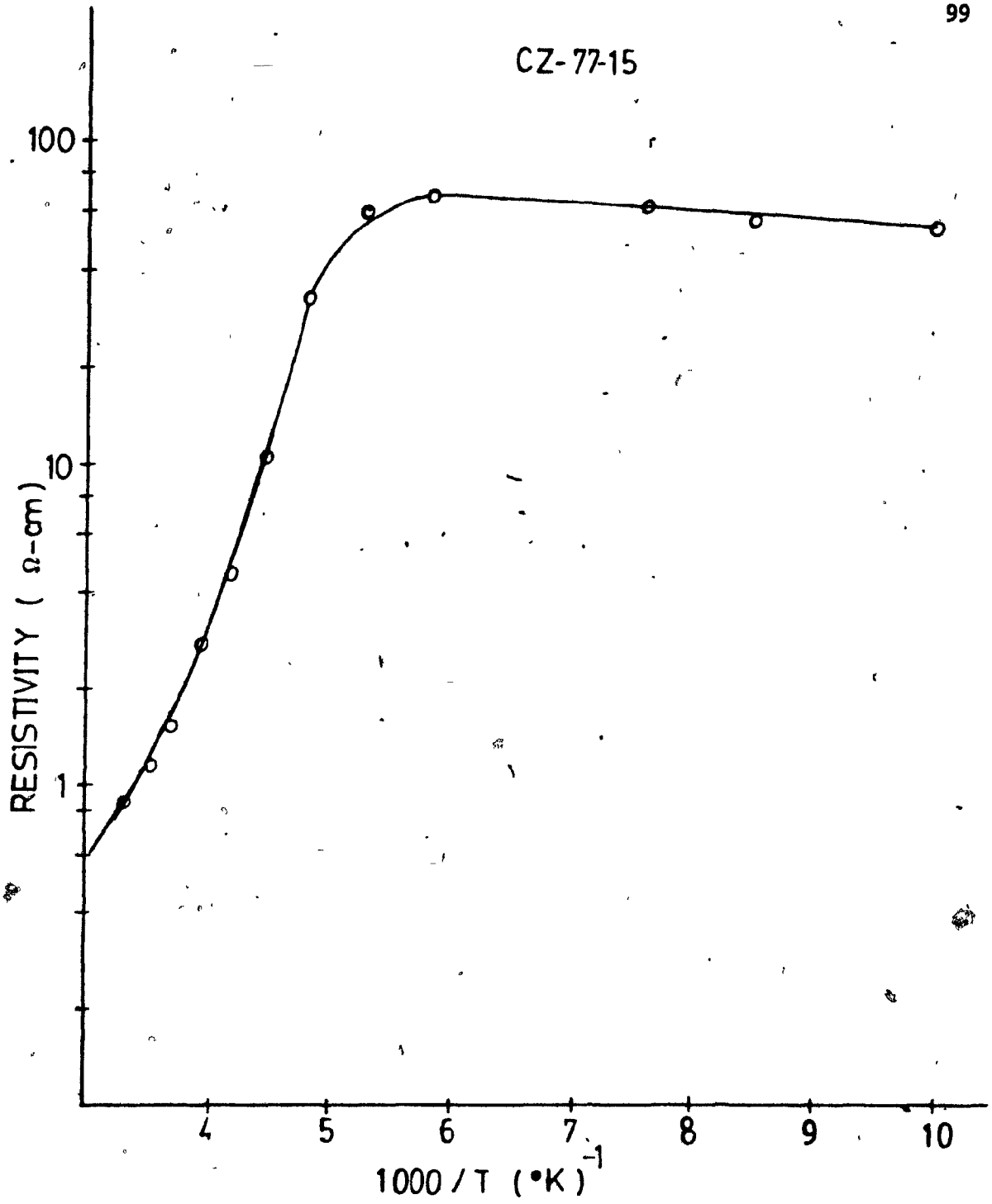

Figure (6-17) Variation of the Resistivity as a Function of the Temperature for Samples Originating from Ingot CZ-77-15

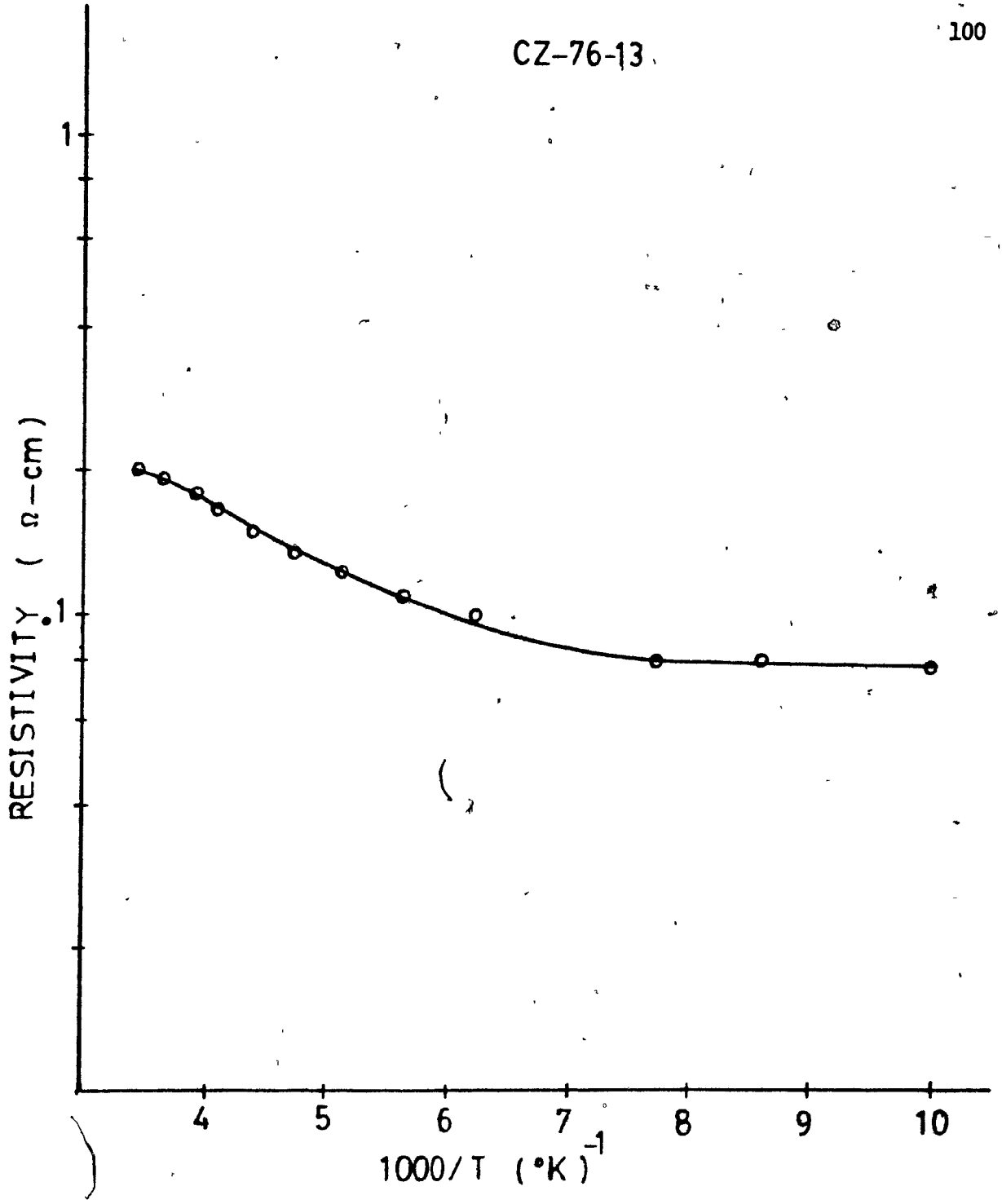

Figure (6-18) Variation of the Resistivity as a Function of the Temperature for Samples Originating from Ingot CZ-76-13

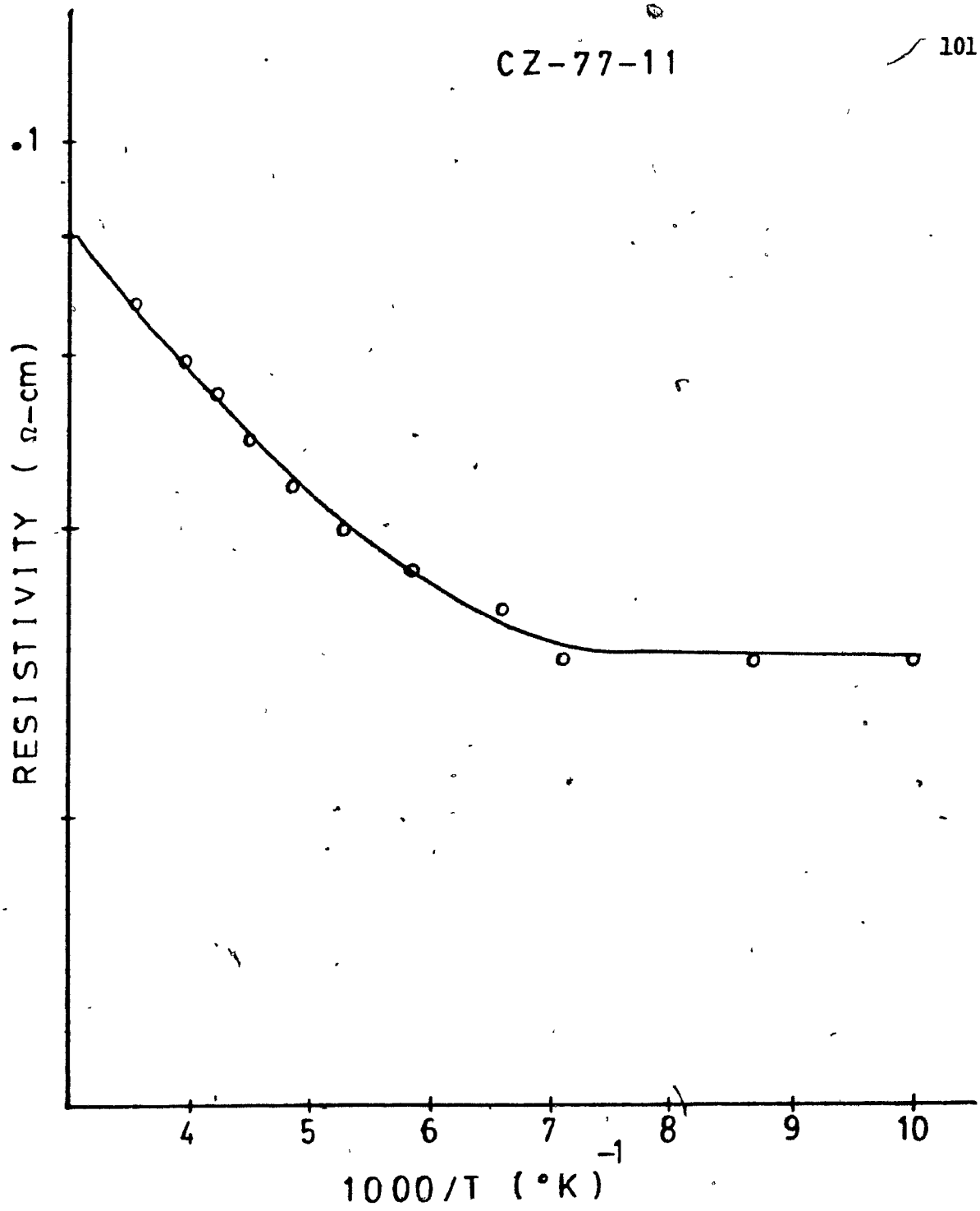

Figure (6-19) Variation of the Resistivity as a Function of the Temperature for Samples Originating from Ingot CZ-77-11

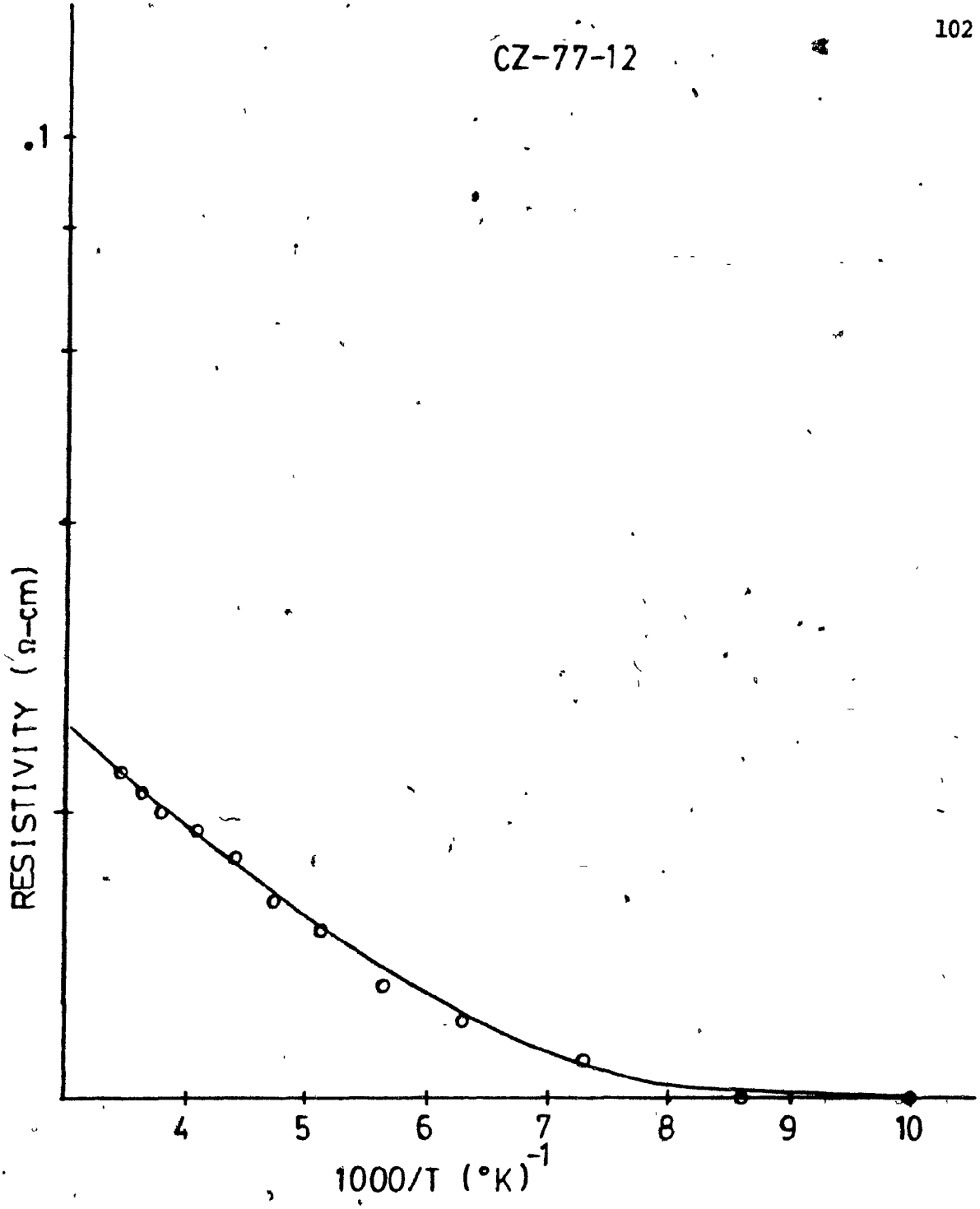

Figure (6-20) Variation of the Resistivity as a Function of the Temperature for Samples Originating From Ingot CZ-77-12

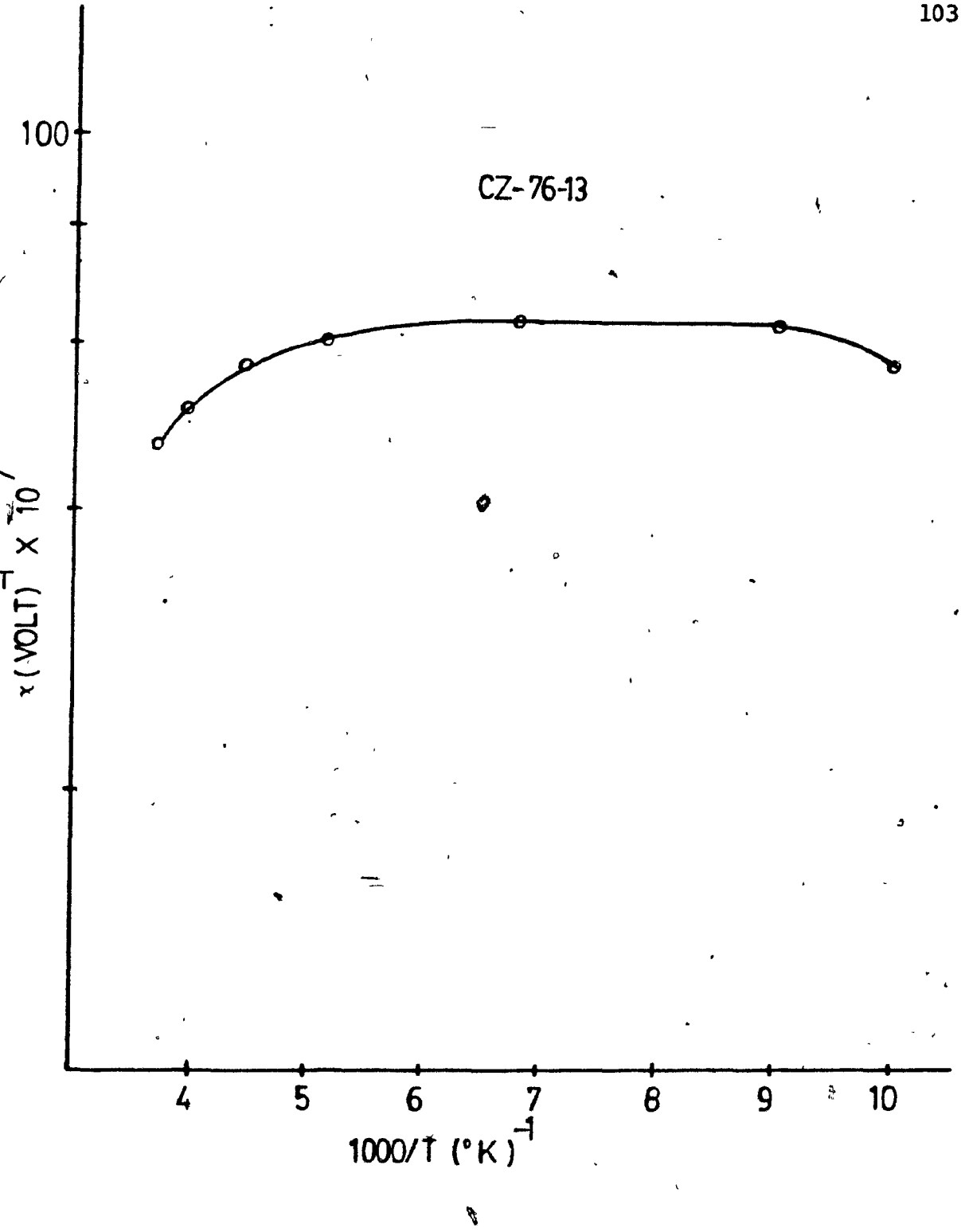

Figure (6-21) Temperature Dependence of the Rectification Tensor χ for Samples Originating From Ingot CZ-76-13

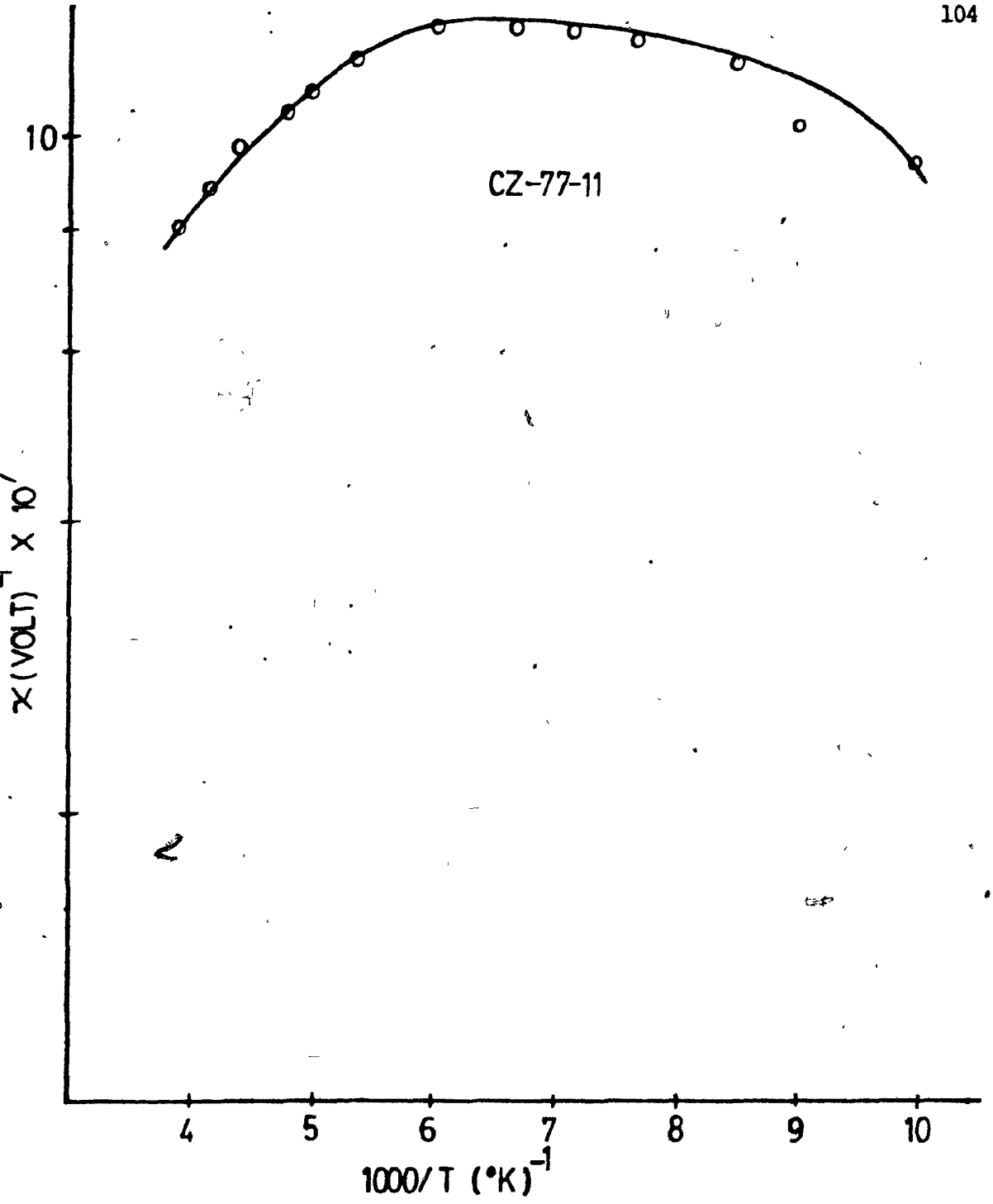

Figure (6-22) Temperature Dependence of the Rectification Tensor χ for Samples Originating From Ingot CZ-77-11

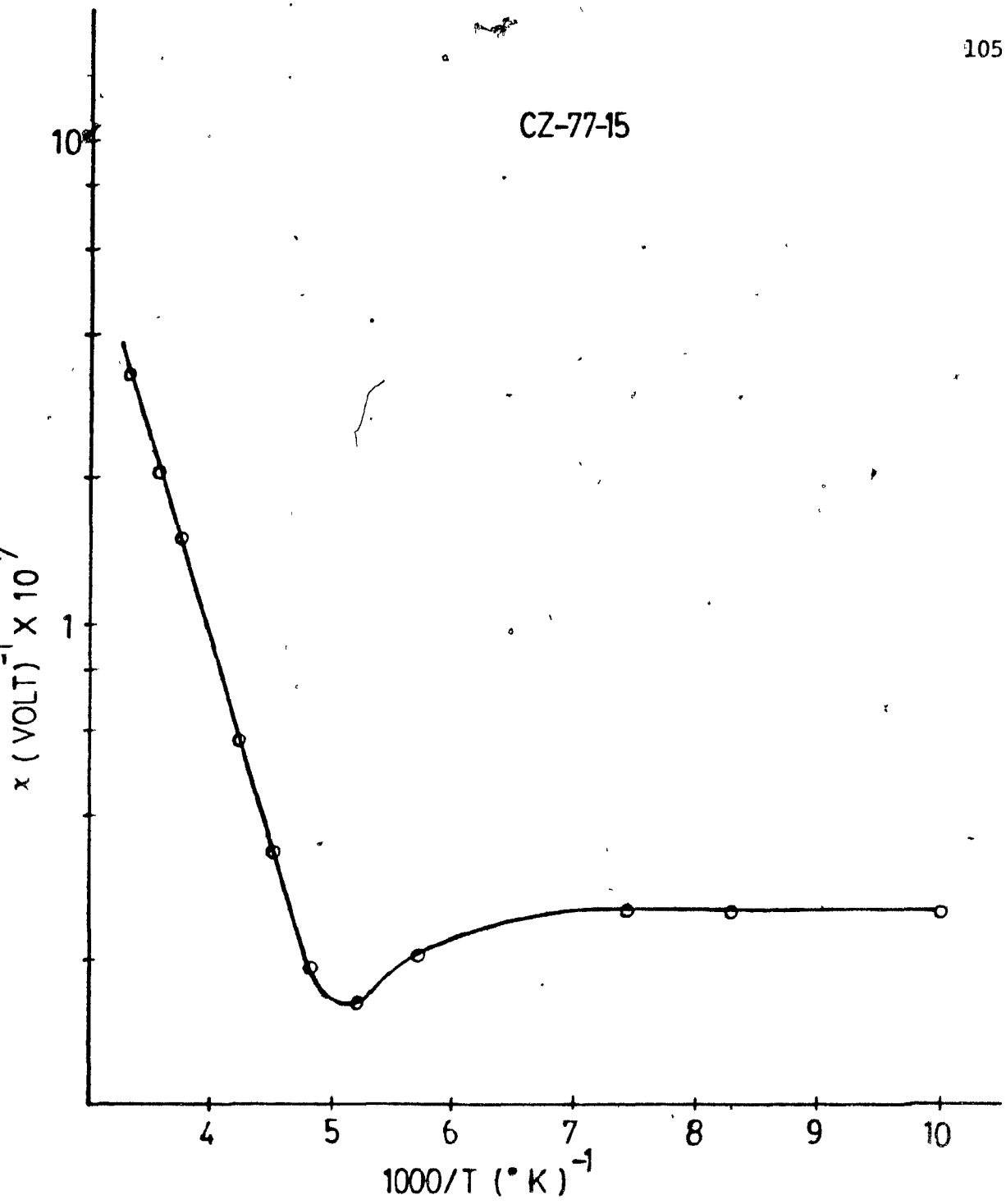

Figure (6-23) Temperature dependence of the Rectification Tensor χ for Samples Originating From Ingot CZ-77-15

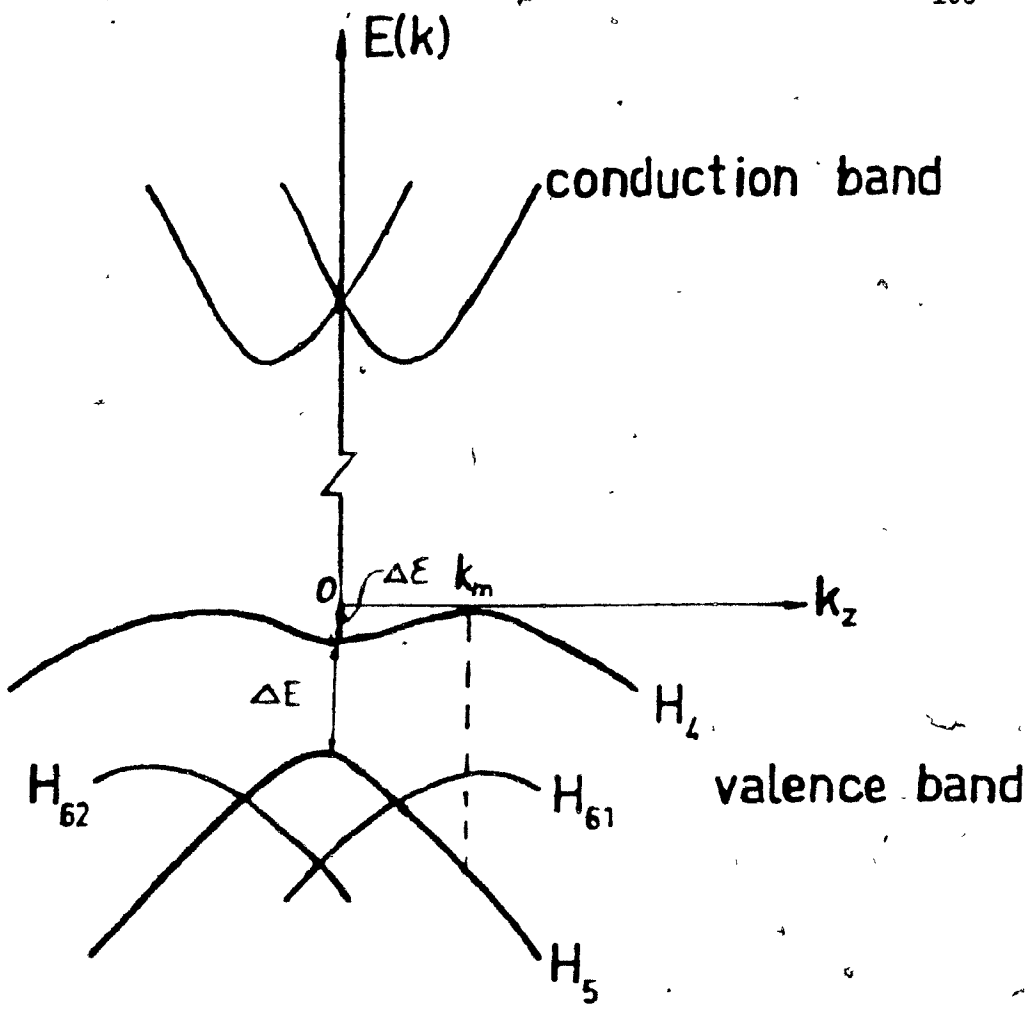

Figure (6-24) **Conduction and Valence Bands in Tellurium.**

On the other hand, in doped samples, the variations are much less pronounced. χ is relatively constant throughout the whole temperature range except at both ends of the latter where it has a tendency to decrease. This behaviour is the same for all doped samples. It is important to observe that the magnitude of χ increases substantially with impurity concentration.

In what follows, our objective shall be to interpret the above mentionned behaviour of the optical rectification tensor in terms of the theoretical expression obtained in Chapter V. It is understandable that numerical estimates of absolute magnitudes cannot be expected realistically from the complex relations presented in the latter chapter. However, a qualitative discussion of the experimental results in terms of the theory should be possible.

6.3.4 Discussion

6.3.4.1 General Considerations

A basic feature of the theoretical expression for χ as given by equation (5-16) is its strong dependence on sub-valence band populations, more specifically on population differences. Moreover, the presence of singularities in the denominator at some preferred frequencies implies that sub-bands separated in energy by an amount corresponding to the photon-energy of the laser should contribute very significantly to the overall optical rectification effect. Obviously, however, the exact behaviour of χ with respect to the populations is difficult to calculate.

Figure (6-14) is a schematic representation of the valence band structure of Tellurium in the neighborhood of point H of the Brillouin zone, that is to say, in the vicinity of the valence band edge. Transitions between bands H_4 and H_5 are allowed only for $\vec{E}$ polarized parallel to the c-axis [38]. However, direct electronic transitions between the H_6 and H_4 valence bands are allowed for this polarization condition and will contribute to χ provided the proper electronic population conditions prevail.

The discussion of the electronic population conditions at different energy levels within the Te band structure requires the specification of the Fermi function f(E,T)

$$f(E,T) = \frac{1}{1 + \exp\{E-E_F(T)\}/kT} \qquad (6\text{-}6)$$

where E represents the energy and $E_F(T)$ is the temperature dependent Fermi energy. Figure (6-25) is a typical plot of the Fermi function.

As it has been mentionned, χ is expected to depend on population differences at energy intervals of the order of the laser photon energy. It is clear that f(E,T) is completely defined when the position of the temperature dependent Fermi level is known. Figure (6-26) gives the result of a numerical computation of the Fermi level position as a function of the temperature for different doping levels, as discussed in Appendix B. Refering to figure (6-25) it is clear that electronic population differences will depend strongly on the average position of the energy intervals relative to the Fermi energy. For example, comparing the cases shown in figure (6-25), population differences from energy intervals corresponding to ΔE_2 would have a much higher contribution to expression (5-16) than those corresponding to ΔE_1 and ΔE_3. Finally, a well known feature of the Fermi distribution function to be taken into account is the increase of the width of the step with temperature.

6.3.4.2 Variations of the Magnitude of χ with respect to the Doping Level at Room Temperature

In terms of the previous discussion, it is clear that in the case of the undoped crystals where E_F at room temperature is well above the top of the valence band, energy intervals contributing to χ within the latter are expected to be of the type ΔE_1, figure (6-25), and hence will be associated with small population differences, i.e., will contribute weakly.

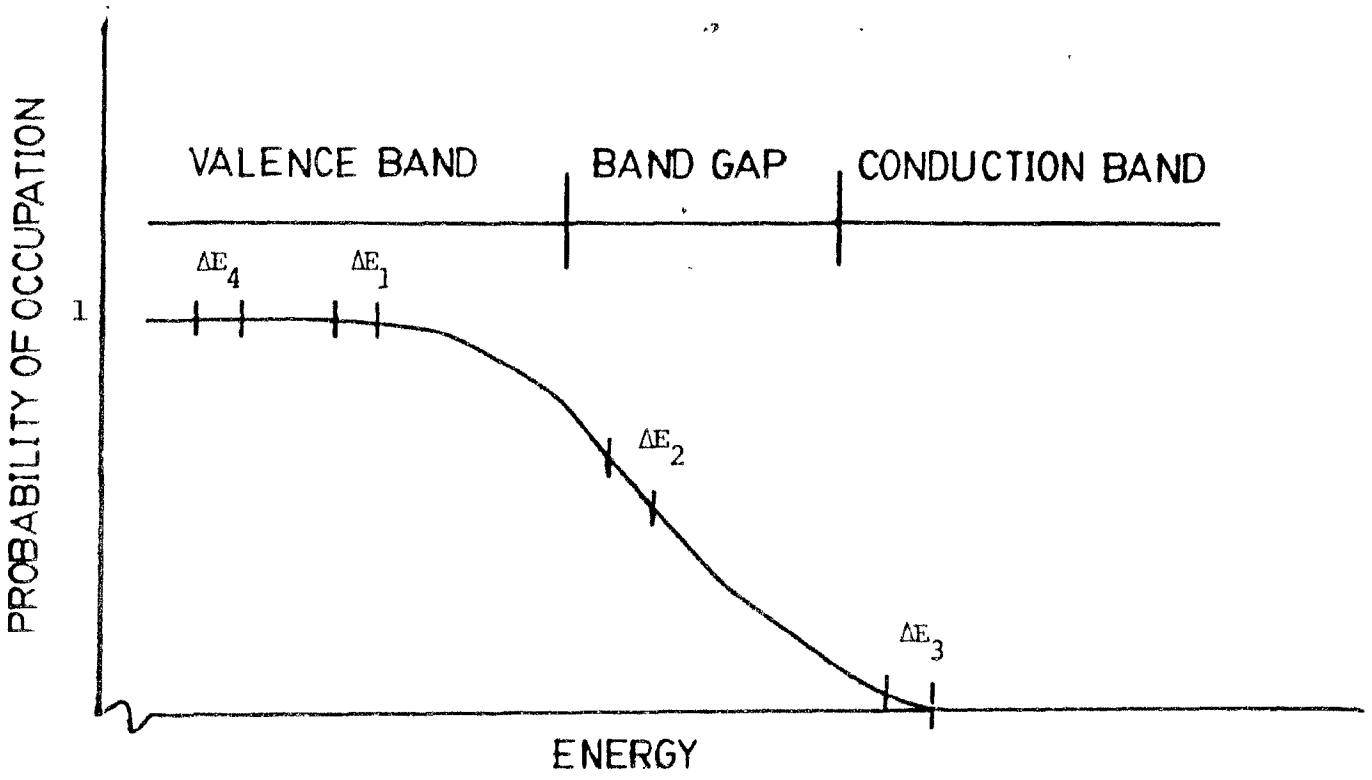

Figure (6-25) A Typical Plot of the Fermi Distribution Function.

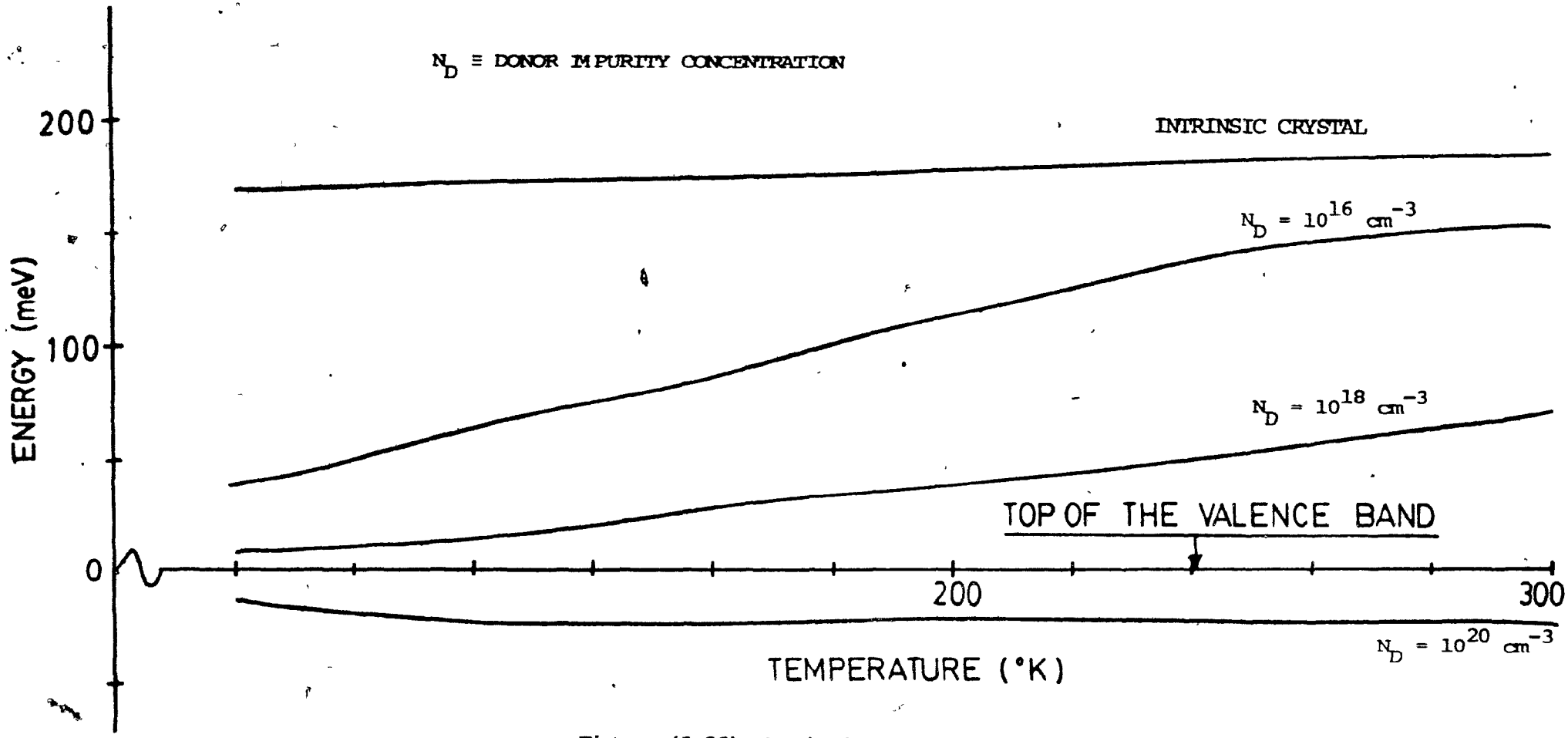

Figure (6-26) Variation of the Fermi Energy Level with the Temperature

This is to be compared with the case of doped crystals where E_F according to figure (6-26) lies increasingly closely to the valence band. In this case, energy intervals contributing to χ are clearly rather of the type ΔE_2 of figure (6-25) and hence will be associated with substantial population differences, i.e. a stronger contribution is expected. This behaviour is confirmed by the experimental results showing a strong increase in the magnitude of χ with an increase in the impurity doping levels (see paragraph 6.3.3)

The case of the very heavily doped samples from ingot CZ-77-12 for which it has not been possible to observe any signal seems at first sight to contradict the above statement. However, in spite of the expected further increase in the rectification effect in heavily doped samples, two parameters tend to decrease strongly any observable signal at the terminal of the device; indeed, the general reduction of the resistivity on the one hand and the sharp increase in the free carrier absorption on the other, can easily account for more than an order of magnitude in the observable voltage signals. It would then be expected that both of these effects can be reduced by reducing the thickness of the sample drastically and make the induced signal observable. This has been confirmed in our observations on thin samples as presented in paragraph 6.2.3.

6.3.4.3 Variations of χ in Doped crystals as a Function of the Temperature

Since the position of the Fermi energy level is relatively independent of the temperature in doped crystals, figure (6-26), it is expected that χ will not be strongly dependent on the latter. This expectation is confirmed experimentally by figures (6-21) and (6-22) which are essentially flat.

6.3.4.4 Variations of χ in Undoped Crystals with Respect to the Temperature

Figure (6-22) illustrates the behaviour of χ with respect to T in undoped crystals; it differs significantly from that of the doped crystals, exhibiting a saturation after a relatively fast decrease with decreasing temperature.

In order to discuss this behaviour in terms of the Fermi function, we note that the Fermi energy level E_F in ideal intrinsic crystals remains practically fixed at the centre of the energy gap, figure (6-26). Simultaneously, the step transition which is of the order of a few eVs decreases with decreasing temperature. Referring to figure (6-25) it is clear that the transitions that contribute to χ in such samples will correspond at room temperature to energy intervals of the type ΔE_4 , and, as the temperature decreases, they will be shifted towards transitions of the type ΔE_3 since the position of the Fermi energy remains fixed. This would result in continously decreasing χ with temperature. Actually, however, since the undoped crystals contain an inevitable small amount of impurities ($\simeq 10^{15}$ cm^{-3}), the Fermi level will tend to move toward the valence band as the temperature is decreased as shown in figure (6-26). In this case the combined effects of the shift in the Fermi energy level and the reduction of the step transition width will, at low temperature, make transitions near the top of the valence band behave as ΔE_4 transitions of figure (6-25). This will tend to reduce the decrease in the value of χ and possibly lead to a saturated profile such as obtained in the experimental results.

6.3.4.5 Enhanced Signals in Thin Samples ,

The case of thin samples presents a particular interest since, by reducing the thickness of the samples and ideally arriving at thin film configurations, we expect an improvement in two respects:

(1) The reduction in the observable signal associated with the finite absorption of the radiation along its trajectory in the sample, as discussed in paragraph 6.2.5 will now be completely eliminated.

(2) It is also generally expected that very thin samples will exhibit a higher average resistivity due to the influence of surface and other imperfections which will impede current flow in such samples. This will cause an effective increase in χ * for a given bulk value of χ.

The experimental results reported in this paragraph 6.2.3 are consistent with the above prediction; the most striking observation beeing that of the most heavily doped samples where a sizable signal is present whereas no signal could be observed in normal ones.

6.4 Conclusion

This chapter has presented a detailed experimental account for the observation of the optical rectification in Tellurium exposed to the 10.6μ radiation of a TEA-CO_2 laser and the results have been critically discussed in terms of the previously developed theory. Good qualitative agreement has been obtained.

CHAPTER VII

Conclusions

The reseach work undertaken in this thesis was originally directed towards the understanding of the physical nature of a third rank optical rectification tensor in Tellurium which had been identified and measured experimentally in a previous investigation by G. Ribakovs {6}.

Optical rectification resulting from non-linear dielectric behaviour in insulating solids seems to be a well understood phenomenon; on the other hand, although the occurence of a rectified signal from optical rectification in conductive solids has been experimentally reported by several workers {11,12,13,14}, the theoretical accounts for the latter have been unsatisfactory due to the use of different terminologies to characterize this effect and the lack of a unified approach.

In the present thesis, a theoretical discussion has been developed to obtain an expression for generalized conduction in solids at optical frequencies on the basis of the classical work of Butcher and McLean {21}; in particular, a phenomenological relaxation constant was introduced to obtain a non-singular form for the generalized conductivity; hence, an explicit expression for the second order conductivity has been given for non-centrosymmetric crystals. Finally, an explicit expression for the optical rectification tensor resulting from second order conductivity has been obtained. This work has established that the so-called Bulk Photovoltaic Effect (BPVE) defined by von Baltz {23} as a novel behaviour in materials is, in fact, identical to the behaviour predicted by our theory.

An attempt has been made to obtain a physical model to illustrate the physical significance of our theoretical expression; although in the case of low optical frequencies compared to interband transition frequencies an interpretation in terms of the standard semi-classical model of the effective mass tensor could be given, such a simple model to account for the general case has not been possible to obtain. This is suggested to be the subject of further investigation in this area.

A careful experimental program was then undertaken to substantiate the theory developed in the particular case of Tellurium, using a wide range of impurity concentration levels. Our results have, on the one hand reconfirmed those obtained by G. Ribakovs [6] in the case of undoped samples and on the other hand, gave a good qualitative agreement with the theory for both doped an undoped samples. Finally, experimental observations in very thin samples of Tellurium have confirmed the expected enhencement of the generated signal voltage at the device terminals. It is suggested that further work be conducted in investigating this area, possibly using in the limiting case deposited thin film samples.

APPENDIX A

Free Carrier Absorption

In the relaxation time approximation, the motion of a charge carrier with effective mass m * can be described as though it were in a viscous medium with a loss factor $1/\tau = \omega_o$, where τ represent a characteristic relaxation time. This model is called Drude's model and can be used to calculate the high frequency conductivity. It is easy to show that

$$\vec{J} = \sigma\vec{E} = \sigma_o\omega_o \frac{\omega_o + j\omega}{\omega_o^2 + \omega^2} \qquad (A\text{-}1)$$

where $\sigma_o = en^2\tau/m$ * represents the usual d.c. conductivity.

The imaginary part of the conductivity can be considered as a contribution to the real part of the relative static dielectric constant ε'.

$$\varepsilon' = \varepsilon_L - \frac{1}{\varepsilon_o\omega} \mathrm{Im}(\sigma) \qquad (A\text{-}2)$$

where ε_L represents the "background" dielectric constant associated with the lattice ions which is assumed to be frequency independent. The real part of the complex conductivity is associated with the imaginary part of the relative permittivity through

$$\varepsilon'' = \frac{\mathrm{Re}\ (\sigma)}{\omega\varepsilon_o} \qquad (A\text{-}3)$$

Both ε' and ε'' are expressible in terms of the real and imaginary parts of the complex refractive index, namely n and k.

$$\varepsilon' = n^2 - k^2 \qquad (A-4)$$

$$\varepsilon'' = 2nk \qquad (A-5)$$

k is usually called the extinction coefficient, and n is refered to as the refractive index.

The absorption coeffcient α is related to k by

$$\alpha = \frac{2\omega}{c} k \qquad (A-6)$$

where c is the speed of light.

From our knowledge of the properties of intrinsic Tellurium, it is possible to obtain the value of k for $\lambda = 10.6\ \mu$.
With {37}

$$\sigma = 100\ \Omega^{-1}m^{-1}$$
$$\alpha = 18\ m^{-1}$$
$$\varepsilon_L = 23$$
$$n = 4.8$$
$$\omega = 2\pi/\lambda = 1.778 \times 10^{14}\ rd/s$$

we get

$$k = 1.52 \times 10^{-5}$$

This value permits a rough evaluation of ω_o, by using equations (A-2) and (A-5).

$$\omega_o \simeq 8.5 \times 10^{12} \quad s^{-1}$$

From this result, the absorption coefficient α can be estimated for each of the samples in the present experiment since the values of ω_o are known from the resistivity data.

APPENDIX B

Numerical Computation of the Position of the Fermi Energy Level in Function of the Temperature

The determination of the Fermi energy level position in a semiconductor is in general a very complex problem. It requires the knowledge of the density-of-states functions for both the conduction and the valence band. The latter are complicated functions of the $E(\vec{k})$ Bloch wave dispersion relation. More specifically, the density of states is given by

$$g(E) = \frac{1}{4\pi^3} \oint\!\!\oint \frac{ds}{|\vec{\nabla}E(\vec{k})|} \qquad (B-1)$$

where the integration is to be performed over constant energy surfaces.

Once the density-of-states is known, the density of carriers at equilibrium can be evaluated by integrating $g(E)$ over the whole bands using the fermi function as a weighting factor. By invoking local charge neurality, one then gets an implicit non-linear equation for the Fermi energy.

In the simplest case, it is usual to assume that the bands are both parabolic and isotropic and therefore that the density-of-states varies like the square root of the energy. A better approximation can be obtained by using the following expression for the density-of-states in the valence band of Tellurium [39]

$$g(E) = \frac{1}{4\sqrt{2}\pi^2 AB}\left[\sqrt{2BE + S^2/2 - \frac{8\Delta_1^2 B^2}{S^2} + \sqrt{4BS^2E}} - \sqrt{2BE + S^2/2 - \frac{8\Delta_1^2 B^2}{S^2} - \sqrt{4BS^2E}}\right]$$

$$\text{for } \left(S^2/4B + 4\Delta_1^2 B/S^2 + 2\Delta_1 \right) < E < 0$$

and

$$g(E) = \frac{1}{4\pi\sqrt{2}\,\hbar^2 AB} \sqrt{2BE + S^2/2 - 8\Delta_1^2 B^2/S^2 + \sqrt{4BS^2 E}}$$

$$\text{for } E < \left(S^2/4B + 4\Delta_1^2/S^2 + 2\Delta_1 \right)$$

(B-2)

where
$$A = 3.4 \times 10^{-15} \text{ eV-cm}^2$$
$$B = 4.6 \times 10^{-15} \text{ eV-cm}^2$$
$$S = 2.67 \times 10^{-8} \text{ eV-cm}^2$$
$$\Delta_1 = 32.2 \text{ meV}$$

and by using the standard square root function

$$g(E) = \frac{\sqrt{2}}{\pi^2} \frac{m_n^*}{h^3}^{3/2} \sqrt{(E-E_c)} \qquad \text{(B-3)}$$

where m_n^* is the electron effective mass, and E_c is the position of the bottom of the conduction band, for the density-of-states in the conduction band.

REFERENCES

{1} A.J. Beaulieu, " Transversly Excited Atmospheric Pressure CO_2 Lasers ", Appl. Phys. Letters 16, 504 (1970).

{2} A.J. Alcock. A.C. Walker, " Fast Linear Detection System for TE CO_2 Lasers ", Appl. Phys. Letters 23, (1973).

{3} W.W. Duley, " A Simple Room Temperature Detector to Use with Carbon Dioxide Lasers ", J. Sci. Instrum. 44, 629 (1967).

{4} A.F. Gibson, M.F. Kimmitt and A.C. Walker, " Photon Drag in Germanium ", Appl. Phys. Lett. 17, 75 (1970).

{5} J. Auth, D. Genzow, K.H. Herrmann and M.Wendt, " Longitudinal Photon Drag in p-Type Tellurium ", Phys. Stat. Sol. (b) 65, 293 (1974).

{6} G. Ribakovs, " Investigation of Tellurium for the Detection of Pulsed CO_2 Laser Radiation ", Thesis, McGill University (1976).

{7} G.Ribakovs and A.A. Gundjian, " Photon Drag and Other Emfs Induced in Te by a TEA CO_2 Laser ", Appl. Phys. Lett. 24, 377 (1974).

{8} G.Ribakovs and A.A. Gundjian, " Theory of the Photon Drag Effect in Tellurium ", J. Appl. Phys. 48, 4609 (1977).

{9} G.Ribakovs and A.A. Gundjian, " TEA Laser Radiation Induced Emfs in Te ", J. Appl. Phys. 48, 4601 (1977).

{10} G. Ribakovs and A.A. Gundjian, " CO_2 Pulsed Laser Radiation Tellurium Detectors ", IEEE Journal of Quantum Electronics QE-14, 42 (1978).

{11} K.H. Hermann and R. Vogel, " CO_2 Laser-Induced Photoeffects in Te", Proc. Eleventh Intern. Conf. on Physics of Semicond. Warsaw (1972) publ. by PNW Warsaw (1972), p. 1251.

{12} C.R. Hammond, J.R. Jenkins, C.R. Stanley, " Optical Rectification in Tellurium from 10.6 μ ", Opto-Electronics 4, 189 (1972).

{13} A.F. Gibson, C.B. Hatch, M.F. Kimmitt, S. Kothari and A. Serafetinides, " Optical Rectification and Photon Drag in n-type Gallium Phosphide " J. Phys. C: Solid State Phys. 10, 905 (1977).

{14} J.M. Doviak and S. Kothari
Proc. Twelfth Intern. Conf. on Physics of Semiconductors, Stuttgart (1974). Publ. by Teubner, Stuttgart (1974) p. 1257.

{15} W.T.H. Koch, R. Miser, W. Ruppel and P. Wurfel
Ferroelectrics 13, [illegible] (1976).

{16} V.M. Fridkin and A.I. Rodin, " Anomalous Photovoltaic Effect in Ferroelectric SbSI and Cubic Piezoelectric ZnS ", Phys. Stat. Sol. (a) 61, 123 (1980).

{17} J. Auth, D. Genzow, K.H. Herrmann and M. Wendt, " Longitudinal Photon Drag in p-type Tellurium " Phys. Stat. Sol. (b) 65, 293 (1974).

{18} H. Heyszenau, " Electron Transport in the Bulk Photovoltaic Effect ", Phys. Rev. B 18, 1586 (1978).

{19} V.I. Belinicher, " Photogalvanic Effect Due to Free Carriers in Noncentrosymmetric Crystals ", Sov. Phys. JETP 48, 322 (1978).

{20} E.L. Ivshenko and G.E. Pikus, " Photogalvanic Effect in Semiconductors with Complex Bands ", Sov. Phys. Semicond. 13, 579 (1979).

{21} P.N. Butcher and T.P. McLean, " The Non-linear Constitutive Rela Relation in Solids at Optical Frequencies ", Proc. Phys. Soc. 81, 219 (1963).

{22} V.N. Genkin and P.M. Mednis, " Second-order Non-linear Conductivity for Band Electrons ", Sov. Phys. Sol. St. 10,1 (1968).

{23} R. von Baltz and W. Kraut, " Theory of the Bulk Photovoltaic Effect in Pure Crystals ", Phys. Rev. B 23, 5590 (1981).

{24} P. Kubo, " Statistical-Mechanical Theory of Irreversible Processes I. " J. Phys. Soc. Japan 12, 570 (1957).

{25} R.C. Tolman, " The Principles of Statistical Mechanics", Oxford University Press 1938 .

{26} E.O. Kane, " The Semi-Empirical Approach to Band Structure", J. Phys. Chem. Solids 8, 38 (1959).

{27} W. Kraut and R. von Baltz, "Anomalous Bulk Photovoltaic Effect in Ferroelectrics: A quadratic Response Theory ", Phys. Rev. B 19, 1548 (1979).

{28} R. von Baltz, to be published.

{29} M. Sachs, " Solid State Theory ", McGraw-Hill 1963.

{30} A. Yariv, " Quantum Electronics ", John Wiley and Sons 1975.

{31} N. Bloembergen, " Nonlinear Optics ", W.A. Benjamin 1965.

{32} C.G.B. Garrett and F.N.H. Robinson, " Miller's Phenomenological Rule for Computing Non-Linear Susceptibility ", IEEE J. Quant. Elect. QE-2, 328 (1966).

{33} M. Bass, P.A. Franken and J.F. Ward, " Optical Rectification ", Phys. Rev. 138, A534 (1965).

{34} J. di Persio, J.C. Pouhhan and G. Saada, " Deformation Plastique du Tellure Monocristallin ", Phys. Stat. Sol 42, 281 (1970).

{35} S. Ades, " Optical Properties of Intrinsic Tellurium Between 4 and 20 microns ", Thesis, McGill University (1975).

{36} J.I. Pankove, " Optical Processes in Semiconductors ", Prentice-Hall 1971.

{37} W.C. Cooper ed., " Tellurium ", Van Nostrand Reinhold Co. 1971

{38} E. Bangert, D. Fisher, P. Grosse, " Intervalence Band Transitions in Tellurium ", Phys. Stat. Sol. (b) 59, 419 (1973).

{39} T. Doi, K. Nakao and H. Kamimura, " The Valence Bance Structure of Tellurium II : The Infrared Absorption ", J. Phys. Soc. of J. 28, 4 (1980)